Simultaneous Fluorescence and Atomic Force Microscopy to study Mechanically-Induced Bacterial Death in Real Time

Tesis presentada por: **Adrián del Valle García**

para optar al título de Doctor en Física de la Materia Condensada, Nanociencia y Biofísica

Madrid, junio 2020

Facultad de Ciencias

Departamento de Física de la Materia Condensada

Universidad Autónoma de Madrid

Directora de tesis: **Dra. Cristina Flors**

Tutor de tesis: **Dr. Pedro José de Pablo Gómez**

Publications

The following publication was a result of the development of this thesis:

1. **del Valle, A**; Torra, J; Bondia, P; Tone, C; Pedraz, P; Vadillo-Rodriguez, V; Flors, C. Mechanically-Induced Bacterial Death Imaged in Real-Time: A Simultaneous Nanoindentation and Fluorescence Microscopy Study, *ACS Applied Materials & Interfaces,* **2020** https://doi.org/10.1021/acsami.0c08184

Other publications not included in the thesis:

2. Bondia, P.; Torra, J.; Tone, C. M.; Sawazaki, T.; **del Valle, A**.; Sot, B.; Nonell, S.; Kanai, M.; Sohma, Y.; Flors, C., Nanoscale View of Amyloid Photodynamic Damage, *Journal of the American Chemical Society* **2020**, 142 (2), 922-930.

A mi madre, a mi padre y a mi hermano

Acknowledgements

Ha sido duro, muy duro, pero ya estamos aquí. Me he caído muchas veces, pero me he levantado, una, otra y otra vez. Sin embargo, de no ser por aquellas personas que me han apoyado día a día, no sólo en el ámbito profesional, sino en el personal, no hubiera sido posible estar en el punto que estoy ahora. Por ello, me gustaría dedicarles unas palabras a todas estas personas que han hecho posible todo esto.

En primer lugar, como no podría ser de otra forma, a mi directora de tesis la Dra. Cristina Flors, por darme la oportunidad de realizar mi tesis doctoral, guiarme en todo este camino que era muy nuevo para mí y haber tenido la paciencia de enseñarme y transmitirme sus conocimientos en la materia. Por otro lado, me gustaría destacar el apoyo personal que ha supuesto, dado que a cada congreso que he viajado siempre me ha facilitado mucho las cosas, sabiendo mis peculiaridades. Para alguien como yo no son fáciles esas cosas, pero siempre lo ha planeado y llevado a cabo de tal forma que he podido disfrutar de esas experiencias, cuidando hasta el último detalle. Y, por último, por aguantar mis chapas y teorías/expedientes X que se maquinaban en mi cabeza, y por reírte conmigo cuando algunas de ellas eran algo disparatadas. ¡Gracias Cristina!

Quiero agradecer también a la Comunidad de Madrid por financiar mi trabajo con la beca PEID-2016/IND-2774.

Por otra parte, quiero agradecer a mi tutor de la Universidad Autónoma de Madrid, el Dr. Pedro José de Pablo Gómez, por su disposición en todo momento, así como su ayuda con todos los trámites implicados en la realización de esta tesis. También por las contribuciones e ideas que me ha dado para la realización de la tesis, teniendo en cuenta su excelente investigación en el estudio de virus. Agradecer al Dr. Pawel Hermanowicz por su ayuda con el AtomicJ y la implementación de la versión 2.1.2.

El grupo de investigación, la clave de todo esto. ¿dudas? ¿discutir teorías? ¿ideas? ¿ayuda? Ahí estaban ellos, dispuestos a allanarme el camino cuando encontraba trabas. La primera, no puede ser de otra forma, la Dra. Patricia Bondia. Desde que llegué a IMDEA ha sabido guiarme, aceptarme, apoyarme y, sobre todo, ayudarme. Era un nuevo reto en mi vida, en un campo científico alejado de mis procesos químicos, de mis simulaciones, de mis cálculos... y entre ella y Cristina supieron guiarme y darme todo lo necesario para que rápidamente fuese hilando todo. Siempre se ha portado genial conmigo, y ha sabido animarme en aquellos momentos difíciles. Pero no todo ha sido dificultades, sino que hemos reído mucho, muchísimo diría yo. Estaremos unidos por *click*, como la película, no lo olvides. Su tocaya, la Dra. Patricia Pedraz, otra de los grandes artífices. Cierto es que, al poquito de entrar yo, tú presentabas tu tesis y te teníamos que decir adiós. En ese tiempo, hicimos buenas migas y me ayudaste también a integrarme en el grupito que teníais todos. Tu vuelta ha sido una de las mejores cosas

que han pasado por Imdea, no solo personalmente, sino profesionalmente. Sabes tanto de AFM que me has facilitado mucho las cosas, a la hora de analizar o interpretar datos. En lo personal ya sabes que te he dado mucho la tabarra y siempre has estado ahí en los momentos claves, donde he pasado por una situación parecida a la que pasaste tú en su día, y has sabido entenderme y apoyarme.

Toda mente creativa, innovadora y curiosa (o loca, como quieras decirlo) necesita un fiel seguidor, que le siga, con todas las de la ley. Creo que el Dr. Joaquim Torra ha sido una persona que me ha ayudado mucho, no sólo ayudándome a solucionar los problemas que tuvimos con la proteína o con el plásmido, sino por las ideas y sugerencias bastante buenas que siempre ha sabido darme y que hemos aplicado con grandes resultados, pero nos falta una, amigo. Tenemos una cita pendiente con el *B. subtilis*, ¡no lo olvides! Estamos cerca de conseguirlo. Ingrid fue el último fichaje del grupo, y ya desde el minuto uno sabía que sería una gran compañera, y ha sido probablemente con la que más teorías locas he discutido. Siempre ha estado ahí para escucharme, y para facilitarme las cosas, sobre todo con el análisis de las oscilaciones. La Dra. Caterina Tone estuvo poco tiempo con nosotros, pero también es necesario agradecer su contribución dado su amplio conocimiento con el AFM, donde me ayudó a interpretar aquellos datos que resultaron ser complejos.

Por otro lado, agradecer al Dr. Santiago Casado su tiempo invertido en enseñarme a usar el JPK de manera autónoma, y poder acometer los experimentos presentes en esta tesis. Al Dr. Alberto Pulido, por explicarme todo lo relativo al cultivo bacteriano, a preparar las muestras y ayudarme en mi vuelta a tareas de laboratorio. Espero que no me tengas en cuenta el primer día que maté las bacterias por error y no pudimos medirlas. También me gustaría expresar mi agradecimiento al Dr. Johann Mertens, por haberme solucionado todas las dudas que tenías acerca de la indentación de bacterias, por haberme dado infinidad de ideas y sugerencias, y siempre dispuesto a escucharme. A la Dra. Virginia Vadillo, por su gran contribución al desarrollo de estos experimentos, donde sus grandes estudios en bacterias han arrojado luz en aquellos momentos que había sombras. Gracias por tus sugerencias y apoyo.

Me gustaría dar las gracias a IMDEA nanociencia por darme la oportunidad de hacer mi doctorado en un centro tan interdisciplinar donde se nos da la oportunidad de entender la ciencia desde distintos puntos de vista y trabajar en un ambiente en el que la gente disfruta con lo que hace convirtiendo esta pasión en algo contagioso. Y a todas las personas que han participado de una forma u otra del progreso de esta tesis como: la Dra. Adriana Arnaiz por enseñarme todo lo necesario para realizar cultivos celulares y hacerme el training para poder ser autónomo, o el grupo administrativo… por ser solucionadores de problemas y hacer la vida más sencilla a todos los que trabajamos en IMDEA. Especial mención quiero hacer al Dr. Jose Luis Casillas, que me ha ayudado

mucho personalmente. Algún día entrenaré a tu hijo en futbol sala, y me darás las gracias porque conmigo va a aprender a jugar al futbol de verdad.

Y especialmente, quiero agradecer a todas aquellas personas que empezaron siendo compañeros de trabajo y que, en este tiempo juntos dentro y fuera de IMDEA nos ha convertido en amigos, en grandes amigos. Aquí, hay que empezar por Lucía, sí o sí. Mi gran apoyo durante toda la tesis, con la persona que probablemente más tiempo he pasado. Solo puedo decir que se merece un monumento, porque aguantarme no es fácil, pero aguantarme tanto tiempo... es complicadísimo. Nunca una mala cara, nunca ha faltado cuando la he necesitado, y siempre ha sabido alegrarme los días con una sonrisa, detalle o con un abrazo. ¡Mis dieces Lusy Lú! Iván, ¡qué voy a decir de ti, si hacíamos todo juntos! Sé tanto de Helio y de trasvases como tú de AFM y bacterias. Has sido un gran compañero, y nos lo hemos pasado muy bien, y te has convertido en uno de mis grandes amigos, por todas las risas que nos hemos echado allá donde íbamos: casa rural, IFEMA, scape rooms... brutal. Andrea, otra de las joyas de la corona, con nuestras muchas conversaciones y apoyo mutuo en esos momentos donde necesitamos desahogarnos. He disfrutado muchísimo de tu compañía, dentro y fuera de IMDEA, y por esas sesiones de gimnasio de 20 min de bici y a casita. Sergio R, sencillamente espectacular. Ha sido mi compañero de office y la verdad que he compartido con él de todo. Experto en futdraft, aunque paquete en el futbol. Nos hemos reído mucho y me has hecho los días muy amenos. Gonzalo, el último en unirse al clan de payasetes. Encajaste desde el minuto uno, y no me extraña dada la personalidad que tienes, extrovertido y sin vergüenza. También destaco tu habilidad como informático, para poder conseguirme mi ordenador 33 meses después (33, ya tu sabes jaja). No me olvido de mi sevillana, Marina, que siempre ha sacado tiempo para venir a darme un abrazo o preguntarme cómo me iban las cosas. Gracias por preocuparte por mí y darme ánimos cuando las cosas iban regular. Jenny, porque supuso para mí un fuerte apoyo en mis primeros meses de tesis, y luego tuvo que irse... fue un momento duro, dado todo el cariño que te cogí, y lo bien que nos entendíamos. Allá donde vayas, seguirás siendo una de las mejores compis que he tenido. Ale Alejandra, Alejandra por ser la mejor jugadora de Counter-Strike de IMDEA. Una gran persona que me ha tratado siempre como a un rey, y he disfrutado mucho con ella, aunque a día de hoy, 3 años después, sigue sin jugar una partida conmigo. Si tan buena eres, ¡enséñame! Maite A, por ser la base de todo lo que he aprendido en temas biológicos y bacterianos. Siempre has sacado tiempo para resolver mis dudas, ayudarme con mis bacterias o enseñarme a plaquear. Mucho ánimo en lo tuyo. Víctor R, por todos esos momentos de risas que hemos pasado, siempre con tu carácter alegre, sabiendo hacer desconectar a los demás y ayudarles a evadirse cuando más lo necesitaban.

Por supuesto, también a aquellas personas que, aunque no haya tenido tanto contacto en el día a día, han aportado su granito de arena, como Maite M, Andrés,

Manu, Sergio (técnico), Iván, Jaime, Sergio (Maite), Miguel (Maite), Gudín, Rial, Marzoa, Felipe, Fer, Irene y Fran.

Y a esa gente que ha sido mi apoyo fuera de IMDEA, como Chicho, Amín, Toñete, Iván, que han sabido hacerme desconectar de mis ralladas en cada partido de fútbol como en los entrenamientos. La verdad que todas las risas que nos hemos echado no tienen nombre, sois unos desgraciados jaja. Y como no, a mi queridísima Leti o, mejor dicho, Lessi, una de las mejores personas que he conocido. Fue un placer entrenarte, pero es toda una suerte disfrutar día a día de tu persona. Tienes un carácter espectacular, una forma de ser que ojalá el resto del mundo fuera así. Siempre te has preocupado por mí, por mi salud y por mi tesis. Has estado ahí siempre, cuando lo necesitase, y has sabido animarme con abrazos o con chucherías/bollos. Sencillamente espectacular.

Finalmente, quiero agradecer a las personas más importantes de mi vida, como son mi familia y mi pareja, las cuales me han apoyado en mi decisión de empezar una carrera investigadora. A mis padres, porque son sencillamente maravillosos y son la principal razón de que haya podido llegar hasta donde he llegado, siempre allanándome el camino, ayudándome a levantarme cuando me caía, y dándome solución a aquellos problemas que me atormentaban. Mi hermano, simplemente para mí, es como Dios. Desde pequeño me ha ayudado con mis problemas, me ha hecho volverme disciplinado y aplicado en mis estudios, y si yo estoy aquí es por todo lo que me ha inculcado. A parte que eres la persona más inteligente que conozco, y para mí, no habrá nadie que iguale esa cabecita tan privilegiada que tienes. ¡Eres un grande bro! Y por supuesto, a Ester, por saber adaptar su vida a mis continuos problemas, ralladas, dudas, incertidumbres, manías... y entenderme y apoyarme en cada decisión que he ido tomando desde que apareciste en mi vida. Te construirán una plaza en tu nombre en Colmenar Viejo algún día, estoy seguro.

Contents

List of acronyms and symbols

AFM	Atomic Force Microscopy
AM	Amplitude Modulation (tapping mode)
AMP	Antimicrobial peptides
BSi	Black Silicon
CT	Cell-Tak™
CM	Contact Mode
DNA	Deoxyribonucleic acid
EMCCD	Electron Multiplying Charge-Coupled Device
GFP	Green Fluorescence Protein
GO	Graphene Oxide
JM	Jumping mode (force mapping)
LB	Luria Bertani
LPS	Lipopolysaccharides
NAG	N-acetylglucosamine
NAM	N-acetylmuramic acid
OD	Optical Density
PEG	Polyethylene Glycol
PLL	Poly-L-lysine
PBS	Phosphate-buffered saline
PI	Propidium Iodide
RNA	Ribonucleic acid
ROI	Region of Interest
ROS	Reactive oxygen species
STM	Scanning Tunneling Microscopy

SWCNTs	Single Wall Carbon Nanotubes
TEM	Transmission Electron Microscopy
TIRF	Total Internal Reflection Fluorescence

F	Force
d	Cantilever deflection
z	Distance (i.e. piezo displacement)
k_{eff}	Slope of the F-z curve
k_c	Cantilever spring constant
k_b	Bacterial spring constant
s	Slope of the d-z curve
E	Young´s Modulus
δ	Indentation
F_r	Rupture force
l_d	Indentation depth
t_{osc}	Oscillation time

List of figures

Abstract

In the last decades, advanced imaging techniques have improved our ability to analyze biological systems at the micro and nanoscale, and in real time. Microscopy techniques have their own strengths and limitations, so their combination has the potential to provide a more comprehensive understanding of biological processes. This thesis is focused on the development and application of simultaneous fluorescence and atomic force microscopy (AFM) to study mechanically-induced bacterial death. The results reported here provide a quantitative understanding of the mechanical interactions between the AFM tip and bacteria, in the context of emerging mechano-bactericidal nanomaterials.

This manuscript is divided into six chapters and one appendix. Chapter 1 provides an overview of the bacterial world and the strategies used over the years to combat the increasing bacterial contamination of surfaces, emphasizing the recent strategy based on mechanical damage. It also describes the microscopy techniques used, highlighting the strengths and weaknesses of each one, and discussing why correlative microscopy is more suitable to study this kind of processes. Chapter 2 describes the general materials and methods applied in this thesis and the software used to analyze experimental data. Chapter 3 provides the groundwork to develop a methodology to successfully combine AFM nanoindentation and fluorescence microscopy simultaneously using fluorescent polymer beads, focusing on the challenges that may arise when simultaneous measurements are performed. In Chapter 4, the methodology was adapted to image bacteria in physiological conditions, and optimal protocols to perform reproducible experiments on living bacteria were found. This optimized methodology in combination with a fluorescent cell membrane integrity marker was successfully applied to quantify the forces needed to rupture the bacterial cell wall. Moreover, a correlation between the forces exerted on bacteria and the kinetics of the fluorescence response is found. Chapter 4 is complemented by Appendix A, which provides the mechanical characterization of the bacterial wall below the rupture point, in order to give a more complete overview of the mechanical properties of the bacterial surface. Chapter 5 explores a different method to assess bacterial viability upon nanoindentation by monitoring the oscillation of the Min system, which reflects bacterial physiology. This method reveals that forces below the breakage point of the cell wall produce a fatigue effect, and provides a quantitative framework to understand low force collisions between bacteria and nanomaterials. These experiments also emphasize the limitation of integrity markers to provide a comprehensive view of bacterial response. The aim of Chapter 6 is to provide coherence and perspective to the main results of the thesis, as well as an outlook on how advanced microscopy methods and future experiments may impact the study of interactions between bacteria and nanotopographical features in the context of mechano-bactericidal nanomaterials.

Resumen

En las últimas décadas, las técnicas avanzadas de imagen han mejorado nuestra capacidad de analizar sistemas biológicos a la micro y nanoescala, y en tiempo real. Las técnicas de microscopía tienen sus propias fortalezas y limitaciones, por lo que su combinación tiene el potencial de proporcionar una mejor comprensión de los procesos biológicos. Esta tesis se centra en el desarrollo y la aplicación de fluorescencia y microscopía de fuerza atómica (AFM) simultánea para estudiar la muerte bacteriana inducida mecánicamente. Los resultados presentados proporcionan una comprensión cuantitativa de las interacciones mecánicas entre la punta de AFM y las bacterias, en el contexto de los emergentes nanomateriales mecano-bactericidas.

Esta tesis está dividida en seis capítulos y un apéndice. El Capítulo 1 proporciona una visión general del mundo bacteriano y las estrategias utilizadas a lo largo de los años para combatir la creciente contaminación bacteriana sobre las superficies, enfatizando la reciente estrategia basada en el daño mecánico. También describe las técnicas de microscopía utilizadas, destacando las fortalezas y debilidades de cada una, y discutiendo por qué la microscopía correlativa es más adecuada para estudiar este tipo de procesos. El Capítulo 2 describe los materiales y métodos generales aplicados en esta tesis y el software utilizado para analizar datos experimentales. El Capítulo 3 proporciona la base para desarrollar una metodología correlativa que permita combinar con éxito la nanoindentación de AFM y la microscopía de fluorescencia simultáneamente, usando microesferas poliméricas fluorescentes, y centrándose en los desafíos que pueden surgir cuando se realizan mediciones simultáneas. En el Capítulo 4, la metodología se adaptó para poder medir bacterias en condiciones fisiológicas, y se encontraron unos protocolos óptimos para realizar experimentos reproducibles en bacterias vivas. Esta metodología optimizada en combinación con un marcador fluorescente de integridad de la membrana celular se aplicó con éxito para cuantificar las fuerzas necesarias para romper la pared celular bacteriana. Además, se encuentra una correlación entre las fuerzas ejercidas sobre las bacterias y la cinética de la respuesta de fluorescencia. El Capítulo 4 se complementa con el Anexo A, que detalla la caracterización mecánica de la pared bacteriana por debajo del punto de ruptura, con el fin de proporcionar una descripción más completa de las propiedades mecánicas de la pared bacteriana. El Capítulo 5 explora un método diferente para evaluar la viabilidad bacteriana como consecuencia de la nanoindentación mediante el seguimiento de la oscilación del sistema Min, que refleja la fisiología bacteriana. Este método revela que las fuerzas por debajo del punto de rotura de la pared celular producen un efecto de fatiga y proporciona un marco cuantitativo para comprender las colisiones de baja fuerza entre bacterias y nanomateriales. Estos experimentos también enfatizan la limitación de los marcadores de integridad para proporcionar una visión integral de la respuesta bacteriana. El objetivo del Capítulo 6 es proporcionar coherencia y perspectiva a los principales resultados de la tesis, así como una proyección de cómo los

métodos avanzados de microscopía y futuros experimentos pueden mejorar el estudio de las interacciones entre bacterias y nanotopografías en el contexto de los materiales mecano-bactericidas.

Chapter 1

Introduction

1. Introduction

1.1 The bacterial world

The world we live in today is mostly composed of bacteria. The total biomass of the smallest organisms on Earth, i.e. bacteria and archaea, has been estimated to equal that of terrestrial and marine plants.[1] Bacteria were among the first forms of life to emerge, before animals and plants. Through two extraordinary events, bacteria made possible the human life: firstly, bacteria (cyanobacteria) started to release oxygen as a consequence of photosynthesis, creating the atmosphere of the earth.[2, 3] Secondly, bacteria, in symbiosis with other cells, created the complex cells present in plants and animals necessary for their life and evolution.[2-4] Therefore, bacteria built the world we live in today.

Bacteria are unicellular prokaryotic organisms that reproduce by binary fission. As a main feature, prokaryotes do not have intracellular compartments delimited by membranes, so they lack a nuclear membrane, unlike eukaryotes, and the prokaryotic DNA is circular and closed.[5] The bacterial cell is about 70-80% water, 15% proteins and 7% nucleic acids (predominantly RNA), 3% carbohydrates and 2% lipids and several other components in small percentages.[6]

The bacterial cell envelope can vary considerably in its structure, and it plays a central role in the properties and capabilities of the cell.[7, 8] In general, the bacterial cell envelope falls in two major types[9]: Gram-negative bacteria, which have two membranes, a cytoplasmic and outer membrane separated by the periplasm in which is a thin cell wall made up of peptidoglycan, and the Gram-positive bacteria which have only a cytoplasmic membrane surrounded by a much thicker peptidoglycan layer (Figure 1.1).

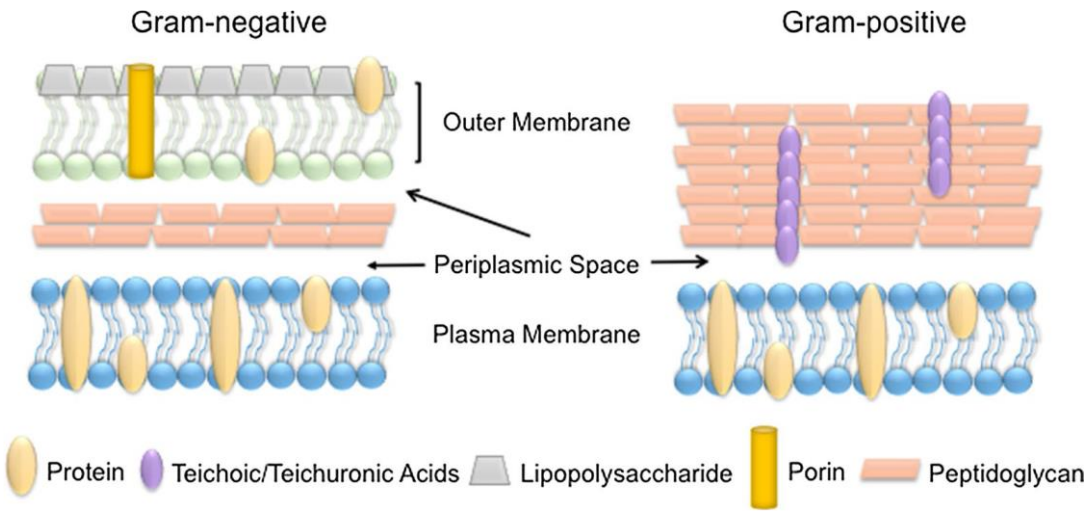

Figure 1.1: Scheme highlighting the differences between the cell wall structure of Gram-negative and Gram-positive bacterial cells. Reproduced from.[10]

The *cytoplasmic membrane or plasma membrane* is about 7.5 to 10 nm thick and composed of phospholipid and protein molecules. The cytoplasmic membrane encloses the cytoplasm of the bacterium and is a selectively permeable membrane that determines and regulates what goes in and out of the organism (i.e. flow of nutrients, or chemical needed for metabolism). Functions associated with the cytoplasmic membrane include energy production or waste removals, among others.[11]

Lying outside of this membrane there is a semirigid, tight knit molecular complex wall that determines the shape of the bacterial cell. This wall is made of a huge molecule called peptidoglycan (or murein). *Peptidoglycan* is a vast polymer consisting of interlocking chains of identical monomers, which consists of two joined amino sugars, N-acetylglucosamine (NAG) and N-acetylmuramic acid (NAM), with a pentapeptide coming off of the NAM. The peptidoglycan prevents osmotic lysis. As seen earlier, bacteria concentrate dissolved biomolecules and ions, making the bacterium's cytoplasm usually hypertonic to its surrounding environment so the net flow of free water is into the bacterium. Without a strong cell wall, the bacterium would burst from the osmotic pressure of the water flowing into the cell.[11]

Gram-positive bacteria have a relatively thick continuous cell wall, which is composed largely of peptidoglycan multilayers (20 to 100 nm ~ 60 to 90 % cell wall).[6-9, 12, 13] Other cell wall polymers are covalently attached to the peptidoglycan, such as teichoic acids, polysaccharides and peptide-glycolipids. In contrast, the peptidoglycan layer in Gram-negative bacteria is thin (up to 10 nm thick ~ 10 to 20 % cell wall). [6-9, 12, 13], representing probably one to a few layers. Outside the peptidoglycan layer in the Gram-negative envelope is an outer membrane structure (about 7.5 to 10 nm thick, similar to plasma membrane), composed of phospholipids, lipoproteins, lipopolysaccharides (LPS).

This Gram-positive and negative major division owes its name to the Danish physician Hans Christian Gram for one of the most useful staining reactions called the Gram stain, developed in 1884.[14] In Gram-positive bacteria the peptidoglycan forms a thick meshlike layer that retains the blue dye of the Gram stain by trapping it in the cell. In contrast, in Gram-negative bacteria the peptidoglycan layer is very thin (only one or two molecules deep), and the blue dye is easily washed out of the cell.[15]

The ratio of bacteria-to-human cells is of the order of 1.3:1 or even 10:1, depending on the estimates.[16, 17] These figures highlight the biological importance of the microbiota. Bacteria are needed to keep ourselves healthy, since they help us in tasks such as fighting against foreign invaders or in processes such as digestion.

However, not all bacteria we know are beneficial for humans. Pathogenic bacteria can cause serious diseases such as infections, pneumonia or cancer, and therefore it is necessary to develop strategies or protocols to combat them, even preventing their colonization if possible.

1.2 Antibacterial strategies: surfaces and colloids

The number of strategies investigated to fight bacterial infection is also growing, and this field represents a very active area of research in the biomaterials community. [18-26]

Bacterial contamination is detrimental to industrial processes and hazardous to human health.[27, 28] The scientific and industrial interest in antibacterial surfaces has significantly increased in recent times due to the persistent bacterial contamination, especially in medical implant surfaces.[20, 29] This is evident in those patients who have undergone a recent surgery, with some type of biomedical implant, where colonization of resistant pathogens can occur at the transplant-tissue interface. In this scenario, what we call "race to the surface"[30] occurs, in which cells compete against pathogens to colonize the surface. If the cells achieve this, rapid proliferation will occur, creating a cell layer discouraging pathogen attachment and reducing the risk of infection. On the contrary, if the pathogenic bacteria manage to colonize the surface faster than the cells, the adhesion and formation of a bacterial biofilm[31-33] will seriously compromise the osteointegration. Unfortunately, in most cases, it is the pathogen that just prevails.

1.2.1. Classical approach: Antifouling vs Bactericidal

Antibacterial strategies for surfaces can be explained by two different mechanisms. While *antibiofouling* refers to the presence of a surface that is inherently resistant, or has the ability to limit the attachment of microbes (i.e. an unfavorable surface architecture for attachment or the presence of an unattractive surface chemistry for the attaching microbial species), *bactericidal surfaces* try to disrupt any cells that have adsorbed onto the surface, resulting in the death of the cells. Bactericidal surfaces possess characteristics that can either physically or chemically disrupt the cell morphology.[34, 35]

Thus, a classical classification is to divide antibacterial treatments as passive or active, depending on their ability to discourage bacterial cell attachment or actually kill contaminating bacteria, respectively. [18] (Figure 1.2).

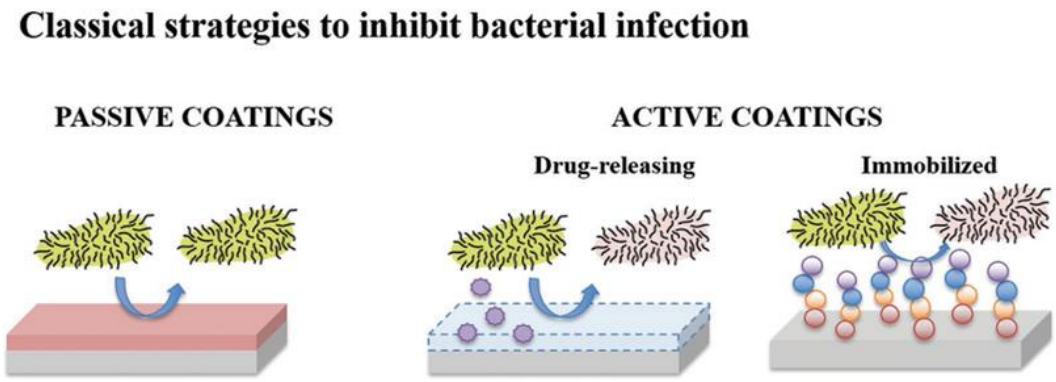

Figure 1.2: Schematic summary of classical strategies of antibacterial surface functionalization. Reproduced from.[18]

Passive coatings are typically based on antiadhesive polymers that prevent bacteria attachment. Among all polymers, polyethylene glycol (PEG) is probably the most widely used to confer antifouling properties to a material surface[22, 36], with promising results tested in *S. aureus, S. epiderrmis, S. mutans and P. aeruginosa.* [37] Its repelling properties are related to its flexible and hydrophilic chains. These coatings can easily be applied to a broad range of materials and have the advantage of being simple, effective, and not requiring the use of drugs.[18]

In contrast to passive coatings*, active coatings* exert their antibacterial action by directly killing bacteria. This may be achieved by a very diverse range of molecules, including bactericidal polymers (e.g., chitosan, cationic polymers), quaternary ammonium salts, ions (e.g., silver, zinc), antibiotics, bactericidal agents (e.g., chlorhexidine), and antimicrobial peptides (AMPs).[18-21, 23-26]

These strategies are largely reliant upon two physicochemical approaches (Figure 1.2):

i. the incorporation of antibacterial agents (e.g., antibiotics or silver ions) on the biomaterial via physical adsorption or entrapment in polymeric matrices (drug-releasing mechanism)
i. the covalent functionalization of the materials with bactericidal molecules (e.g., AMPs).

Although drug-releasing approaches are commonly applied and have proven their efficacy in many reports, the second approach (i.e. immobilization of the antibacterial molecule) warrants further research because the release of antibacterial agents entails several risks in terms of (off target) toxicity, rapid decreasing concentration due to release and loss of activity over time; these latter effects necessitate the use of very high doses, increasing toxicity and increasing probability of bacterial resistance.[18]

In any case, even when a surface is chemically unfavorable, ions and macromolecules such as proteins and polysaccharides secreted by bacteria or from the local environment can form a “conditioning film” on the surface. This acts to mask antibacterial functional groups so that adhesion and bacterial proliferation can proceed, rendering the covalently functionalized material inefficient.[38-40]

1.2.2. New paradigm: Mechano-bactericidal mechanism

In the past decade, a new strategy has emerged to deal with bacterial contamination. Bacterial functions have proven to be greatly influenced when contact is made with other nanoscale materials in their environment.[41-43] Thus, the use of nanostructure geometry to deliver lethal mechanical forces, causing bacterial cell death, is starting to be explored. Due to this mechanism of action, this strategy may be promising since there is no need for dose control or replacement as there is no metabolic consumption. Its action, merely by direct contact with bacteria, could potentially overcome the problems

found in chemical-based methods, such as resistance, and offer new and alternative solutions to biomaterial infections.[38]

These mechano-bactericidal nanostructures can be prepared as dispersed nanoparticles suspended in media, referred to as colloids, or fabricated as surface nanotopography (Figure 1.3):

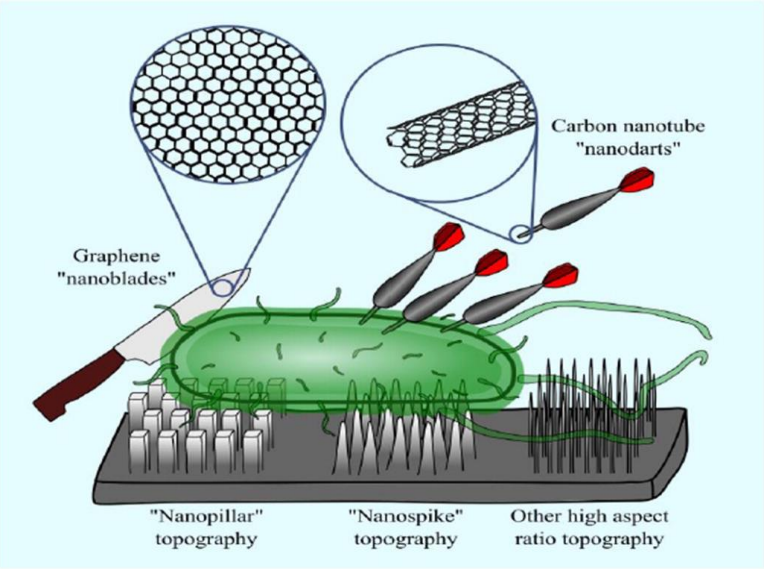

Figure 1.3: Scheme of different mechano-bactericidal nanostructures. Mechano-bactericidal nanostructures can be designed to act as suspended colloidal systems, as is the case for carbon nanotubes and graphene nanosheets, or patterned as surface nanotopography, such as nanopillars and nanospikes. Reproduced from.[38]

➢ Colloids: Carbon nanotubes and graphene family nanomaterials

The first evidence of these mechano-bactericidal nanostructures is attributed to single wall carbon nanotubes (SWCNTs). In direct contact with *E. coli*, they were able to puncture and pierce the cell membrane, causing irreversible damage, as a consequence of the sharp geometry of the SWCNTs, hinting at the potential of SWCNTs as antibacterial materials.[44] Further investigations in both Gram-positive (*B. subtilis* and *S. aureus*) and Gram-negative *(E. coli* and *P. aeruginosa*) bacteria led to the conclusion that the high aspect ratio geometry of the SWCNTs were primarily responsible for the bactericidal effect, behaving like *nanodarts* while other possible cell death factors, like oxidative stress and toxic impurities resulted to be minimal.[38, 45, 46] Aside from SWCNTs, strong antibacterial activity of graphene nanomaterials has been discovered.[47-50] Satisfactorily tested in both Gram-positive and Gram-negative, with high levels of bacterial inactivation, these results reveal that the sharp sheets of the graphene walls, in direct contact with the bacterial cells, were responsible for the membrane damage and consequent efflux of cytoplasmatic material[48, 49] due to a so-called mechano-

bactericidal effect: an atom-thin layer of graphene acts as a *nanoblade* to cut the cell membrane.[51]

In another study, simulations made with graphene oxide (GO) nanosheets revealed that in suspension, very small GO nanosheets were only able to cause very little membrane perturbation and tended to accumulate on the outside of the cell while large GO nanosheets were able to pierce through the membrane.[52] This result was confirmed by TEM analysis, where bacterial cells exposed to GO nanosheets in suspension had the cell membrane totally broken and had lost some intracellular medium, leading to the conclusion that irreversible damage to the membrane by graphene nanomaterials had occurred via some physical means.[51, 53]

Despite all these evidences, the bactericidal activity of SWCNTs and GO nanosheets is not unanimously accepted as an exclusively mechanically-dependent killing mechanism, and more complex pathways have been proposed. Through modeling and experimentation, it was discovered that nanomaterials can interact with the bacterial cell membrane by adsorbing onto the membrane, passing through it, extracting its lipids, inducing pore formation, altering osmotic pressure and culminating in cell inactivation.[38, 54-59] Other commonly reported antibacterial mechanisms are related to oxidative stress initiated by ROS or by charge transfer.[59-61]

- **Surface nanotopography**

Although sharp colloid nanostructures were investigated long before, the existence of nanotopography with bactericidal properties was not known until recently. [18, 34, 38, 62, 63] Natural bactericidal surfaces are widespread in nature in different shapes (e.g. nano-spikes, cones, wires, pillars or spinules), ranging from insect wings[64-71] to gecko skin[72-75] and moth eyes[76-79] (Figure 1.4A). These bactericidal surfaces typically consist of high aspect ratio nanopillars of diameter between 50–250 nm, with different heights and densities, capable to induce self-driven membrane rupture of the bacterial cells during cell-surface adhesion.[34, 63, 80]

One of the pioneering investigations in this area concerned the cicada wings with *P. aeruginosa*.[64] It was revealed that, despite the superhydrophobic nature of the cicada wing, there was significant bacterial adhesion on the nanostructured surface. On contact, the adhered bacteria went through a rapid morphological change and were killed within few minutes as estimated through imaging techniques (Figure 1.4A1).[63, 64] It was concluded that the anti-bacterial nature of cicada wings was not due to its ability to repel the bacteria, rather to its ability of kill them upon contact.[63, 64] For further insight, the wing was also made hydrophilic with a 10 nm gold coating while its surface topography was retained, and it was found that its bactericidal activity was preserved, confirming that cell lysis is largely unaffected by surface chemistry, free energy, or

hydrophobicity, meaning that the mechanism is physical in nature.[62, 64, 71, 81] In light of this result, a physical-mechanical mechanism was proposed, whereby the high-aspect-ratio nano-pillars ruptured and consequently killed the bacterial cells upon surface adhesion (Figure 1.4C1-4).[82]

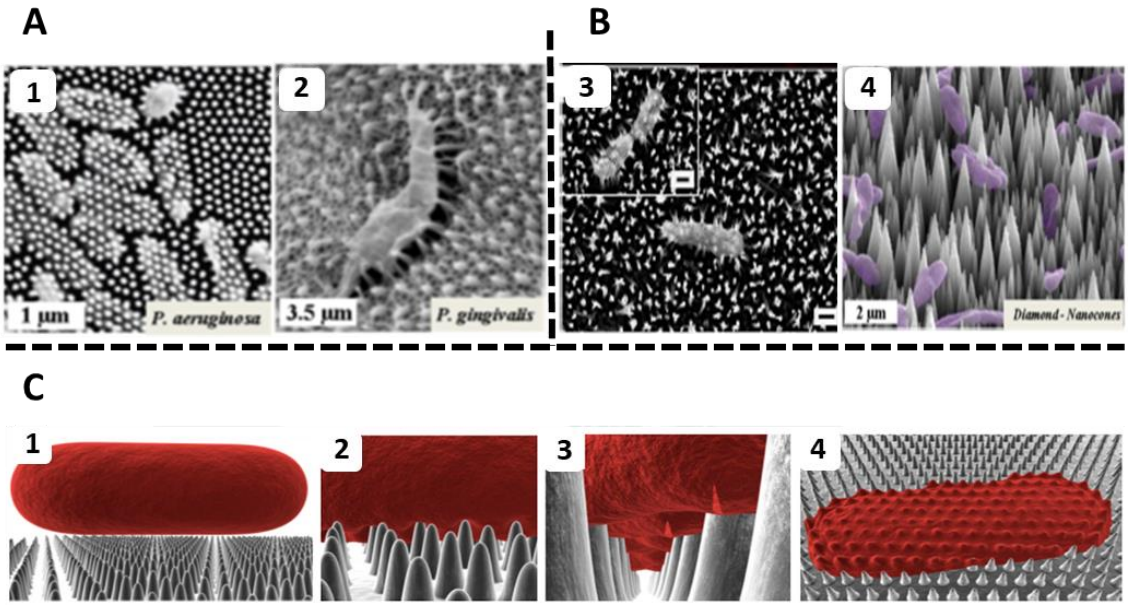

Figure 1.4: Natural and biomimetic bactericidal surfaces. A) SEM images of natural bactericidal surfaces of (1) cicada wings (*Psaltoda claripennis*) and (2) Gecko Skin (*Lucasium steindachneri*), which reveal the mechanical disruption of the *P. aeruginosa* and *P. gingivalis*, respectively. B) SEM images of biomimetic bactericidal surfaces (3) black silicon nanowired (bSI) and (4) diamond nano-cone surface, both in contact with *P. aeruginosa* cells. C) Schematic representation of bacterial attachment onto the cicada wing nano-pillars showing (1) cellular approach, (2) initial adhesion buckling the cell membrane, (3) the apparent rupture of the cell wall in the region suspended between the nano-pillars, and (4) cell collapse (death) onto the nano-pillars. Figure A1 adapted from[64], Figure A2 adapted from[72], Figure B3 adapted from[81], Figure B4 adapted from[83] and Figures C1-C4 adapted from[82]

Natural bactericidal surfaces have provided scientists with the template for the next-generation of artificial bactericidal substrates, through silicon[81, 84-86], diamond coated silicon[83, 87, 88], titanium and its alloy[89-95], a range of biopolymers[73, 96-98], graphene[59] and more recently carbon nanotubes[99] (Figures 1.4B3 and 1.4B4). To carry out all these investigations, a large number of nano/microtechniques have been used, including reactive-ion beam etching[81, 83], plasma etching[87], laser ablation[81], microwave plasma chemical vapor deposition[83], nano-imprint lithography[97] and bench-top nano-templating[73], among others.[73, 89, 97, 100]

The first successful attempt to artificially produce nature-inspired bactericidal structures was through silicon substrates, which were altered to incorporate high-aspect-ratio nanopillars that mimicked those found on the wings of one species of dragonfly.[81] Among the silicon substrates, black silicon (bSi) is a synthetic nanomaterial obtained by reactive-ion etching to possess high aspect-ratio nanopillars. Despite bSi was developed for photovoltaic and sensing application[101-104], its application also

includes the biomedical field.[105-108] The resulting substrate (Figure 1.4B3) differed in nano-architecture from that of the dragonfly wings, in that the nano-protrusions were sharper and more discretely arranged, displaying a lower degree of clustering.[34, 81] The bSi surface was found to be highly bactericidal against both Gram-negative and Gram-positive bacteria and, notably, the bSi substrate often displayed higher degrees of bactericidal efficacy than their biological blueprints (cicada and dragonfly wings), establishing the realistic opportunity to develop effective, optimized, next-generation antimicrobial nano-materials[34, 81] (e.g. implant material[81, 85, 87, 109], water treatment devices[110], medical sutures[111], and surgical instruments.[90, 112, 113]

1.2.3. Forces involved in the rupture of the bacterial cell wall

Clear advantages of mechano-bactericidal strategies compared to traditionally chemical ones have been discussed above. However, the real effect of mechanical action on the antibacterial activity is under debate in the literature.[51, 60, 62, 69, 99, 114-118] In addition, there is still a lack of quantitative information on the mechanisms involved in the physical damage of the bacterial cell wall, although some insight has been gained with atomic force microscopy (AFM) experiments as well as modelling.[46, 64, 70, 82, 119, 120]

Previous work using AFM nanoindentation with sharp cantilevers on a live Gram-negative bacterium *Salmonella typhimurium* determined that forces of about 1-2 nN were necessary to rupture its cell wall (Figure 1.5AB).[119] This study also suggested that bacteria were still viable after multiple puncturing, which was interpreted as a rapid reorganization of the phospholipids in the cell membrane, resealing the cytoplasm after AFM tip penetration (Figure 1.5C).

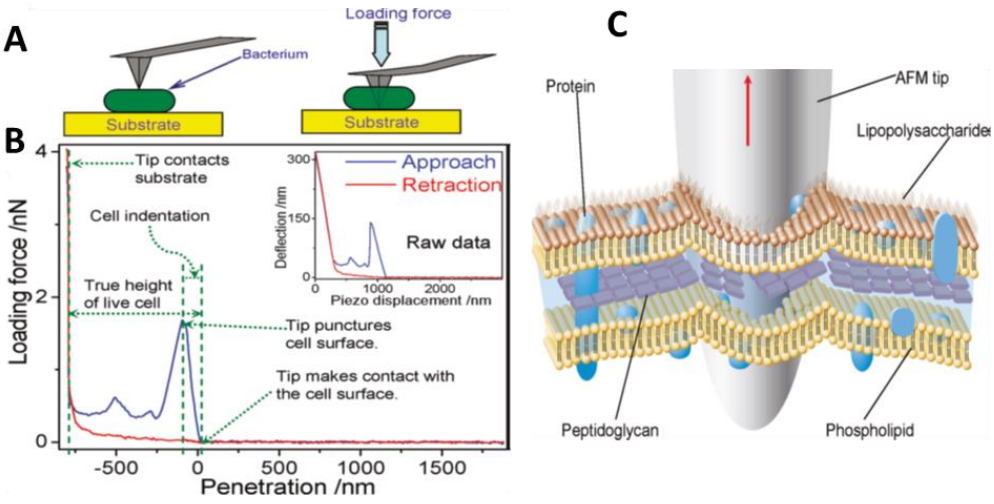

Figure 1.5: Schematics of AFM indentation on bacteria. A) An AFM tip was brought into contact with the surface of a live bacterium immobilized on a silicon substrate. B) A typical puncturing curve obtained with a biolever tip. Puncturing curves reveal a variety of information, including the true height of a live bacterium, its initial elasticity under physiological conditions, the pressure required to puncture the cell wall and the cell indentation before the cell wall was punctured. C) Illustrative schematics of an AFM tip body as it is pulled out interacting with a punctured three-layer cell wall. Adapted from.[119]

In another study, ultrasharp AFM tips were used to simulate the interaction between SWCNTs and bacteria.[46] It was found that forces above 10 nN were necessary to exert permanent damage on *E. coli* and *B. subtilis* cell walls, although the measurements were performed on air-dried bacteria, which may not be representative of physiological conditions (Figure 1.6). This value was used to conclude that a single collision between a SWCNT in solution and a bacterium was not able to produce enough force to cause mechanical damage on the bacterium surface.[46] Instead, antibacterial activity would require the cumulative effect of a large number of individually dispersed nanodart-membrane interactions over time[121]. On the other hand, other processes such as filtration through membranes containing SWCNTs would produce forces higher than 10 nN that could result in physical damage.[46, 122]

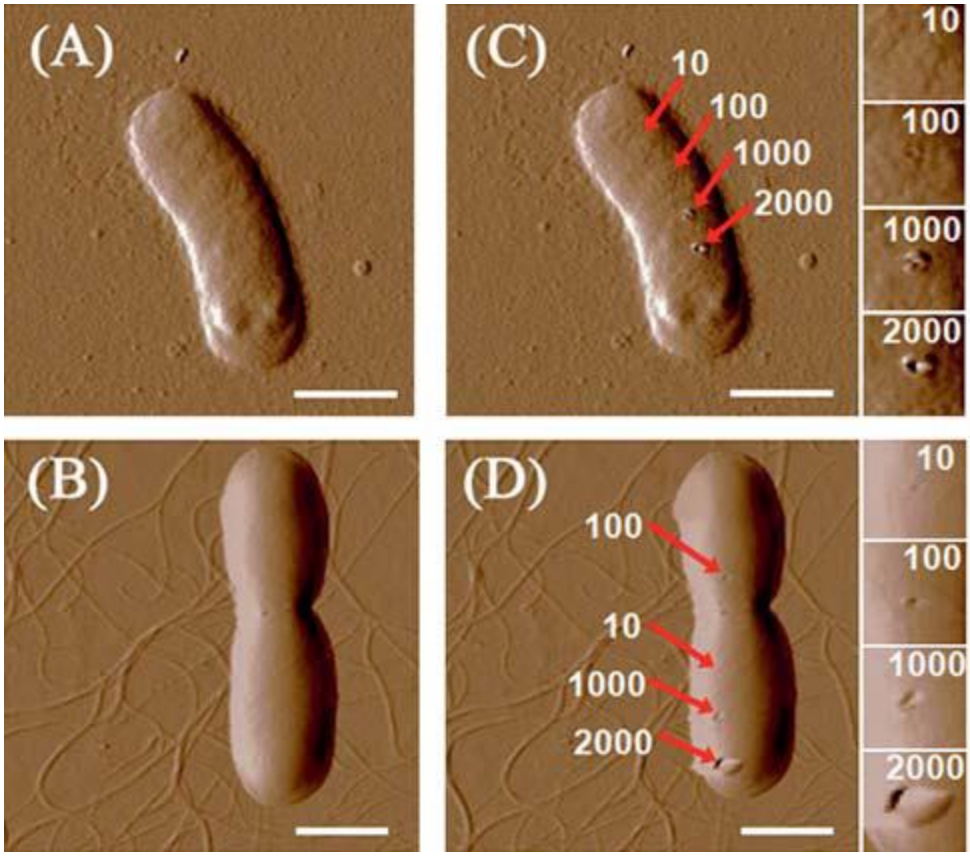

Figure 1.6: Bacterial damage caused by AFM indentation. AFM amplitude images of (A) *E. coli* and (B) *B. subtilis*. (C) and (D) are, respectively, *E. coli* and B. subtilis after piercing by a 2 nm AFM tip for 200 times at different locations. Small images on the extreme right are enlarged images of areas punctured by the tip. The deflection set points of the AFM tip are 10, 100, 1000, and 2000 nN. All scale bars are 1 μm. Adapted from.[46]

1.3 Microscopy techniques

1.3.1. Atomic Force Microscopy

Atomic Force Microscopy (AFM) is a powerful imaging technique to obtain nanometer-resolved topographic images. However, its potential is not limited to that, but it is an appreciated tool to study the properties of materials, such as friction[123], electrical forces[124], adhesion[125], magnetic forces[126], conductivity[127], or mechanical properties[128], for example. AFM can also be used to manipulate or dissect biological structures such us cells[129], nanoindent virus[130] or bacteria[131] and to study protein folding and unfolding mechanisms[132] or molecular recognition events.[133] Therefore, this technique has played a big role in materials science, biology and solid-state physics over plenty of years. Its origin arises in 1986[134] and it was developed from Scanning Tunneling Microscopy (STM). STM was invented in 1982 by Binning and co-workers[135] to investigate surfaces of conductive materials, leading them to get the Nobel Prize in Physics in 1986.

The primary element in the AFM is a tip located at the end of a cantilever. When the tip comes into contact with the surface of the sample, it scans the sample line by line and from this tip-movement a topographic image from the sample is built up. The ability to extract a topographic image from the sample is based on the attractive and repulsive forces between the tip and the sample. These forces cause the deflection of the cantilever, which depending on the attractive or repulsive nature of the force, will be deflected towards or away from the surface. At this point, it is necessary to use a device capable of converting that cantilever deflection into a topographic image. The standard AFM method is based on the optical lever principle[136], where a laser beam is focused on the cantilever and its reflection is collected on a detector (photodiode). When scanning the sample, the cantilever deflects, meaning that any small change in the bending of the cantilever is converted to a measurable deflection in the position of the reflected spot in the photodiode (Figure 1.7). The majority of AFM has a four-quadrant photodiode, allowing the position of the reflected spot to be calculated in two directions: vertical deflection (normal) and lateral twisting (torsion). A piezoelectric scanner is used to control the movement of the tip over the sample, adjusting its movement in Z to the topography of the sample through a feedback loop from the photodiode signal.

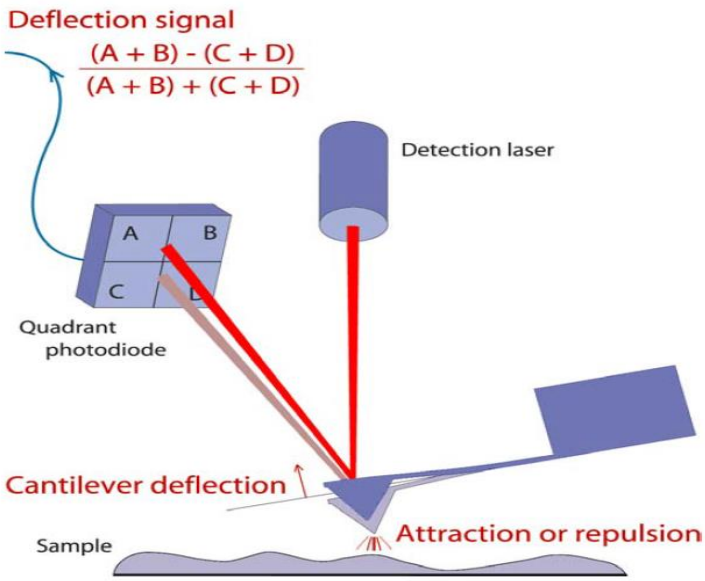

Figure 1.7: Main components of AFM basic principle. Reproduced from[137]

Different imaging modes are available for the AFM, which differ in the movement of the tip when scanning the sample and the controlled variable used by the feedback loop. The choice of one method or another depends fundamentally on the nature of the sample, as well as the measurement conditions (air or liquid), or the type of measured properties, among other factors. Most common operating modes are briefly summarized hereafter:

- **Contact Mode**

It is considered the simplest and pioneering method of AFM.[134] In contact mode (CM), or also called static mode, the tip always remains in contact with the sample during scanning, so it has been considered one of the modes that provides the best resolution (Figure 1.8A). It is also a very useful mode when it comes to measuring lateral forces (e.g. friction[123]), since being permanently in contact is able to detect areas with the same height but have other properties. In contact mode, the controlled parameter is the cantilever deflection, so a good control of the force applied is achieved.

However, due to the permanent tip-sample contact, the latter is subject to possible damage or irreversible deformation, which restricts its use for biological samples.

- **Dynamic Mode**

The dynamic mode tries to solve those limitations present in the contact mode. In this mode, the tip performs continuous cycles of oscillation near or at its resonant frequency[138], so the tip is not in contact with the sample most of the time (Figure 1.8B). One of the most typical mode is Amplitude Modulation (AM), which operates at the

resonant frequency of the cantilever, and where the amplitude of the oscillation is the parameter used to control the tip-sample distance, providing the topographic image.

This means that the damage caused to the sample and the lateral forces experienced are much smaller, making this mode very suitable for biological or delicate samples. Due to that, the resolution obtained in the images is lower than the one obtained in the contact mode. Nevertheless, several challenges can be found when operating in dynamic mode, like the difficulty to control the force applied, especially in liquid, where the frequency peaks have a lower quality factor or dragging effects.

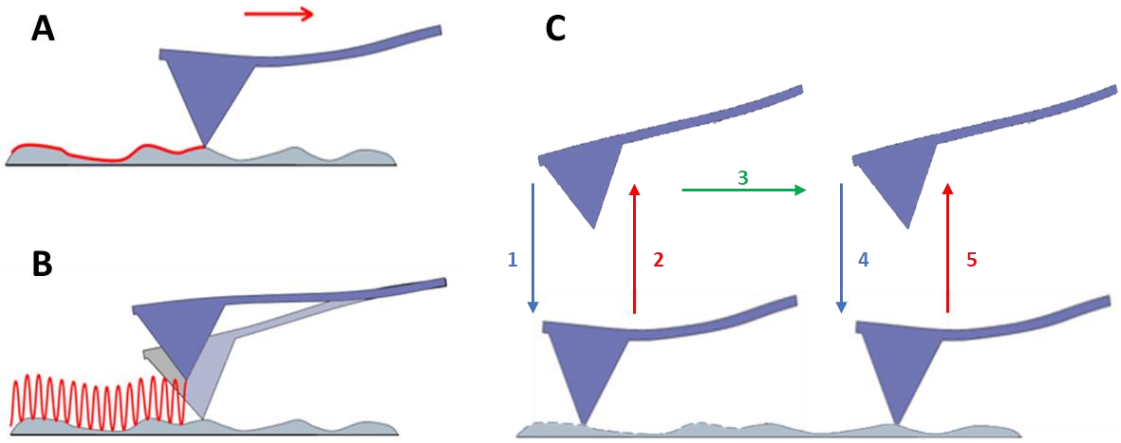

Figure 1.8: Imaging modes of AFM. A) Contact Mode, B) Dynamic Mode and C) Jumping Mode. Adapted from[137]

➢ Jumping Mode (Force mapping)

At present, there are other methods that come to improve the previous ones, trying to minimize the inconveniences that both modes can present, Jumping Mode (JM)[139] performs successive force - distance curves at each scan point of the sample while the lateral movement is done away from the sample, resulting in a lateral force of zero (Figure 1.8C). JM is a very used mode, since it allows controlling the force applied at each point, avoiding lateral displacements of the sample and with a good resolution (however, the acquisition data speed depends on the AFM electronics). This makes JM a very convenient way to measure samples in liquid where adhesion is delicate and small forces are required.

1.3.2. Overcoming AFM limitations: Combining with optical microscopy

As discussed above, AFM is highly suitable for imaging biological samples, as it can be operated in buffered solution and at controlled temperature, thereby providing high-resolution imaging of structural surface features and analyzing forces in the pico- and nano-Newton regime even on individual cells, bacteria, virus particles, etc. However, this technique also has some limitations: AFM cannot be used to image intracellular features because it is only used to investigate the sample surface, and usually with no chemical or functional information.

To overcome these limitations, AFM can be combined with optical techniques, for example Raman or Infrared spectroscopy.[140-142] But most often, it is combined with fluorescence microscopy, which is based on the detection of fluorescent molecules (fluorophores) attached to a molecule or structure of interest within the sample, acting as a reporter that provides contrast in the image. Fluorophores absorb light energy and, as a consequence, emit light with lower energy (longer wavelength). Thus, in a standard fluorescence microscope, a light beam (e.g. a laser) is used to excite the fluorophores and the objective lens focuses the emitted fluorescence from the sample to a detector (e.g. a camera) (Figure 1.9). Indeed, fluorescence microscopy is the method of choice in the biological sciences due to its ability to use specific molecular labels and access deep into a sample, allowing imaging of different cellular, subcellular or molecular components, and in real time.[143-147]

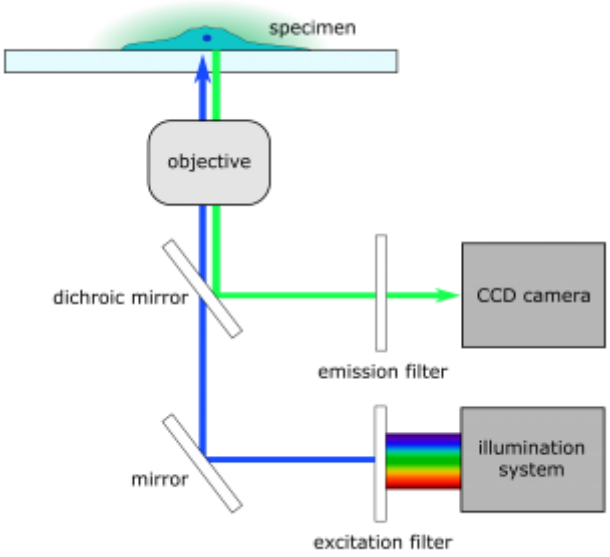

Figure 1.9: Inverted microscope basic scheme.

Combining AFM and fluorescence microscopy, two techniques with complementary strengths and weaknesses, yields a powerful tool for the investigation of biological samples. Thus correlative AFM and fluorescence microscopy enables us to gain complementary information of the same sample area, since each technique provides information about a specific aspect of the sample (e.g. specific localization of a fluorescent molecule of interest in the topography map). This strategy has been used for example to detect individual exocytic events correlated to structural changes in epithelial cells.[148] AFM topography imaging detected the disappearance over time of surface protrusions after exocytosis stimulation, which could be confirmed by monitoring fluorescently-labeled lamellar bodies.

This correlative technique was also applied in cell viability experiments, for example, to visualize the drug-induced effects on single tumor cells[149], monitor the antimicrobial peptide effects on bacteria with live/dead fluorescent indicators.[150] or assessment of bacterial resistance to organic solvents.[151] In all cases, bacterial structural changes exposed to bactericidal compounds were imaged by AFM and correlated with fluorescent labeling. Fluorescence here plays a crucial role to discriminate those live cells which are not influenced by the antibacterial agent (green) to those who are dead (red). Measuring topographical changes or mechanical properties over live/dead cells by AFM and correlate with bacteria fluorescence state over time can provide a better understanding of how cells response upon bactericidal effects.

Since AFM is also exploited for nanomanipulation applications, it is also possible to inject fluorescent particles in single cells by AFM and monitoring them by fluorescence microscopy.[152] Fluorescent particles were attached to the AFM tip and injected to the cell by AFM indentation. Thus, AFM tip penetrated the cell wall, and irradiated before retracting, leaving the nanoparticles inside the cell as could be visualized by fluorescence. Since the AFM potential is limited to topographical changes on the surface, this experiment is useful to highlight the importance of fluorescent labeling to observe internal physiological processes or targets that could not be monitored directly by AFM.

Our laboratory has developed advanced versions of correlative AFM and fluorescence microscopy in the last years, with applications from materials science to biology.[153-158] Most recently, this technique was used to reveal topography-dependent binding of a photoactive drug to model amyloid fibers, highlighting the influence of amyloid polymorphism on potentially different therapeutic outcomes.[158]

As a next major step, the aim is to fully exploit the combination of these techniques by operating them simultaneously rather than sequentially. Numerous biological processes occur rapidly, and high temporal resolution is required to monitor surface changes of the sample and correlate them to specific events by fluorescence. Despite the fact that it is a complex challenge and most of the experiments in the literature are

carried out sequentially and not simultaneously, a good example of this simultaneous technique is the study of selective virus disassembly by AFM nanoindentation with fluorescent indicators.[159] Here, virus capsid disruption by AFM tip indentation can be observed by fluorescence, tracking the genome release in the presence of YOYO-1 dye, which binds to DNA and becomes fluorescent. Firstly, AFM nanoindentation was used to simulate slow genome unpacking by applying consecutive forces below the capsid rupture (e.g. mimicking the uncoating process of human adenovirus with fatigue experiments). Fluorescence tracking over time allowed to observe the sequential steps until capsid disruption, where a slight rise in fluorescence signal was observed when the viral particle lost its first capsomer vertex, and a clear fluorescence enhancement when the capsid was totally disrupted, indicating that DNA genome was fully accessible to YOYO-1. Later, they simulated a fast disruption of the virus capsid, by applying a single puncture with a force above the rupture point. In this experiment, no fluorescence enhancement was observed until the puncture was applied, where clear peaks observed in the force-time curve matched with the onset of the fluorescence enhancement, providing a method to investigate real time changes in genome organization with more detail.

Thus, since the AFM potential is limited to topographical changes on the surface, correlative AFM and fluorescence microscopy could highlight internal physiological processes or targets that could not be monitored directly by AFM. When AFM and fluorescence techniques are operated simultaneously, a more comprehensive understanding of the system and its dynamics can be achieved.

1.4 Thesis motivation

Despite the interest and potential advantages of mechano-bactericidal strategies, there are still many open questions about the real effect of mechanical force on bacterial death. While some initial studies have proposed different mechanisms of cell rupture, a more systematic and quantitative approach is needed to start to comprehend mechanically-induced bacterial death. This insight will have an impact on the design of improved antibacterial surfaces with high-aspect ratio topography. Therefore, this thesis focuses on the characterization of the mechanical interaction between nano-objects and the bacterial cell wall. To that end, an experimental strategy using simultaneous AFM-fluorescence in a systematic and quantitative way is used, which may help to provide a deeper insight into the range of forces that are relevant to "mechano-bactericidal" mechanisms of action, contributing in the development of new materials and more efficient antibacterial surfaces.

The combination of these two techniques, which are based on very different principles, is not trivial. For this reason, this thesis has an important component of technical development and optimization of sample preparation and nanoindentation-imaging protocols. It is necessary to find a compromise between the requirements and the limitations of each technique. These technical challenges have been overcome in this thesis, which allows to study bacterial cell behavior in real time with fluorescence microscopy upon AFM nanoindentation. The quantitative results presented here reveal the magnitude of the forces that significantly affect bacterial viability, as well as the physiological response to different ranges of force.

1.5 Objectives

The aim of the thesis is the application of combined AFM and fluorescence microscopy to study mechanical effects on *E. coli* physiology and viability, in the context of a better quantitative understanding of bacteria-nanomaterials interactions. The objectives of this thesis are:

1) The development of advanced protocols for simultaneous correlative AFM nanoindentation and fluorescence microscopy of immobilized *E. coli* cells.

2) The systematic quantification of the forces necessary to produce bacterial cell wall rupture in immobilized *E. coli*.

3) To obtain relations between force applied and bacterial cell wall response beyond rupture.

4) To obtain relations between force applied and bacterial physiological state, before and beyond rupture, including the study of fatigue effects.

5) To explore complementary methods for fluorescence monitoring of bacterial physiology and viability.

Chapter 2

Materials and general methods

2. Materials and general methods

2.1 Correlative AFM and fluorescence microscopy system

The setup is an adaptation of a commercially available platform that integrates an AFM (Nanowizard II, JPK Instruments) and an inverted optical microscope (Nikon Eclipse Ti).[158] This set up is placed on an active vibration isolation optical table (Thorlabs) (with no acoustic enclosure). It has been adapted for simultaneous AFM-fluorescence measurements by adding an electron-multiplying charge-coupled device (EMCCD) camera (iXon Ultra 897, Andor Technology) (Figure 2.1).

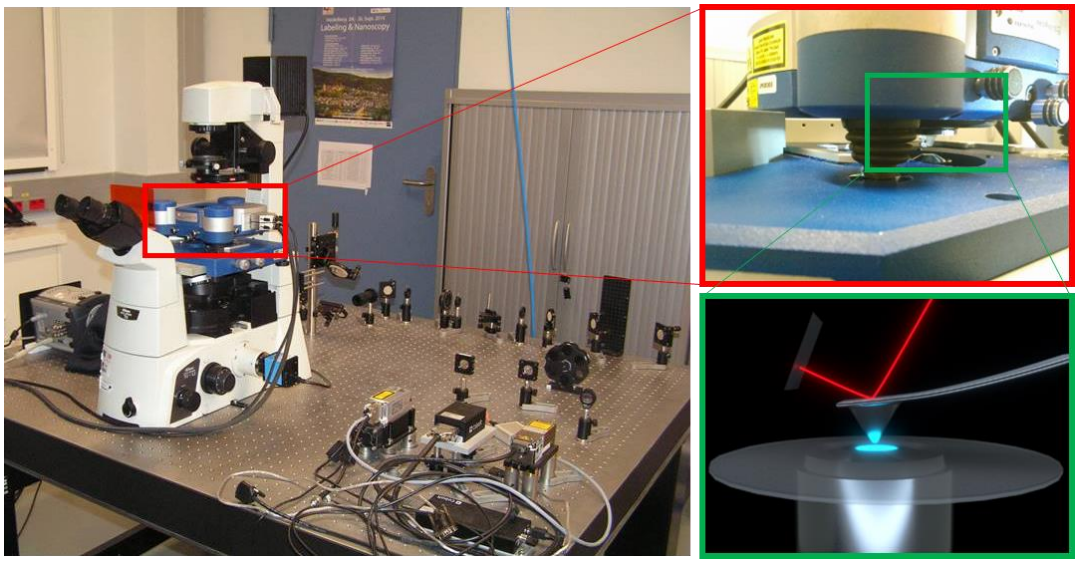

Figure 2.1: Correlative AFM-Fluorescence setup. Adapted from[156]

For fluorescence imaging, different lasers were used as excitation source depending on the sample: Luxx Omicron (488 nm, nominal 100 mW) and Cobolt Samba (532 nm, nominal 100 mW). Wide-field illumination was achieved by focusing the expanded and collimated laser beam onto the back focal plane of the objective (Total Internal Reflection Fluorescence (TIRF), 60x, 1.49 NA, oil immersion, Nikon). Emission light was selected through a dichroic mirror depending on the laser used (z488rd or ZT532rdc, Chroma Technology, respectively) and additional spectral filters (HQ500 LP and HQ525/50, Chroma Technology, or 641/75 Brightline, Semrock, respectively). The use of additional lenses resulted in a final magnification of 148x, equivalent to a pixel size of about 108 nm.

For AFM imaging, the suitable imaging mode was determined depending on the purpose of the experiments (see Chapters 3-5), and the type of sample (adherence or composition). In Chapter 3, in which a methodology was developed for AFM and fluorescence simultaneous correlative measurements, polymer beads were used due to their bright fluorescence and ease of handling. In that case, the measurements were performed in dynamic mode and in air, since the sample has better adhesion to the

surface and the cantilever tuning is simpler. For Chapter 4-5, the methodology developed in Chapter 3 was optimized and applied to achieve reproducible and optimal measurement conditions with live bacteria, which present challenges such as low adhesion to the surface. Thus, Force Mapping mode[160] (a JPK tool with the same working principle as jumping mode, with slower data acquisition electronics) was used for imaging bacteria for being the less invasive imaging mode and having the better control of forces applied on adhered bacteria. Experiments were carried out in liquid because, to address biological questions, measurements near to physiological environment provide more relevant conclusions since drying of biological samples could modify their structure.[161]

Different types of AFM tips were selected to carry out the experiments presented in this thesis, depending on the conditions of measurement, sample and purpose of the experiment: HQ:NSC35/CR-AU BS (MikroMasch, 8 nm nominal radius, 5.4 – 16 N/m, 150 – 300 kHz) and HQ:NSC36/CR-AU BS (MikroMasch, 8 nm nominal radius, 0.6 – 2 N/m, 65 – 130 kHz). For each type of experiment, a compromise had to be found between the low stiffness necessary for topography imaging and the relatively high values of force that needed to be exerted on the sample for indentation beyond rupture. This compromise is particularly critical for soft samples like bacteria.

2.2 Sample preparation

0.1 μm and 0.5 μm Ø polymer beads (ThermoFisher, TetraSpeck™ fluorescent microspheres sampler kit) were used for the set-up and calibration process developed in Chapter 3. *E. coli* DH10β strain was used as a model to study the bacteria response to mechanical forces exerted by AFM, discussed in Chapters 4 and 5.

E. coli DH10β were growth aerobically until early exponential phase was reached (i.e optical density (OD) ~ 0.3 – 0.5). Absorption spectra were recorded on a Cary 50 UV-vis spectrophotometer in a 1 cm pathlength quartz cuvette at various moments of bacterial growth. Growth conditions, like incubation time and temperature or specific treatments made, are specified in Chapter 4 and 5.

For improving bacterial adhesion, functionalization of the surface (glass) with Poly-L-lysine (PLL) or Corning Cell-Tak™ (CT), an acidic solution of polyphenolic proteins purified from marine mussels. was performed for successfully immobilize bacteria. The optimal amount of adhesive needed was determined experimentally in Chapter 4.

For fluorescence imaging, Propidium Iodide (PI, ThermoFisher, 3.34 mg/mL in water) was used as a cell death marker. PI is a red-fluorescent cell viability dye which is excluded from live cells with intact membranes, but penetrates dead or damaged cells. For experiments related to the physiological state of bacteria (see Chapter 5), a plasmid with

GFP-MinD[162] was incorporated into *E. coli*, allowing to monitor the oscillations of the Min system as a reporter for the physiological state of bacteria through fluorescence microscopy.

2.3 Mechanical characterization by AFM: Nanoindentation

AFM is best known for its ability to obtain high resolution topographic images, but it is also a powerful tool for force experiments. For this purpose, valuable information can be extracted from the measurement of changes based on the separation of the tip-sample at the same point, instead of scanning the lateral position of the tip. This is called Force Spectroscopy. In this mode, the cantilever moves always in vertical direction towards the surface using the piezo and then retracts. Vertical displacement of the cantilever and its deflection are recorded simultaneously. Data collected from this experiment is displayed as force-distance curves (Figure 2.2), where the important events are plotted as A-F:

The cantilever is retracted and far from the surface (A). The cantilever starts approaching the surface until point B, called "jump to contact", where the attractive forces make the tip snap to the surface. From then, the cantilever starts pushing into the surface and deflecting itself until the programmed deflection value (or force) specified by software (i.e. setpoint value) is achieved (C). In this region, mechanical properties of the sample, like stiffness or Young´s Modulus, can be investigated. Once the set point is reached, the cantilever starts to retract from the surface (D), until it snaps off from the surface (E) where the adhesion force can be measured. Finally, the cantilever returns to its initial starting position (F).

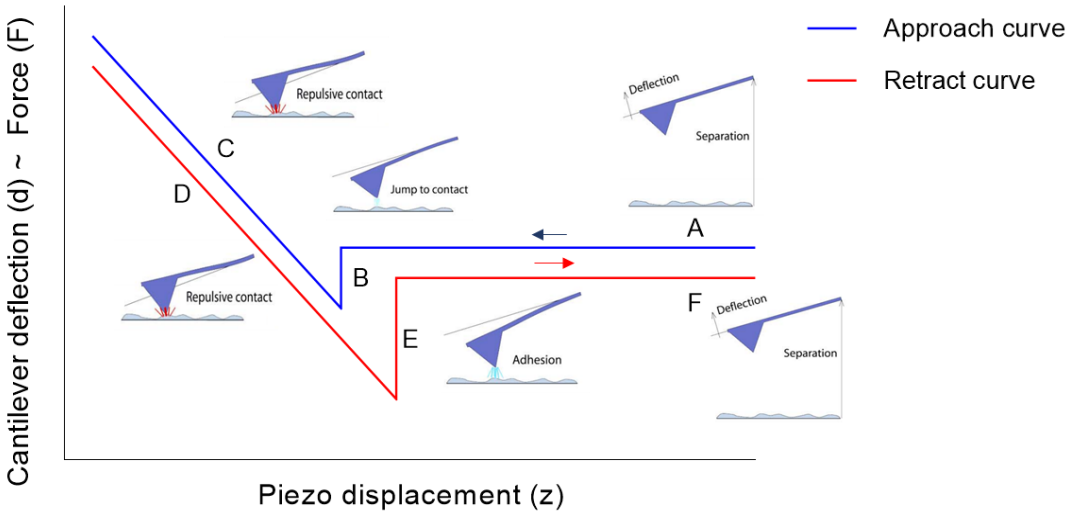

Figure 2.2: Schematic diagram of the vertical tip movement during the approach and retract parts of a force spectroscopy experiment. Adapted from[137]

The region "C" is where indentation takes place. Assuming that the cantilever is harder than the sample, when a force is applied on it, the sample experiences a

mechanical deformation depending on the force applied, geometry of the tip or loading rate, among others.[131, 163-170] The tip acts as an indenter, while the cantilever behaves like a Hookean spring (k_c). Because the AFM is able to measure cantilever deflection with high precision, the applied force can be easily computed as:

$$F(nN) = k_C\left(\frac{nN}{nm}\right) \cdot Sensitivity\left(\frac{nm}{V}\right) \cdot Deflection(V) \qquad \text{Equation 2.1}$$

The sensitivity parameter corresponds to the elastic response of the cantilever when a force is applied in a hard and non-deformable substrate. Since all the deflection corresponds to the deformation of the cantilever and no indentation is present, this value allows converting the voltage detected by the photodiode to force units (nN).

Once this conversion is integrated in the AFM software, Equation 2.1 adapts the form:

$$F = k_C \cdot \Delta d = k_C \cdot (d - d_o) \qquad \text{Equation 2.2}$$

Where the deflection (d) is now in length units (nm). The indentation depth (δ) is calculated by subtracting the cantilever deflection Δd from the piezo translation Δz (Figure 2.3):

$$\delta = \Delta z - \Delta d = (z - z_0) - (d - d_0) \qquad \text{Equation 2.3}$$

where z_0 is the translation of the piezo at the contact point.

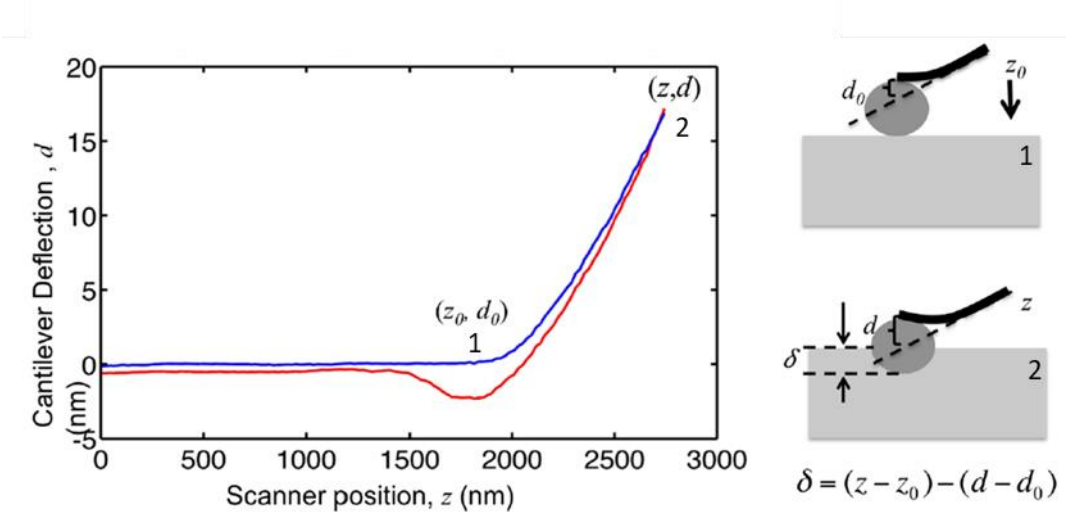

Figure 2.3: Typical AFM force-distance curve collected when a sample is indented. Adapted from[171]. Right panels show the tip position on points 1 (above) and 2 (below), where data is computed to obtain the indentation (δ) by subtracting the cantilever deflection (d) to the piezo displacement (z) based on initial (z_o,d_o) and final tip position (z,d).

2.4 Data analysis

AFM imaging processing was performed using Gwyddion software (v2.48).[172] Basic treatment functions were applied to every image data: Plane subtraction, flattern base and rows alignment.

AFM force-distance curves were processing using JPK Data Processing[173] and AtomicJ software[174] (version 2.1.2) to convert the raw data, i.e. cantilever deflection vs. z piezo position, into force-indentation (F-δ) and force-time (F-t) curves. Appendix A, analysis data section, gathers the software used for the processing and analysis of nanoindentation curves obtained in this thesis.

Fluorescence data were acquired and processed with Andor Solis[175] software. The software's region of interest (ROI) tool was used to analyse any change in fluorescence signal while AFM measurements were being performing. ImageJ[176] software was used when required for a more advanced representation of fluorescent data (kymograph builder plugin[177]). Kymographs are space-time plots which display intensity values along a predefined path over time[178]. This tool was used in Chapter 5 to graph the physiological state of bacteria in a more visual and perceptible way.

Chapter 3

Methodology development for simultaneous AFM nanoindentation and fluorescence imaging

3. Methodology development for simultaneous AFM nanoindentation and fluorescence imaging

3.1 Introduction

Recent advances in imaging tools have greatly improved the ability to monitor and analyze biological processes at the micro and nanoscale. By applying several microscopy techniques to the same sample, scientists can obtain complementary morphological, structural and chemical information that exceeds what is possible with any single technique, particularly suited to address insights questions of the modern biological sciences[179].

However, combining techniques is not a trivial process. Some problems, such as those arising from different requirements for sample preparation or imaging conditions, can make this task challenging.[155] If the correlative procedure is sequential, some of these problems can be mitigated by individually optimizing each step in the correlative workflow as required by the technique to be used. For example, in sequential correlative AFM and fluorescence microscopy, the sample can be reconditioned to facilitate measurements in each of the techniques used (i.e. AFM imaging in dry conditions but fluorescence imaging in liquid conditions.[155] By contrast, for correlative simultaneous measurements, the optimization of the system has to be carried out globally, and it is where incompatibilities and greater challenges are found (e.g. same environment, dry or liquid conditions, for both microscopy imaging techniques).

The purpose of this chapter is to develop a methodology to successfully combine AFM nanoindentation and fluorescence microscopy simultaneously, enabling its application to the study of bacterial cell behaviour when subjected to mechanical stress on its cell wall. This chapter will focus on the identification of common problems that may arise when carrying out simultaneous correlative measurements. For this, micron-sized fluorescent polymer beads will be used, which are easier to image by AFM compared to bacteria and can be measured in dry conditions.

3.2 Simultaneous AFM nanoindentation and fluorescence imaging of fluorescent polymer beads: Basic methodology development

A test sample for these experiments was prepared by mixing 1 uL of 0.5 Ø μm fluorescent polymer beads (Tetraspeck ™) suspension of with 99 uL of MiliQ water and depositing over a cover glass (Ø 25 mm, #2 thickness) and allow to dry completely at room temperature. While thinner glass slides are more suitable and typically recommended for fluorescence microscopy, thicker slides were used in these experiments to reduce vibrations during AFM experiments. Figure 3.1A shows a fluorescence image of the sample acquired with 532 nm laser excitation, showing the beads as bright spots in an area of 56 x 56 μm^2. Then, the AFM cantilever is moved laterally (x-y axis) to the top left vertex of the (fluorescence) area and a scan of 50 x 50 μm^2 is performed in dynamic mode at 128 x 128 pixels (Figure 3.1B) so that it fits with the optical image outline (red dashed square). If further magnification is required (32 x 32 μm^2, 128 x 128 pixels, blue dashed square), it can be done by scanning a smaller area with the AFM (or by digitally zooming into the acquired image) (Figure 3.1C).

It can be verified that the fluorescent polymer beads have been deposited and fixed to the substrate successfully, because no drag is observed in the AFM images. In the 50 x 50 μm^2 image (Figure 3.1B) we can distinguish the outline of each bead, despite the low resolution, and by increasing the image magnification (Figure 3.1C and 3.1E), the rounded shape of the beads becomes more apparent.

We can also see in the AFM images that the beads appear as comet tails. This is a very common artifact (usually called “flying tip”) indicating that the AFM is not properly tracking the surface.[180] The “tail” of the object appears to the right, since the image was recorded scanning from left to right. This artefact can be corrected with a better optimization of the feedback parameters (see below), increasing setpoint or decreasing scan speed, while trying not to impact sample detachment.

Once the alignment and correlation of the optical and topographic images have been performed, the indentation of one bead is carried out. For this, it is necessary to first perform an additional zoom of the selected bead (6 x 6 μm^2, 128 x 128 pixels), to facilitate the correct indentation in the center of the bead. Adjusting feedback parameters and scan speed fixed the flying tip artifact, improving the quality of the image (Figure 3.1D) A topography profile shows a height of about 480 nm (Figure 3.1E), similar to the nominal specifications provided by the manufacturer.

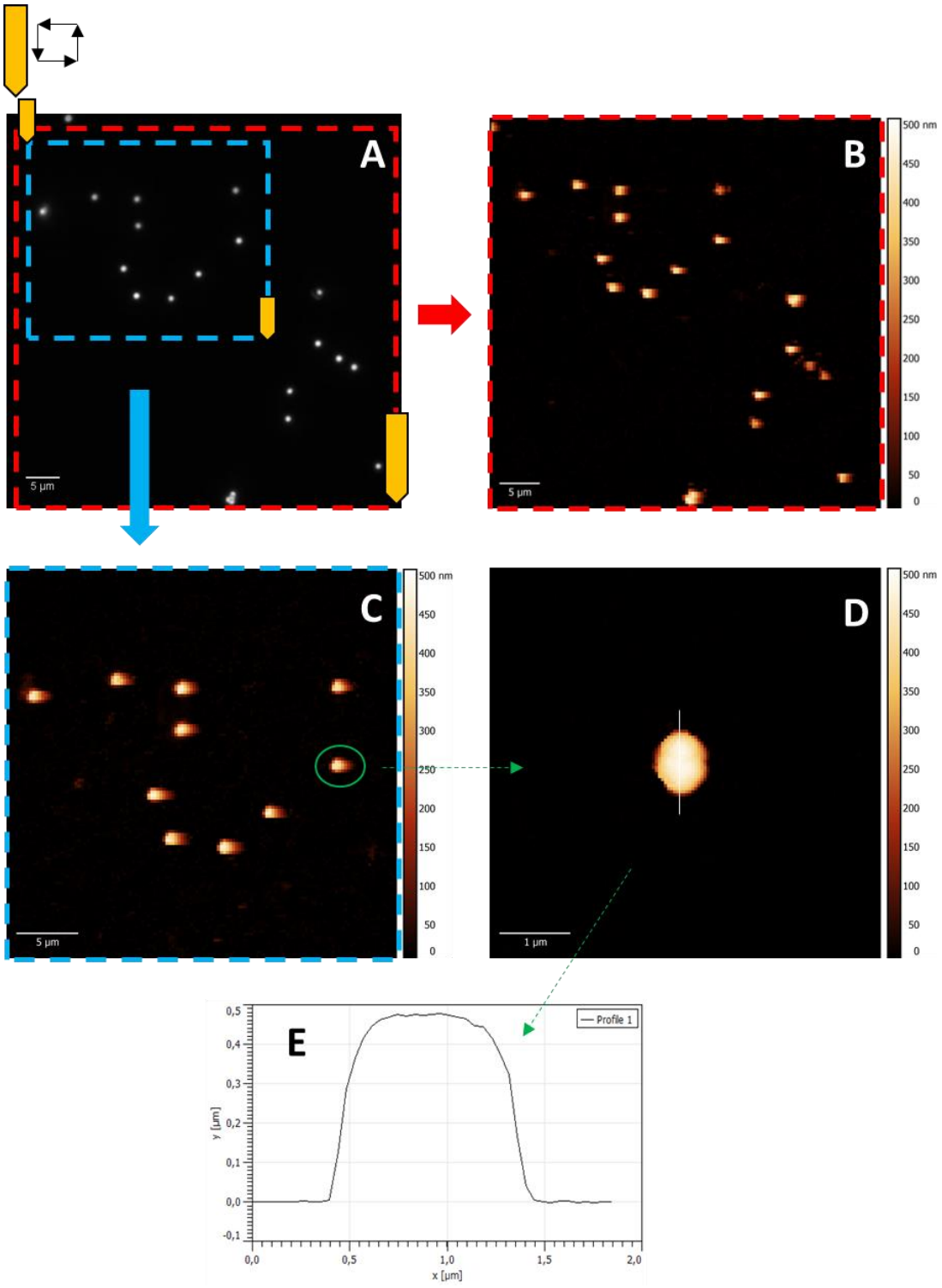

Figure 3.1: Correlative AFM and fluorescence imaging of fluorescent polymer beads.
A) Fluorescence image of the deposited fluorescent polymer beads on glass. Red dashed square represents the 50x50 µm^2 area imaged by AFM. Blue dashed square represents a 32 x 32 µm^2 AFM image zoom of a specific area of the optical microscope. B) AFM image of the red dashed area. C) AFM image zoom corresponding to the blue dashed area. D) Individual zoom of one polymer bead (marked in green). E) Corresponding AFM profile of the polymer bead in D.

The nanoindentation was performed at 2 μm/s, with a vertical deflection setpoint value of 15 nm, maintained during 2 s (Figure 3.2A). The tip position during nanoindentation is indicated with the I-IV indexes. At the beginning of the experiment, the tip rests on the polymer bead (I). Then, the tip retracts 1 μm from the polymer bead (II) and then it approaches the bead surface (III), producing a clear peak in the fluorescence signal (t = 2.5 s). This fluorescence peak is produced by the cantilever movement, without touching the bead, strongly suggesting that it is an artefact arising from reflections, as will be discussed later. Once the contact between tip-bead has been made, the cantilever begins to deflect until the force setpoint value is reached, and remains close to this position for 1 s (IV) before the applied force ceases and it retracts again 1 μm (II). The experiment ends when the cantilever returns to its initial state, so the cantilever approaches the bead again (III) and rests on it (I), producing another clear peak in the fluorescence signal (t = 5.5) during the movement of the cantilever.

This fluorescence artifact due to the cantilever movement was corroborated by varying the residence time of the tip at position IV from 1 to 5 s. The fluorescence peaks appeared in all cases with a time delay that matched the expected residence time, confirming that the peaks are generated when the cantilever is not touching the sample (i.e. approaching and retracting from the sample).

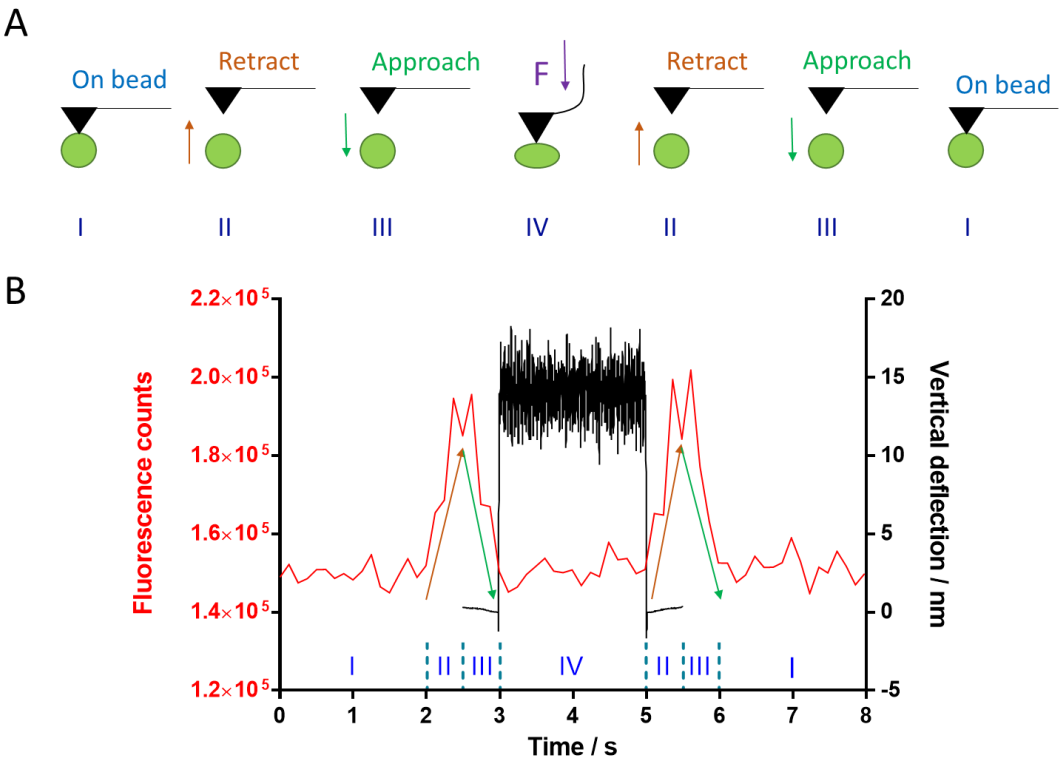

Figure 3.2: Simultaneous nanoindentation and fluorescence imaging on a fluorescent polymer bead. (A) Scheme of the tip position (I – IV) over time during polymer bead indentation. (B) Simultaneous measured force-time curve (black) and fluorescence intensity (red).

While it was possible to implement simultaneous AFM nanoindentation and fluorescence imaging in these preliminary experiments, several limitations were found, mainly related to reflections and interactions between the cantilever, polymer beads and laser.

We found reflections due to the tip movement during scanning (x-y axis motion) and indentation (z axis motion, Figure 3.2B) of the polymer beads.[181] This was probably due to the high fluorescence intensity emitted by polymer beads and the laser reflection on the cantilever.[182] This occurs when the cantilever moves over and on the sample, producing periodical increases and decreases of the fluorescence signal, like is shown in Figure 3.2A for indentation, and becomes more appreciable when scanning a higher bead population or very bright beads (Supporting Movie S3.1, Supporting Movie S3.2 and Supporting Movie S3.3).

To try to alleviate reflections, TIRF microscopy configuration was also tested. A slight reduction of reflections was achieved, although not completely mitigated.

While some studies have pointed to quenching effects between silicon tips and organic fluorophores (e.g. Atto and Alexa fluorophores),[183, 184] quenching is probably not significant in our case since the AFM tip radius is around 8 nm and polymer beads are around 500 nm

Another drawback is that related to the adhesion to the tip of those polymer beads (or fluorophore residues) that could be poorly fixed to the surface. This is a typical problem when imaging fluorescent samples, in which contamination results in a fluorescent tip (Supporting Movie S3.1 – white spot movement). The consequence of this is a decrease in fluorescence image quality and interference with nanoindentation results, because not only the tip surface would have changed but also an external fluorescent signal is being introduced.

We have seen that several challenges appear when simultaneous AFM and fluorescence microscopy is attempted. The high brightness of the polymer beads, together with the interactions of the tip-laser system, produce a series of reflections during the movement of the cantilever. This however is not a major concern for the experiments reported below with bacteria, as the fluorescence signal of interest is delayed or decoupled from indentation.

Supporting Movies

Movie S3.1: 0.5 Ø μm fluorescent polymer beads showing emission fluctuations during AFM scanning with a fluorescent contaminated tip. The white spot moving along the sample corresponds to the fluorescent tip. The fluctuations are caused by the cantilever movement during the scan.

Movie S3.2: 0.1 Ø μm fluorescent polymer beads showing emission fluctuations during AFM scanning. Reflection effects could be easily appreciated when the sample scanned is more populated.

Movie S3.3: 0.5 Ø μm fluorescent polymer beads showing emission fluctuations during AFM tip movement on z axis on the center of the fluorescence area recorded. It can be observed the different degrees of fluctuations according to the size, brightness and position of the fluorescent polymer beads.

Chapter 4

Simultaneous AFM nanoindentation and fluorescence imaging to assess cell wall integrity in live bacteria

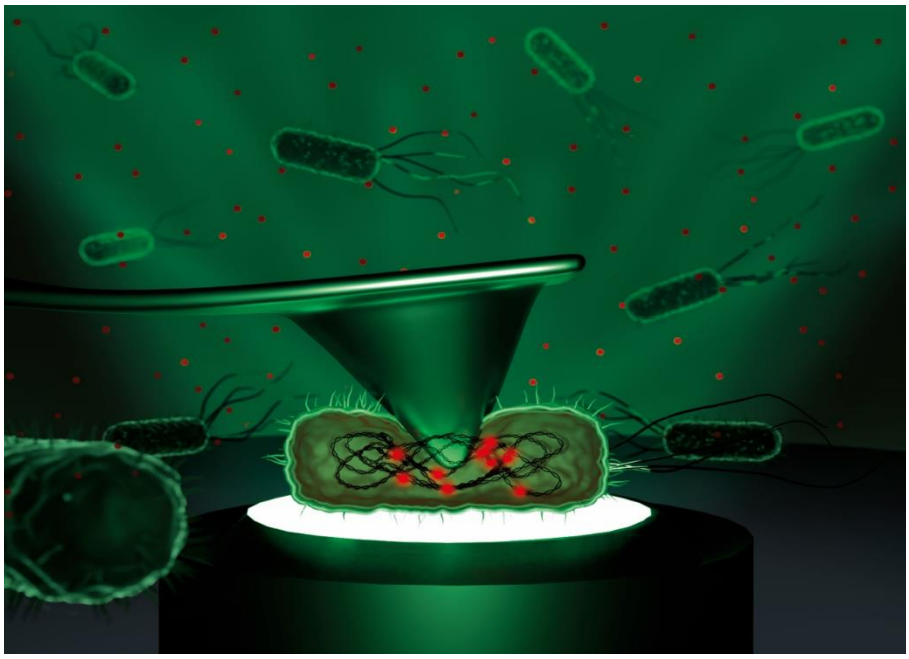

4. Simultaneous AFM nanoindentation and fluorescence imaging to assess cell wall integrity in live bacteria.

Adapted from:

del Valle, A; Torra, J; Bondia, P; Tone, C; Pedraz, P; Vadillo-Rodriguez, V; Flors, C. Mechanically-Induced Bacterial Death Imaged in Real-Time: A Simultaneous Nanoindentation and Fluorescence Microscopy Study, *ACS Applied Materials & Interfaces*, **2020** https://doi.org/10.1021/acsami.0c08184

4.1 Introduction

Once a reliable strategy for simultaneous AFM nanoindentation and fluorescence imaging was developed, the next step was to apply it to image mechanically-induced bacterial damage in real time. These experiments are relevant to provide quantitative information on the mechanisms involved in the physical damage of the bacterial cell wall in the context of mechano-bactericidal strategies, as discussed above.

While previous experiments with atomic force microscopy (AFM) as well as modeling have provided some insight into this matter,[46, 64, 70, 82, 119, 120] they were not performed in physiological conditions or were not systematic. In this context, we set out to design an experimental strategy that enabled higher throughput measurements in order to capture the potential variability within a larger bacterial population, and in living cells. To that end, we performed simultaneous AFM nanoindentation and fluorescence imaging of single *E. coli* cells to quantify in a systematic way the forces necessary to rupture their cell wall. We study the puncture of the cell wall of an immobilized bacterium with a sharp AFM tip while monitoring in real time the fluorescence signal form propidium iodide (PI), a cell membrane integrity marker (Figure 4.1).

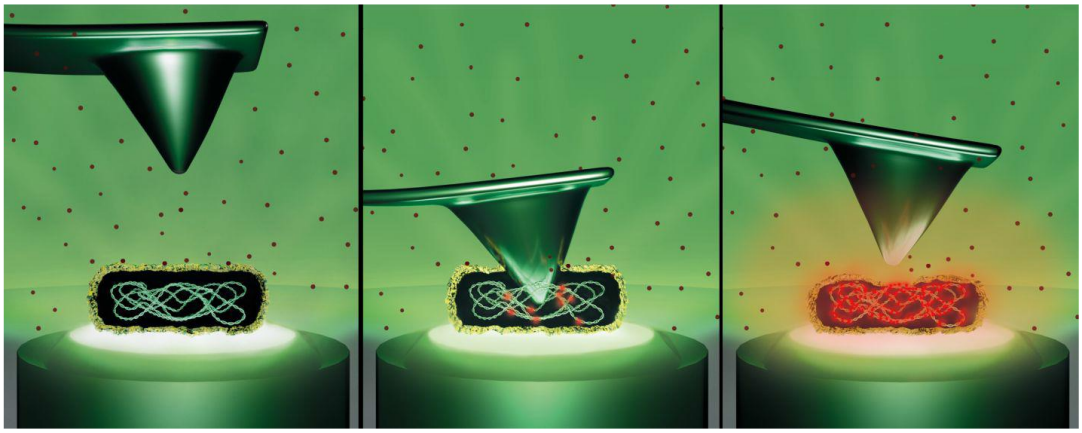

Figure 4.1: Experimental strategy for simultaneous AFM nanoindentation and fluorescence imaging of immobilized *E. coli* cells. Red dots represent PI molecules that are non-fluorescent in solution and light up upon DNA intercalation after cell wall damage.

4.2 Materials and methods

Single colonies of *E. coli* DH10β were grown overnight at 37 °C in 10 mL Luria Bertani (LB) medium (Fisher BioReagents, casein peptone 10 g/L, yeast extract 5 g/L, sodium chloride 10 g/L). 100 µl of the overnight culture was diluted into 10 mL of fresh medium and grown for 2 h at 37 °C - 200 r.p.m, until early growth phase (optical density at 600 nm ~ 0.3) was reached.

Cells were harvested by centrifugation (3000·g, 3 min), washed 2 times with phosphate buffered saline, pH 7.4, 0.01 M, (PBS, Sigma-Aldrich) and further diluted in order to immobilize isolated bacteria on the coverslip. Cells were immobilized by adding a 50 µL aliquot of the bacterial suspension in PBS on the optimal amount of PLL or Cell-Tak™ coated coverslips (see section 4.2.1) and incubated for 20 min at room temperature. After that, non-adhering bacteria were removed by rinsing the coverslip vigorously with PBS. Bacteria were imaged in 100 µL PBS (supplemented with 1 µM PI).

4.2.1. Determining the optimal conditions for imaging living bacteria in real-time

Imaging live bacteria in an aqueous environment is one of the most challenging applications for AFM.[185] The search for optimal conditions was carried out according to the following parameters: viability (lower toxicity effect from adhesive), immobilization[186] (enough fixation to avoid bacteria dragging during AFM scan) and breakage (tip hard enough to be able to break bacteria membrane during nanoindentation).

A greater amount of adhesive will give a better immobilization of the bacteria, but it could alter the physiological properties of the bacteria due to electrostatic stress (e.g. PLL), compromising its viability.[187] On the other hand, a soft cantilever is best suited to avoid damaging or dragging bacteria during the scan, but if it is not stiff enough it will not be able to break and penetrate the bacteria (main objective of this thesis).

Therefore, based on these premises, an iterative search for optimal conditions was carried out, following the procedure below (Figure 4.2). As said above, the adhesives chosen for cell immobilization in this thesis were PLL and Cell-Tak™.

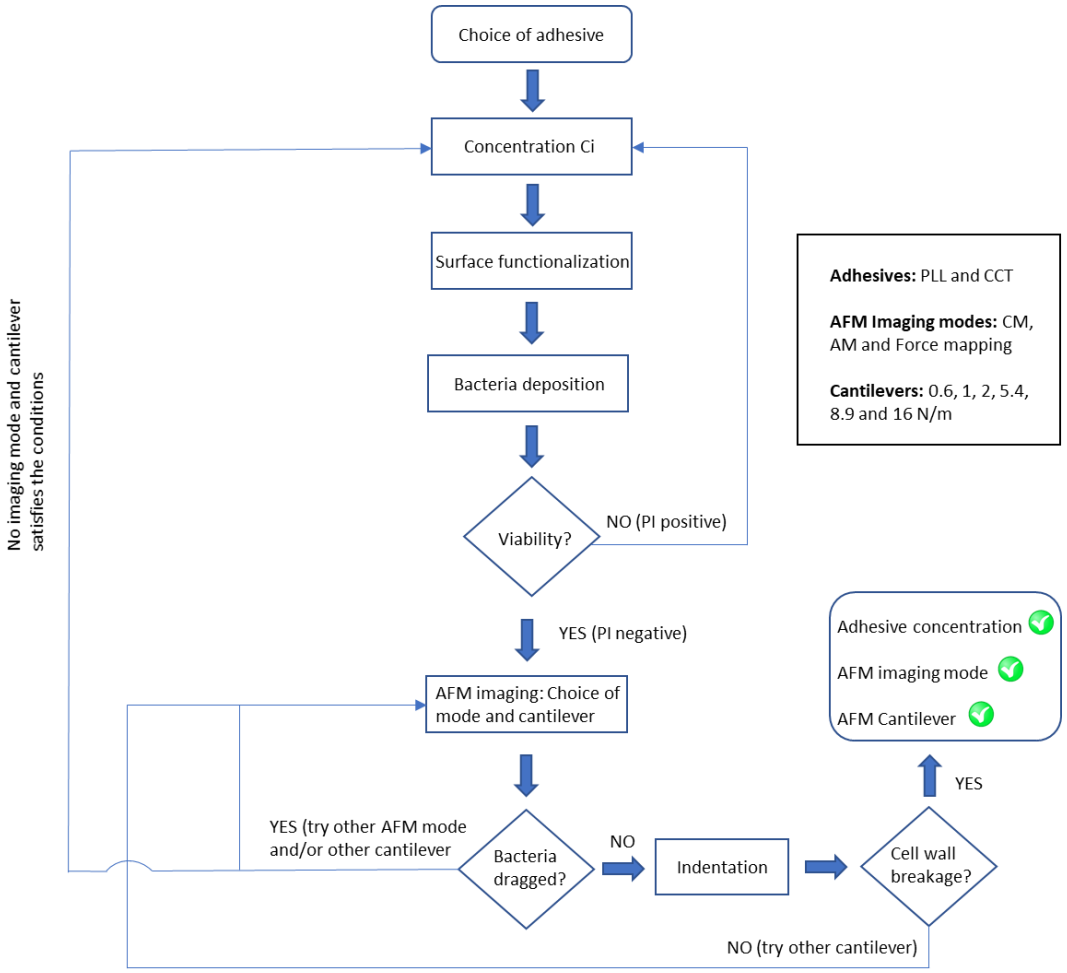

Figure 4.2: Procedure used to search for optimal conditions for immobilization and rupture of the bacterial cell wall.

The amount of adhesive was set to be the minimum as possible, so as not to compromise viability or alter the mechanical properties of bacteria (PI negative for most bacteria – Figure 4.3B). With this restriction, the most suitable AFM scanning mode has turned out to be force mapping (better control of forces) with the 0.6 N/m cantilevers, since they have been proven to be soft enough to image bacteria without dragging them and stiff enough to penetrate the bacterial membrane during indentation (inset Figure 4.3B and Figure 4.3C and Figure 4.3D, respectively). Effective adhesive concentrations and immobilization procedures were:

- PLL solution, 0.1 % (w/v) in H_2O (P8920, Sigma Aldrich) was diluted 1:91 in PBS and 100 µL of this solution was deposited on a coverslip and allowed to dry at room temperature overnight. The coverslip was then submerged in MilliQ water 3-5 times and air dried before cell immobilization.

- Alternatively, 5.7 µL of Cell-Tak™, a strongly adhesive polyphenolic protein extract from *Mytilus edulis*, (1.83 mg/L in 5 % acetic acid) was mixed with 94.3 µL $NaHCO_3$ buffer, pH 7. This solution was deposited on a coverslip and

allowed the protein to settle on the glass for 1.5 h. The coverslip was then submerged in MilliQ water 3-5 times and air dried before cell immobilization.

For the experiments in these optimal conditions, the cantilever spring constant was calibrated before the experiment by thermal noise method (in liquid).[188] The position of the bacteria was first determined optically (brightfield) and then imaged (5 x 5 μm^2) using the force mapping mode, where an array of 32 x 32 force-distance curves are collected over the entire field of view with low applied force (< 500 pN). After individual bacteria were force-mapped, indentation experiments were performed. To investigate quantitatively the nanomechanical properties, a single force-indentation curve was recorded at the center top of each bacterium. Typical force-indentation curves were carried out at typical loading rates of 0.5-2 µm/s and maximal forces of 30-60 nN. After indentation experiments, bacteria were typically imaged again to observe possible changes in morphology caused by the AFM tip during indentation.

For fluorescence imaging, samples were excited by laser irradiation (532 nm, 13 W/cm^2, Cobolt Samba). The emission was collected in the camera according to the laser path and filters chosen described in Chapter 2. Typical fluorescence data consisted on movies of up to 500 frames and 100 ms exposure time per frame.

The experiments carried out in this thesis have been synchronized by clicking on both AFM and fluorescence controls simultaneously, with an error of around 0.5 s between both signals.

4.3 Results

4.3.1. Quantification of forces to rupture the bacterial cell wall

Typical simultaneous AFM nanoindentacion and fluorescence experiments are displayed in Figure 4.3. Figures 4.3A and 4.3B show brightfield and fluorescence images, respectively, of bacteria before AFM nanoindentation, where it can be seen that most bacteria are viable (non-fluorescent) and survive immobilization conditions. Selected viable bacteria were then imaged with AFM at low resolution (inset Figure 4.3B), and subsequently nanoindented in their center (Supporting Movie S4.1 and Supporting Movie S4.2).

Figures 4.3C and 4.3D show the force-distance and force-indentation curves, respectively, corresponding to the left bacterium (“1”). The first peak in the force-indentation curve, which corresponds to the first rupture event upon approach,[130] shows that it occurred at a force of 22 nN, at an indentation depth of about 400 nm, which is about 50 % of the cell diameter. The following features in the curve likely arise from the AFM tip experiencing further resistance as it penetrates into the bacterium, which has gel-like characteristics. Indeed, it has been previously shown that the appearance of several peaks in the force-distance approach curves is characteristic of

low aspect ratio tips, which experience higher resistance to penetration compared to sharp tips.[119] After indentation, brightfield (Figure 4.3E) and fluorescence images (Figure 4.3F) of the same area show that PI fluorescence is only observed for the indented bacterium. This observation confirms that the integrity of the membrane is compromised due to mechanical rupture after it has been indented at a high loading force (bacterium "1"), but not if only low loading forces (of about 500 pN) applied during force mapping. The same procedure was then performed on the bacterium on the right ("2"), with a similar result (Supporting Movie S4.2).

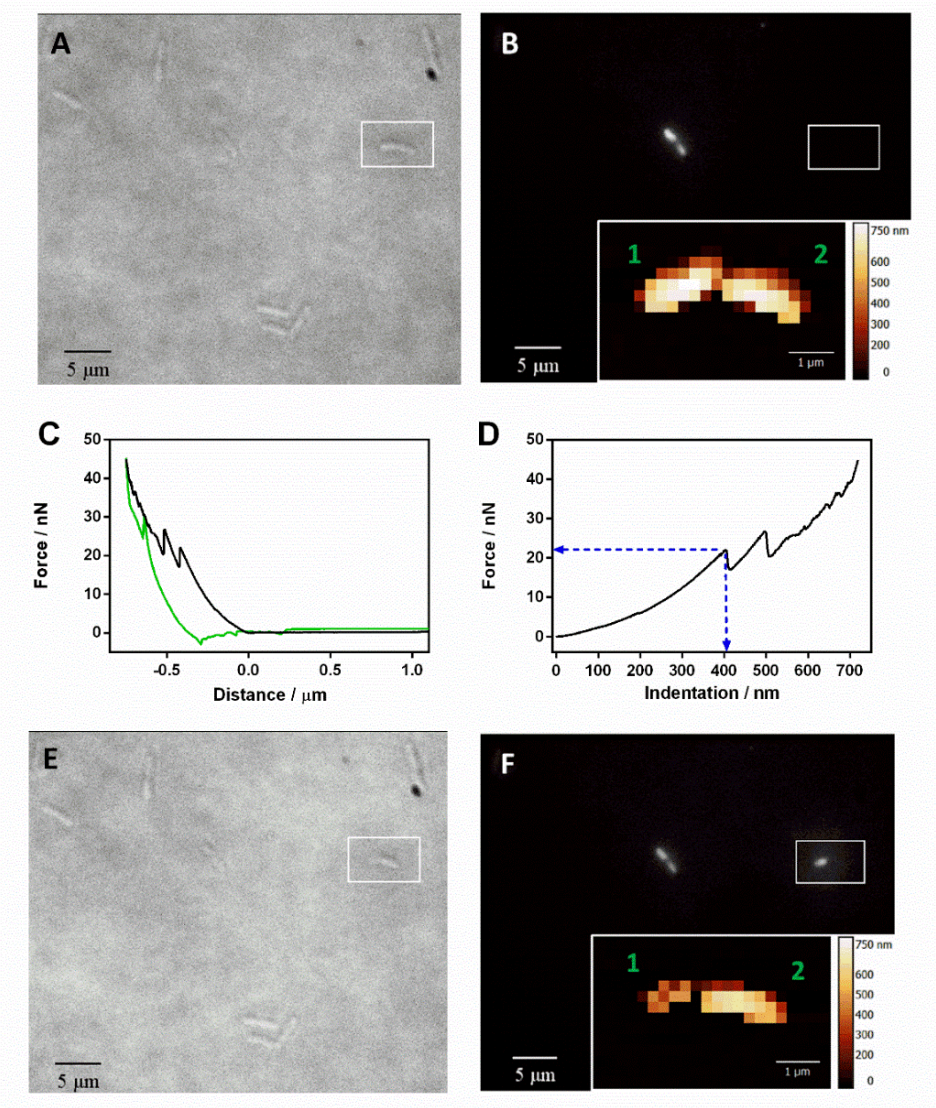

Figure 4.3: Correlative AFM and fluorescence imaging of *E. coli* cells with indentation beyond cell wall rupture. (A) Brightfield and (B) PI fluorescence images of bacteria immobilized on PLL-coated glass confirming that most bacteria do not show PI fluorescence before indentation with the AFM tip. Inset in panel B shows a low resolution AFM topography image of two viable bacteria that are visible in brightfield but are not stained with PI (white rectangle). (C) Force-distance curve (black is approach, green is retract). Peaks in the approach curve reflect resistance to tip penetration, while those in the retract curve likely correspond to random interactions with bacterial components or debris; (D) Force-indentation curve showing a cell wall rupture event (blue arrows). (E) Brightfield and (F) fluorescence images after indentation of bacterium "1", showing PI staining. The AFM topography image confirms that structural damage was inflicted only on the indented bacterium.

Force-indentation curves for 24 *E. coli* cells immobilized on PLL were measured and the values of rupture force and indentation depth are collected in the histograms in Figures 4.4A and 4.4C, respectively. The values for the rupture force (20.3 ± 4.9 nN) (mean ± standard deviation) are consistent with previous AFM work on Gram-negative bacteria that showed that no puncture occurred at forces below 10 nN,[46, 131] but larger than previously reported in the literature for other direct[119] and indirect measurements.[62, 189, 190] In our experimental conditions, we only observed a single rupture event below 10 nN (Figure 4.4A). Values of indentation depth at rupture show a broad distribution (373 ± 157 nm, Figure 4.4C), presumably due to bacterial size variability.

At this point, it is important to recall that the cell wall of Gram-negative and Gram-positive bacteria behaves as a viscoelastic solid material.[164] An important property of this type of materials is that their mechanical properties depend on the rate at which they are deformed. Their stiffness, for example, increases with the loading rate. Thus, for a truly quantitative comparison, nanoindentation experiments on bacteria should to be done under exactly the same experimental conditions, and slight differences may lead to marked discrepancies. Appendix A provides a mechanical estimation of Young´s Modulus and bacterial spring constant (i.e. elasticity and stiffness) before bacteria cell wall rupture, to give a more complete vision of the bacteria cell mechanics.

We further note that higher concentrations of PLL on the surface resulted in even higher rupture forces. This observation might be related to the decrease in fluidity of model membranes induced by PLL,[191] and more generally, consistent with the fact that antibiotic compounds affect the mechanical properties of bacteria.[192, 193] On the other hand, similar values of rupture force (24.9 ± 4.1 nN) and rupture indentation (340 ± 100 nm) as those shown in Figure 4.4A and 4.4C were obtained on 21 *E. coli* cells immobilized on Cell-Tak™, which has been suggested as gentle strategy for bacterial immobilization for AFM experiments.[186]

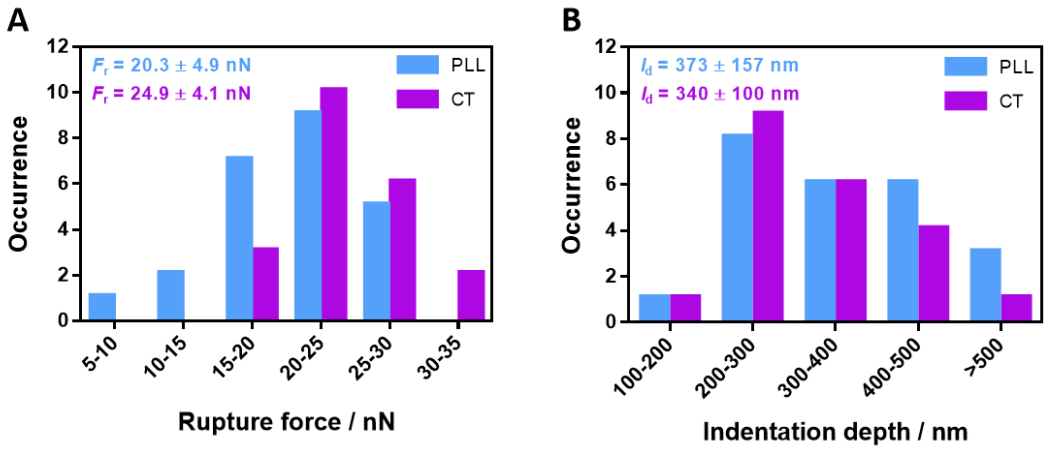

Figure 4.4: Rupture force and indentation depth histograms. Rupture force (A) and indentation depth (B) at for 24 and 21 *E. coli* cells immobilized on PLL (blue) and Cell-Tak™ (purple), respectively. The values correspond to the first clear peak in each force-indentation curve, which were all measured at 1 µm/s.

4.3.2. PI fluorescence response to assess cell wall integrity

As determined above, forces above 20 nN consistently punctured the cells, as judged by the appearance of at least one peak in the AFM force-time curve and PI fluorescence (Figure 4.5). Figure 4.5A shows the temporal evolution of the applied force (up to 35 nN) and a gradual PI fluorescence response upon nanoindentation of an immobilized *E. coli* on PLL, confirming damage to its cell wall. AFM imaging before and after nanoindentation (inset) does not reveal major damage on the bacterium. If larger forces of about 50 nN are applied (Figure 4.5B), the fluorescence response is somewhat faster and major damage can be observed in the AFM image taken after indentation.

In some cases, typically at lower force values, incorporation of PI after rupture was slow (longer than 30 seconds after puncture), and therefore the fluorescence response was assessed sequentially after indentation. The fluorescence response upon indentation for 36 *E. coli* cells immobilized on PLL and 21 *E. coli* cells immobilized on Cell-Tak™ is collected in the histograms in Figure 4.5C and Figure 4.5D, in which "fast" is in the order of a few seconds after puncture and "slow" is > 30 s. It is worth mentioning that, in a few cases, bacteria showed rupture peaks but no fluorescence response. This histogram provides a quantitative correlation between the magnitude of the rupture force and the speed in viability loss, as assessed by PI fluorescence enhancement. This observation is reasonable since larger forces will produce a more dramatic perturbation in the bacterium (i.e. AFM in Figure 4.5B), which will in turn allow PI to enter more rapidly the bacterial cytoplasm and intercalate into DNA. In some occasions, it was also observed that bacterial DNA exited to the solution, as inferred by the build-up of a cloudy fluorescence signal around the indented bacterium (not shown).

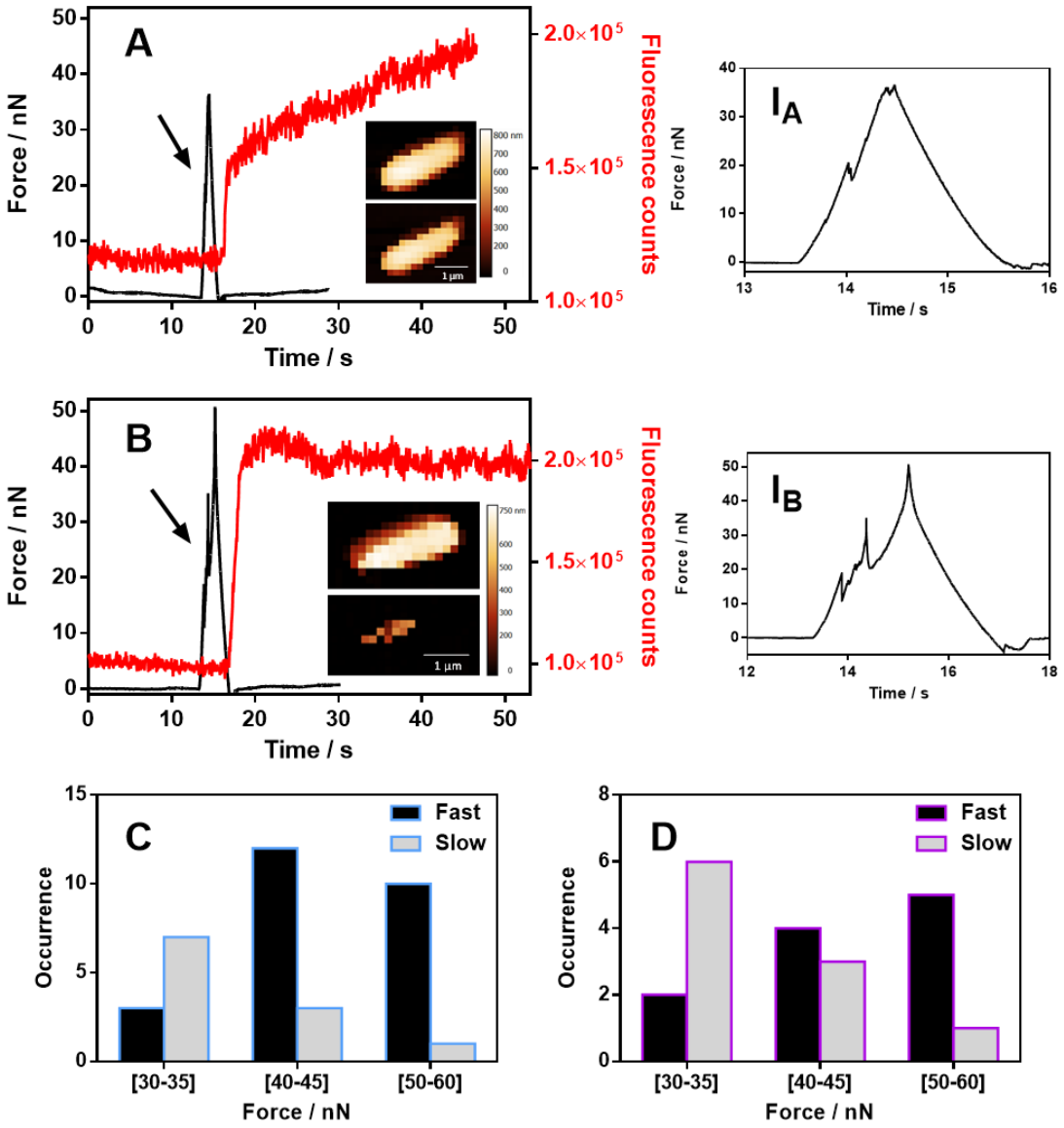

Figure 4.5: Simultaneous AFM nanoindentation and PI fluorescence curves of *E. coli* cells. Simultaneous nanoindentation and PI fluorescence of single *E. coli* cells immobilized on PLL upon rupture, with an applied force of up to 35 nN (A) and 50 nN (B). The insets show low resolution AFM images of the studied bacterium before (top) and after (bottom) rupture. The black arrows show the moment at which puncture occurs, as revealed by the presence of a peak in the force-time curve (not clearly observable at this scale but shown in Insets I_A and I_B, respectively). (C) and (D) Distribution of the PI fluorescence response ("fast" corresponds to an increase of at least 30% of the fluorescence signal in < 30 s after puncture, "slow" is > 30 s), at different ranges of applied force for *E. coli* cells immobilized on PLL (blue contour) and Cell-Tak™ (purple contour).

It is interesting to note that in Figures 4.5A and 4.5B there is a lag of a few seconds between puncture (black arrows) and fluorescence response, compared to similar experiments in single viruses in which the response is instantaneous.[159] We wondered if the inserted AFM tip could be acting as a stopper for PI diffusion into the bacterial cytoplasm. To test that hypothesis, the tip position was maintained for 5 or 10 seconds after rupture (Figure 4.6A and 4.6B, respectively). Indeed, we observed that, in both cases, most of the fluorescence signal appeared only after the tip was retracted.

Therefore, part of the observed lag could be related to the time it takes for the AFM tip to exit the cell. In addition, we speculate that it takes longer for PI molecules to diffuse through the more complex (damaged) bacterial cell wall into the much larger volume of the bacterium compared to a virus, before intercalating into DNA and becoming fluorescent.

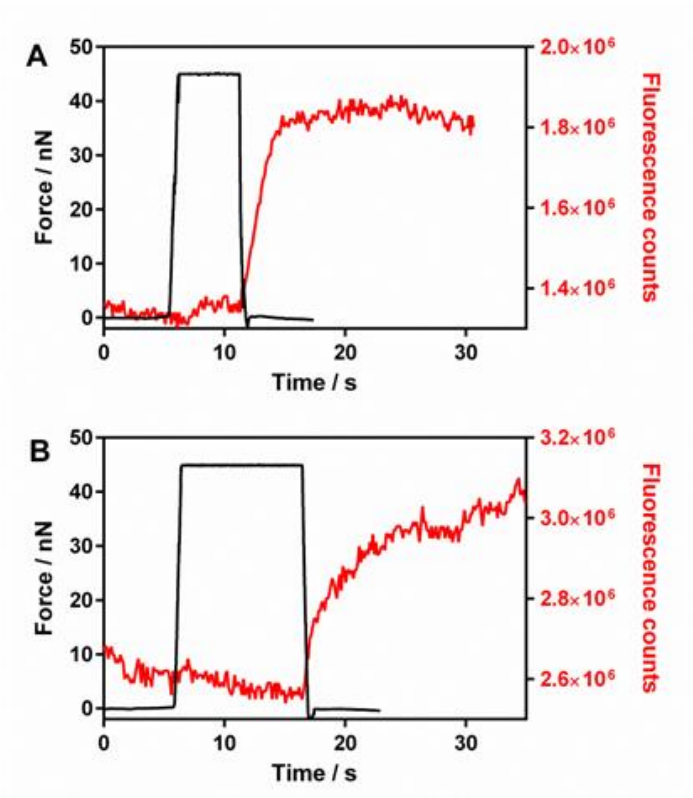

Figure 4.6: Tip influence over PI response. PI fluorescence behavior upon nanoindentation and rupture of a bacterium, maintaining the tip indented for 5 s (A) and 10 s (B). Fluorescence only evolves after the AFM tip is retracted, suggesting that the tip acts as a stopper for PI internalization.

4.4 Conclusions

In conclusion, we have designed a simultaneous AFM nanoindentation and fluorescence imaging strategy to quantify the mechanical forces necessary to damage cell wall in bacteria, upon bacterial cell wall rupture. We find that forces of about 20 nN are necessary to break the cell wall in *E. coli*, which are larger values compared to previous studies in other bacterial systems or using different techniques. Our results indicate that there is a correlation between the magnitude of the force exerted and the loss of bacterial viability and integrity, as assessed by PI incorporation and AFM topography imaging. This fact can be understood in the following way: larger forces produce a greater damage on the bacterial membrane, which would suppose a greater entrance hole for the PI marker, and therefore, the intercalation in the DNA occurs faster, giving rise to what we call "fast response".

Other remarkable fact is the delay between the cell wall rupture and the rise of fluorescence signal, in contrast with similar experiments performed in virus.[159] This has been corroborated through experiments where the PI marker entrance through the membrane has been blocked, using the tip as a stopper. In those cases, the rise of the fluorescence signal did not occur until the tip was removed, suggesting that the PI entrance is not an instantaneous process and cell wall layers may influence the PI propagation into bacteria.

Rupture force and indentation depth values found for *E. coli* resulted to be quite similar between those immobilized in PLL and Cell-Tak™. This fact is expected, since the amount of adhesive was minimized during the optimization procedure in order to reduce its impact on the mechanical properties of the bacteria. Nevertheless, the small deviations observed could be attributed to the bulkier nature of the Cell-Tak™ protein layer, providing some support to the bacterium, and slightly increasing their elasticity and stiffness (see also Appendix A).

From the AFM point of view, a critical aspect of these experiments is to choose the correct cantilevers that will allow not only imaging but also indentation. In order to perform indentation experiments, it is necessary to use cantilevers that are stiffer than the sample, so the indentation occurs. Therefore, the challenge here was to find a stiff enough cantilever to be able to perform higher indentations and consequently rupture the bacteria cell wall, and soft enough to scan bacteria without dragging or damaging them during AFM imaging. In the hypothetical case that several cantilevers meet these premises, it is suitable to use those which stiffness matches the sample stiffness, in such a way that it can deflect the cantilever to a greater extent (always within the linear range of the photodiode), increasing accuracy and decreasing error.

Supporting Movies

Movie S4.1: Bacteria cell wall integrity experiment (I). Fluorescence imaging upon nanoindentation to break the bacterium “1” cell wall (Figure 4.3). The fluorescence emission increases once the bacterium has been penetrated by the AFM tip and tip was retracted. As the movie progresses, the outline of the bacterium is better distinguished, probably due to the diffusion of the PI inside the bacterium. The movie is sped up; the whole experiment took about 60 s.

There is an animation overlaid with the movie to illustrate when the tip makes contact with the bacterium.

Movie S4.2: Same as Movie S4, but on bacterium “2”. In this case, the fluorescence increase after indentation is clearer.

Chapter 5

Simultaneous AFM nanoindentation and fluorescence imaging to assess physiological state in live bacteria

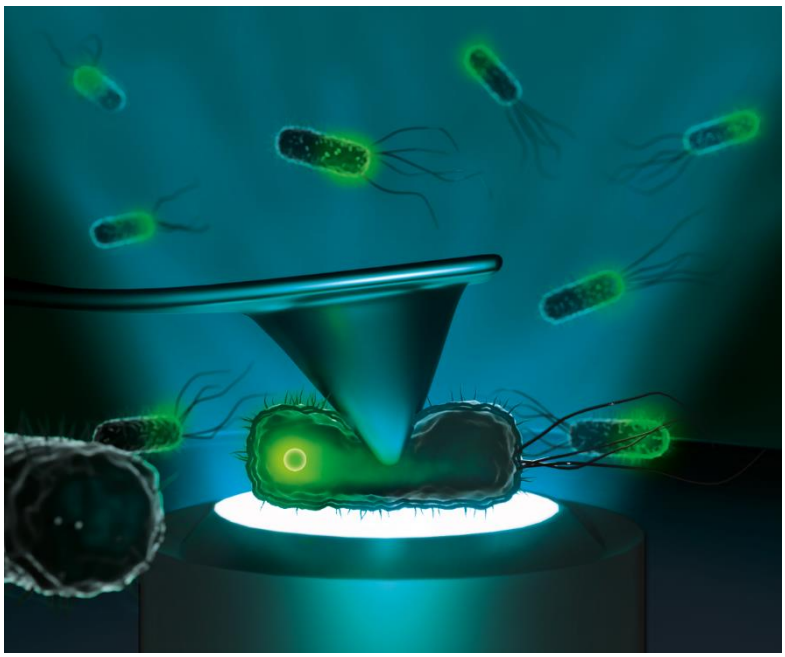

5. Simultaneous AFM nanoindentation and fluorescence imaging to assess physiological state in live bacteria

Adapted from:

del Valle, A; Torra, J; Bondia, P; Tone, C; Pedraz, P; Vadillo-Rodriguez, V; Flors, C. Mechanically-Induced Bacterial Death Imaged in Real-Time: A Simultaneous Nanoindentation and Fluorescence Microscopy Study, *ACS Applied Materials & Interfaces*, **2020** https://doi.org/10.1021/acsami.0c08184

5.1 Introduction

PI staining is a widely used indicator for bacterial viability, however it reports on the integrity of the cell membrane and not on the physiological status of the cell. Indeed, several reports point to the limitations of PI as a viability indicator in different bacterial strains.[186, 194-198] Therefore, our next step was to extend our simultaneous AFM and fluorescence studies by monitoring the bacterial physiological state upon indentation. To that end, we followed the oscillation period of the Min system, a protein complex that helps determining the cell division site in bacteria and that has been proposed as a reporter of bacterial physiology.[187, 199] The Min CDE proteins regulate bacterial fission by oscillating from pole to pole to prevent the formation of the Z-ring septum, formed by the tubulin homolog FtsZ, anywhere but at the midcell (Figure 5.1A).[200-207]. This dynamic process cycles back and forth every one minute or so, depending on a number of factors, including temperature.[205] By labeling the Min system with GFP, oscillations can be monitored by fluorescence microscopy, providing a convenient and intrinsic reporter (Figure 5.1B).

Since this oscillation mechanism is related to bacterial physiological status, the response of the bacterium to induced mechanical damage could be observed in an alternative way. In addition to experiments in which the forces applied are beyond the rupture point of the cell wall as in Chapter 4, monitoring in oscillations of the Min system enable to investigate the response of the bacterium at forces below critical damage. Therefore, this method is complementary to the use of fluorescence viability indicators such as PI, which are limited to cases in which major damage on the bacterial membrane is produced. In this context, the periodic application of forces below the membrane breaking point over time, simulating a fatigue effect, could help to understand the bactericidal effect of an accumulation of SWCNT collisions.

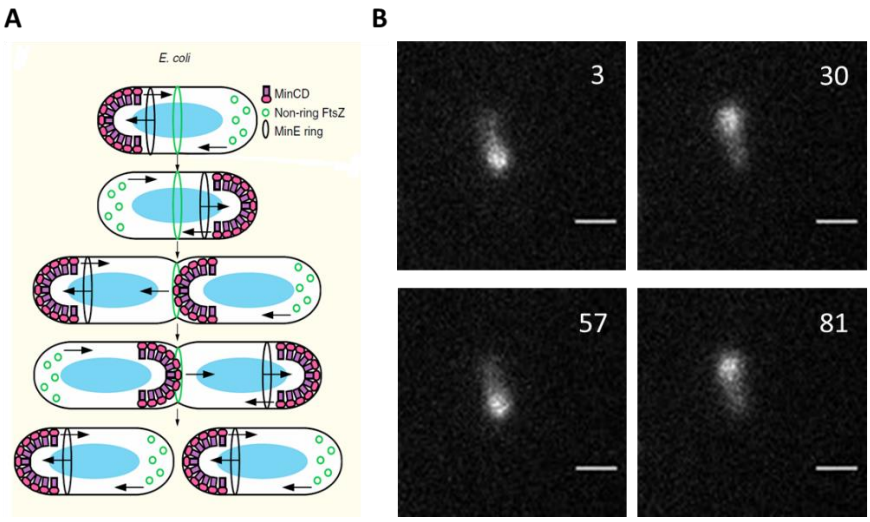

Figure 5.1: Min system basic oscillation principle. (A) Spatial regulation of Z ring positioning in *E. coli* by the Min system. Reproduced from[207] (B) Example of Min-GFP fusion protein oscillations in *E. coli* bacterium. The fluorescence intensity oscillates pole to pole with a period of about 54 s. Numbers represent the time scale (s). Scale bar = 2 μm.

5.2 Materials and methods

For *E. coli* DH10β expressing GFP-MinD (plasmid pDR122),[162] growth medium was supplemented with 100 μg·mL-1 ampicillin (Fisher Chemical). Overnight cultures were grown following the same conditions for section 4.2. 100 μl of the overnight culture was diluted into 10 mL of fresh medium with 100 μg·mL-1 ampicillin, and grown for 2.5 h at 30 ºC. The expression of GFP-MinD was induced by 25 μM Isopropyl β-D-1-thiogalactopyranoside (IPTG) at 30 °C for 3 h in the dark.

Cells were harvested and preprocessed in the same way as in section 4.2. The PLL and Cell-Tak™ coated coverslips were prepared according to the optimal conditions found in section 4.2.1 (i.e. 1:91 in PBS for PLL, 20 minutes and 5.7:100 in $NaHCO_3$ buffer, 1.5 h for Cell-Tak™).

The AFM imaging and nanoindentation procedure was the same as mentioned in section 4.2.1, using the force mapping mode to scan the bacteria after optically locating them. Both AFM tips and procedure to calibrate the cantilever spring constant were also the same. Force-indentation curves were carried out at loading rates of 1 μm/s and maximal forces of 50 nN.

For fluorescence imaging, samples were excited by laser irradiation (488 nm, 27 W·cm-2, Luxx Omicron). The emission was collected in the camera according to the laser path and filters chosen described in Chapter 2. 50-170 frames were typically collected at 3 s intervals and 100 ms integration time per frame. To reduce photobleaching, a shutter (SHB05T - Ø1/2", Thorlabs) connected to a wave generator (TTi TG330) and synchronized with the EMCCD camera was used to restrict the irradiation that reached the sample only during acquisition.

5.3 Results and discussion

5.3.1. Effects of Poly-L-lysine and Cell-Tak™ coatings on attached *E. coli*.

As mentioned above, the Min oscillation periods can be influenced by multiple environmental factors, such as liquid medium (e.g. LB, PBS, M9 minimal salts), pH, temperature or bacteria growth state.[162, 208, 209] Therefore, an initial assessment of the effect of surface adhesive on the Min oscillation period was performed.

The average oscillation time from pole to pole for *E. coli* bacteria immobilized in both PLL and Cell-Tak™ was analyzed and plotted in Figure 5.2. Both histograms have a similar distribution, with close average oscillation times. For 51 *E. coli* cells immobilized on PLL, we found t_{osc} = 60 ± 9 s (mean ± standard deviation), with a close value of t_{osc} = 56 ± 9 s found for 27 immobilized on Cell-Tak™. These results are in agreement with the values reported in the bibliography[205, 210] and the similar values obtained for PLL and Cell-Tak™ confirm the successful optimization process done to minimize the influence of the adhesive. The slightly longer oscillation times for bacteria immobilized on PLL can be explained by the antibacterial activity of PLL, as reported in literature.[187]

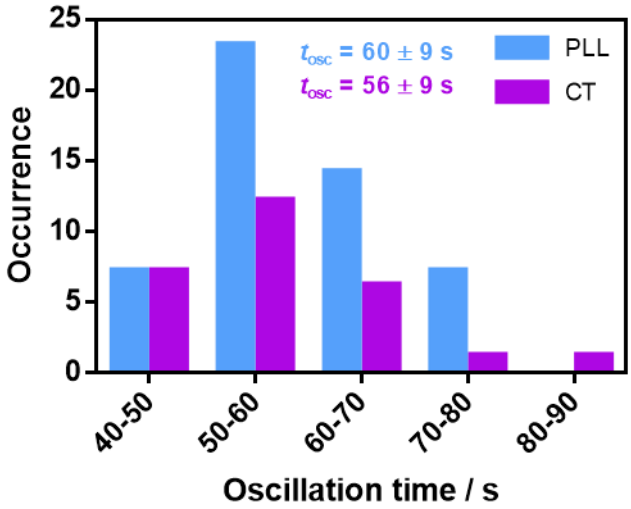

Figure 5.2: Min oscillation time histogram. Oscillation time histogram for *E. coli* cells immobilized in PLL (blue) and Cell-Tak™ (purple).

5.3.2. Monitoring physiological state beyond rupture point

Figure 5.3A shows Min oscillations of an individual *E. coli* cell expressing GFP-MinD.[162] Before puncture, the oscillation period is about 63 s, close to typical values reported,[205, 210] and previously found for our experimental conditions based on immobilization procedures. After one indentation with a low force of about 5 nN (green dotted line), below the rupture threshold estimated above, the oscillation slows down only slightly. However, indentation with about 45 nN (red dotted line) results in the abrupt halt of the

oscillation (Supporting Movie S5.1). Figures 5.3B and 5.3C shows fluorescence images at the beginning of the experiment (t = 0, GFP channel) and the end of the experiment (PI channel), where it can be seen that PI staining is positive for bacteria punctured (P, blue circle) because the cell membrane has been penetrated, while no PI staining is found for the control bacteria (C, orange circle). These observations confirm that forces below the rupture point (Figure 5.3D, green curve) do not have a critical effect, whereas those above 20 nN affect both the integrity of the cell wall (Figure 5.3D, red curve), as seen in the PI experiments, as well as bacterial physiology.

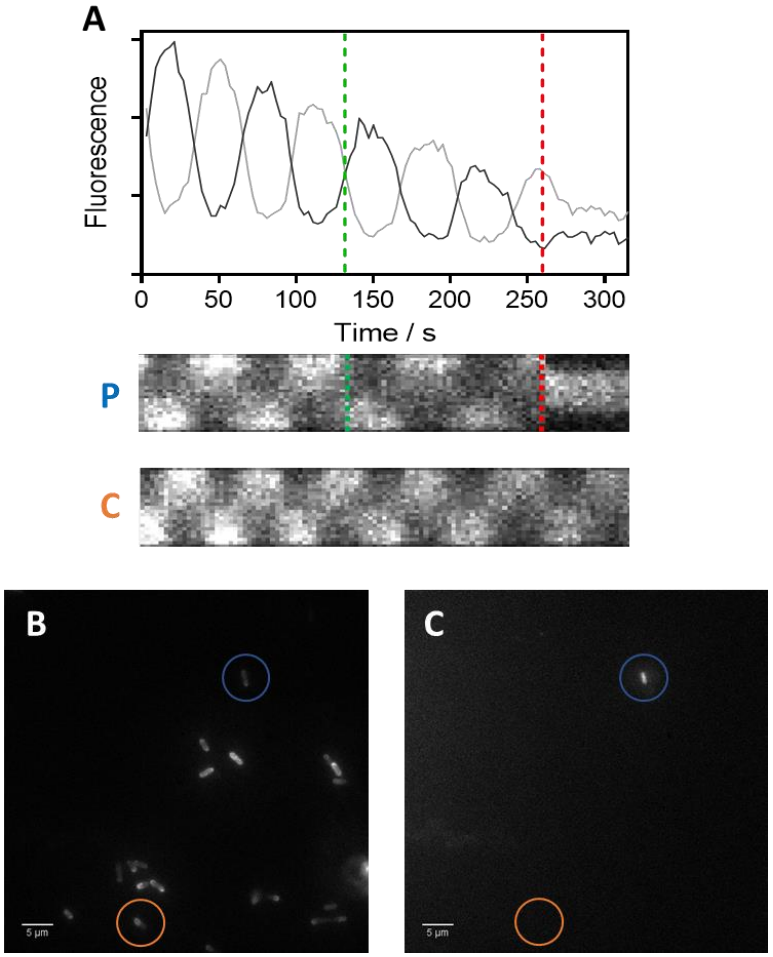

Figure 5.3: Simultaneous AFM nanoindentation and fluorescence imaging of Min oscillations in *E. coli* cells to assess physiological state beyond cell wall rupture. (A) Pole-to-pole oscillations of GFP-MinD upon indentation of an *E. coli* bacterium immobilized on Cell-Tak™ with low force (5 nN, green dotted line) and above rupture (45 nN, red dotted line). Blue and pink curves correspond to the average fluorescence intensity of each pole (dark and light grey lines, respectively. P and C show kymographs of the punctured and a control (non-indented) bacterium, respectively. The dimension of the y-axis in both kymographs is about 2.5 µm. The gradual decrease in fluorescence intensity in all panels is due to GFP photobleaching. (B) MinD-GFP fluorescence images of *E. coli* cells at t=0. (C) PI fluorescence images of the same area than (B), showing PI staining for bacteria punctured (blue circle). Orange circle shows a non-indented bacterium, as a control, with no PI staining.

5.3.3. Monitoring physiological state without rupture: fatigue effects

We also investigated if several consecutive indentations at low forces, with no cell wall rupture, produced a measurable "fatigue" effect on bacterial physiology. In this context, two different indentation experiments were performed. The first one (Figure 5.4) was done by applying 5 nN forces every 10 s (Supporting Movie S5.2). The second one (Figure 5.5) was carried out by applying 2 nN every 9 s, maintaining the indentation during 5 s (Supporting Movie S5.3). Interestingly, in both cases, a halt of Min oscillations could be observed after several indentations, suggesting that bacterial physiology was indeed compromised. It is interesting to note that oscillations halt earlier in the case where the force is maintained for a longer time, even though it is lower (2 nN vs 5 nN). This interesting observation suggests that contact time between nanomaterials and the bacterial envelope is a more important parameter in their mechano-bactericidal activity at this range of force interactions, although more systematic experiments need to be done to clarify this point.

For the second experiment PI staining was monitored after the oscillation halt and, as can be seen in Figure 5.5B, PI fluorescence was not detected, which highlights that cell wall integrity markers do not provide a complete picture of bacterial viability, and that reporters for bacterial metabolism or physiological state can complement viability studies. Moreover, the observed fatigue effect is consistent with the suggestion that the antibacterial properties of high aspect ratio colloidal nanoparticles such as SWCNT may stem from the accumulative action of many low force collisions.[46]

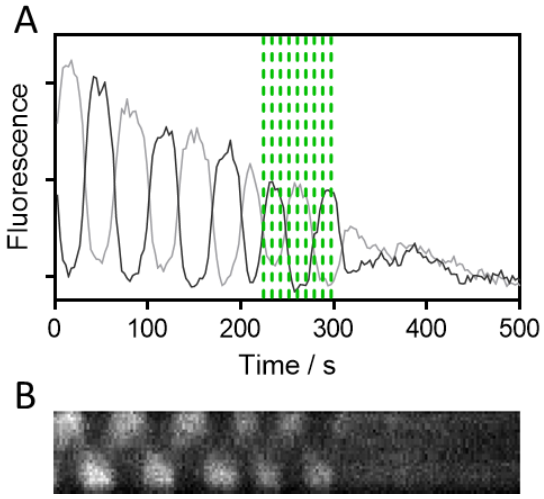

Figure 5.4: Simultaneous AFM nanoindentation and fluorescence imaging of Min oscillations in *E. coli* cells to assess physiological state due to fatigue (I). (A) Pole-to-pole oscillations of GFP-MinD upon repeated indentation (5 nN for each cycle) of *E. coli* bacteria immobilized on PLL. Dark grey and light gray curves correspond to the average fluorescence intensity of each pole. Green dotted lines represent the times at which indentations were performed. (B) Kymograph of the punctured bacteria. The gradual decrease in fluorescence intensity in all panels is due to GFP photobleaching. The dimension of the y-axis in the kymograph is about 3 µm.

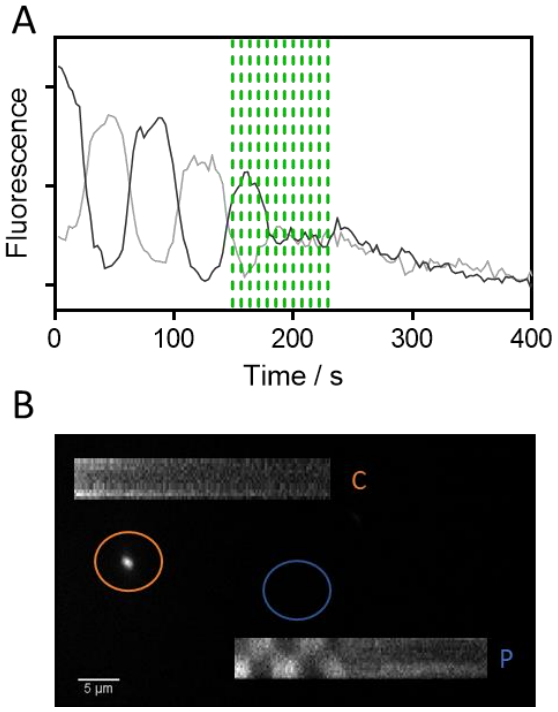

Figure 5.5: Simultaneous AFM nanoindentation and fluorescence imaging of Min oscillations in *E. coli* cells to assess physiological state due to fatigue (II). (A) Pole-to-pole oscillations of GFP-MinD upon repeated indentation (2nN maintained for 5 s for each cycle) of *E. coli* bacteria immobilized on PLL. Dark grey and light grey curves correspond to the average fluorescence intensity of each pole. Green dotted lines represent the times at which indentations were performed. (B) PI fluorescence image after repeated indentation, showing no staining of the indented bacterium (blue circle). Bacteria in orange circle is a control showing PI staining, probably due to immobilization. The insets are the kymographs of punctured and control bacteria oscillations collected during the experiment shown in (A). The dimension of the y-axis in both kymographs is about 2 µm. The gradual decrease in fluorescence intensity in all panels is due to GFP photobleaching.

5.4 Conclusions

We have demonstrated that Min oscillations are a useful reporter for bacterial physiology in these experiments, particularly to study effects of small forces. This method is therefore complementary to the use of classical viability indicators such as PI, which rely on major damage of the bacterial membrane to penetrate and intercalate into DNA. Small disturbances such as fatigue or the effect of immobilization on a surface will be reflected in changes in the oscillation period or, in the extreme case, with the cessation of oscillation.

Indeed, by monitoring Min oscillations we have observed that the adhesive does not have a large impact in the immobilization process, since values obtained for average oscillation time are very similar. This confirms again that the optimization process has been successful, this time monitored with a more subtle and direct method compared to Chapter 4.

For experiments in which forces beyond the rupture point were applied, the obtained results are in agreement with the experiments in Chapter 4, confirming that forces above 20 nN are able to inflict critical damage as observed by a halt of the Min oscillations.

For fatigue experiments, preliminary results show that lower forces (i.e. below rupture point) could be detrimental for bacteria when they are applied repeatedly in a short time frame, supporting the accumulation effect proposed in literature for the antibacterial activity of SWCNTs by multiple collisions. These experiments also highlight the limitations of PI as a fluorescent reporter for experiments with no major cell wall damage.

Supporting Movies

Movie S5.1: Bacterial physiological state experiment (I). Fluorescence imaging of Min oscillations upon a low force indentation (5 nN, i.e. with no cell wall rupture) followed by a high force indentation (45 nN, i.e. with cell wall rupture). It can be observed that a halt of oscillations occurs only when the bacterium cell wall was ruptured (Figure 5.3).

Movie S5.2: Bacterial physiological state experiment (II). Fluorescence imaging of Min oscillations upon six consecutive low force indentations (5 nN, i.e. with no cell wall rupture). It can be observed that there is a halt of oscillation while forces are being applied (Figure 5.4).

Movie S5.3: Bacterial physiological state experiment (III). Fluorescence imaging of Min oscillations upon eight consecutive low force indentations (2nN, i.e. with no cell wall rupture) and maintaining the force for 5 s for each cycle. It can be observed that there is a halt of oscillation while forces are being applied (Figure 5.5).

Chapter 6

General discussion and outlook

6. General discussion and outlook

The aim of this thesis is to provide a more quantitative understanding of how *E. coli* cells response when they are subjected to nanomechanical forces, through a simultaneous correlative AFM and fluorescence microscopy. This aim was pursued through complementary methods that addressed different aspects of bacterial response. The purpose of this chapter is to globally discuss the main findings and current limitations of these methods, while potential ideas for alternative experiments or future work are outlined.

6.1 Technical considerations and potential improvements.

In this thesis, correlative microscopy was successfully applied to analyze immobilized *E. coli* cell wall integrity and physiological state, in the context of the recent emergence of bactericidal nanomaterials based on mechanical-induced damage due to their nanofeatures. These studies are an example of how a better understanding of complex biological systems can be achieved by combining techniques, whilst applying these techniques independently would not allow addressing these questions. Simultaneous AFM force spectroscopy and fluorescence imaging in real time of *E. coli* cells allowed us to quantify the forces needed to be able to penetrate the cell wall.

As with most advanced microscopy applications, compromises between temporal and spatial resolution have to be made. As discussed in Chapter 2 and 4, force mapping was used for topography imaging bacteria, since both contact and dynamic modes did not provide low enough forces to avoid bacteria dragging during imaging in the explored conditions. Thus, force mapping provides low resolution images but at a reasonable acquisition time. Longer acquisition times have the drawback that the environmental conditions and bacterial morphology/state could change during the experiment. This could be solved with a more advanced AFM setup (better than our current JPK Nanowizard II), with better electronics that allow to perform similar experiments faster and with improved resolution. With this upgrade, it would be possible to correlate in a better way the PI entrance and fluorescence response with the local damage induced by the AFM tip when cell wall is ruptured, similar to those performed in air conditions[46] (Figure 1.6) with higher resolution. It is important to note that measurements performed in air generally provide better topography resolution than those performed in liquid, but with an AFM which provides a high enough resolution it would be possible to better appreciate damage caused to bacteria. If imaging could be faster, the changes in environmental conditions and bacterial morphology/state during time are expected to be reduced, and topographic changes between before and after puncturing could be studied more reliably.

On the other hand, successful nanoindentations were performed to analyze the bacterial response for force ranges between 0-60 nN. Cell walls were successfully ruptured, by observing both a PI rise in the fluorescence counts and clear peaks in the force-distance curves. However, the indentation speed was quite high (1 μm/s for a bacterial height around 0.8 μm), and indentation occurred in less than a second. This means that it is very hard to assign the exact peak that corresponds to bacterial cell wall rupture and PI entrance. In this context, the next step would be to perform indentations at lower speeds (e.g. 10-50 nm/s). This would allow us to obtain a higher peak resolution, helping us to determine which is the bacterial cell wall breakage point. This would help to clarify if the few experiments in which a single clear peak was observed but with no PI response could be related to an insufficient cell wall rupture, taking into account that the bacterial cell wall consists of two membranes and a layer of peptidoglycan. Moreover, these experiments would require a better synchronization between AFM and fluorescence, e.g. with more advanced electronics, as the synchronization error of our current protocol is about 0.5 s. The suggested improvements of the indentation experiments would allow to obtain statistic of the number, relative position to PI fluorescence increase and magnitude of those peaks presented in whole force distance curves, and achieving a more in-depth study of the cell layers[7] that are being penetrated by the AFM tip.

This thesis suggests that bacterial cell viability can be compromised without rupturing the cell wall, by applying consecutive forces simulating a fatigue effect. These experiments were preliminary and a more systematic study with improved statistics would be needed to understand how this fatigue effect alters the physiology of the bacteria. However, it is difficult to achieve high statistics in these experiments, mainly due to two factors: the slow oscillation of the Min systems and the incomplete expression of Min-GFP in *E. coli*.[162] As mentioned in Chapter 5, the average oscillation time is about 60 and fluorescence data acquired was about 300 s, longer than cell wall integrity experiments with PI (about 30 s). Thus, physiological experiments take 10 times more than PI ones. In terms of Min-GFP expression, it is important to mention that every bacterium does not correctly express the introduced plasmid (pDR122[162]). This issue was shown to be dependent of the type of plasmid chosen[211], where not all bacteria that contained the plasmid (e.g. pDR113 (MinE-GFP) or pDR119 (GFP-MinD)) and that showed GFP fluorescence exhibited Min oscillations. The percentage of bacteria that showed fluorescence and the percentage displaying fluorescent oscillations from pole-to-pole was 22% and 14% respectively for bacteria with pDR113, and 40% and 21% for bacteria with pDR119. This limitation was partially overcome with the plasmid pDR122 used in this thesis, where the percentage of bacteria displaying fluorescent oscillation increased significantly meaning that experimental throughput could be improved. Looking forward in terms of improved labeling strategies, selective fluorescent sensors for monitoring other parameters related to bacterial physiology, like intracellular pH[212], glucose consumption[213, 214], membrane potential[215] or reactive oxygen species (ROS)

generation inside bacteria could be used.[216] The right choice of fluorescent sensor would enable to obtain quantitative information of environmental or physiological parameters.

In the context of quantitative measurements, improvements in fluorescence labeling could be combined with more sophisticated fluorescence techniques. For example, fluorescence lifetime imaging microscopy (FLIM) or ratiometric fluorescence imaging are two powerful techniques that can measure perturbations on bacterial physiological state in a quantitative way. FLIM microscopy produces spatially resolved images of fluorescence lifetime, which is independent of excitation intensity, optical pathway heterogeneities and fluorophore concentration[217]. FLIM has been successfully used for biological applications such as reporting pH dynamics in living cells after environmental perturbances[218], measurement of dissolved oxygen concentration in single living cells[219] , based on the fact that the fluorescent probe can be dynamically quenched by local oxygen, thereby shortening its fluorescence lifetime or monitoring free and bounded nicotinamide adenine dinucleotide (NADH), a metabolic biomarker coenzyme.[220]

On the other hand, ratiometric fluorescence imaging is the method where the relative intensities of two or more wavelengths of the emission spectrum are measured to detect changes in the local environment. The implementation of ratiometric fuorescence detection in our setup would be easier than FLIM, as only an optical splitting device is needed in the detection path of the microscope. If AFM tip perturbations lead to a slowdown in the consumption of nutrients or ions, or any ROS production, the ratiometric probe will interact with the target species, and produce spectral changes that can be detected and quantified ratiometrically.[221]

Combining these advanced fluorescence techniques with AFM presents additional technical challenges, but would lead to a more quantitative view of bacterial behavior upon nanoindentation.

Finally, it would be interesting to explore a more realistic scenario of interactions between bacteria and nanofabricated topographies. So far, indirect methods have been developed based on the deformation produced on nanopillars by bacteria once they adhere to the surface. In such scenario, the lateral deflection (bending) of each pillar can be described as a function of external applied force, using the nanostructure as a ‘‘force sensor”.[222-225] It should be noted that this approach is an *ex-situ* technique, which requires the dehydration of cells, metal coating, and then SEM imaging[62], so its results may not be as representative as those obtained through an *in-situ* technique, such as with the AFM. In this context, the next step in our experiments to better simulate the interaction between bacteria and nanomaterials is to attach a bacterium to a tipless cantilever and push it against a nanotopographical surface. This experiment involves some challenges, such as the fact that such nanostructured surface should be transparent enough for fluorescence microscopy, but this line of research has potential and will be further explored in the laboratory.

6.2 Further insights into mechanically-induced bacterial death

E. coli DH10β was chosen as a bacterial model for the experiments carried out in this thesis. They are non-pathogenic and widely used for in biology for several applications.[226] They have been successfully characterized in terms of cell response when mechanical forces are induced on their surface, beyond and below the critical point where the bacteria cell wall ruptures. The experiments were done for early phase grown *E. coli* (OD at 600 nm close to 0.3), where the majority of cells are "young". In this context, it would be interesting to perform these experiments on older *E. coli* cells (e.g. in their stationary phase), since bacteria morphology is affected by the growth state[227] and the cell cycle state could also affect to the susceptibility of bacteria to force. Cells are genetic machines which consume energy to survive and replicate, in a continuous cycle.[228] In this context, replication may lead to a transiently weaker cell wall, or on the contrary, a more resistant wall that prevents or combats external threats. While the majority of experiments presented here were performed on individual bacteria, a few experiments were carried out in dividing bacteria. Preliminary observations do not suggest that there was an evident effect, but a better topography and indentation resolution would allow to obtain a potential correlation between cell replication stage and forces required to rupture the bacterial cell wall, if it exists. This could represent a more complete scenario when we talk about bacteria contamination on surfaces, where bacteria in a heterogeneous growth state adhere on the surface.

At this point, it is necessary to remark that this thesis is focused in only one bacteria species and type (i.e. Gram-negative). As shown in Chapter 1, Gram-positive bacteria differ in their cell wall composition from Gram-negative bacteria by the absence of the extra cell outer membrane, but instead a bigger layer of peptidoglycan, among other differences. In this thesis, we were not able to use for *B. subtilis* and *S. aureus* a similar immobilization procedure than for *E. coli*, since the fixation was not strong enough to prevent dragging during AFM imaging, probably due to their different surface composition. Attempts to find optimal conditions for immobilization with no toxicity (assessed by PI staining) for Gram-positive bacteria were unsuccessfully. As discussed above, with a hardware upgrade which provides better control of the applied forces and better stability, this problem could be overcome, and few pico-newtons forces could be applied, maybe reducing or avoiding the bacteria dragging during AFM imaging. In this hypothetic scenario, experiments would be performed in very similar experimental conditions, so the values obtained could be directly compared to those of *E. coli* cells. This would be so assuming that the cantilevers used for these experiments are stiff enough to break the Gram-positive bacteria wall, which is not necessarily the case. Indeed, stiffness and viscoelasticity differences between Gram-negative and Gram-positive bacteria have been discussed in literature[165], probably due to the thicker peptidoglycan layer of the Gram-positive, providing greater rigidity which leads to a greater resistance to being indented, so that the applied forces to break the cell wall

should be different than those applied to the Gram-negative. This fact was in agreement in the only one case in which the experiment could be performed, where fixation was enough to perform one indentation experiment in a *B. subitilis* CECT 356, and PI rise of the fluorescent signal was achieved. Figure 6.1A and B shows brightfield and fluorescence images of *B. subtilis* cells, where no PI staining was detected for the bacterium marked in blue. Figure 6.1C shows the AFM imaging of the same bacterium. It was observed that the rupture force and indentation depth were about 80 nN and 173 nm respectively (Figure 6.1D and E), and therefore stiffer than *E. coli* cells studied in this thesis. Brightfield and fluorescence microscopy (Figures 6.1F and G) shows PI staining for the bacterium after puncture, where damage caused could be observed by AFM imaging (Figure 6.1H). Note that PI staining has been obtained with apparently a single clear peak, bearing in mind that the Gram-positive only has one membrane, suggesting that those *E. coli* experiments with a single break peak without PI staining were insufficient to penetrate both membranes. Nevertheless, the PI response was “slow”, probably due to the little damage caused to the bacterium (Figure 6.1H).

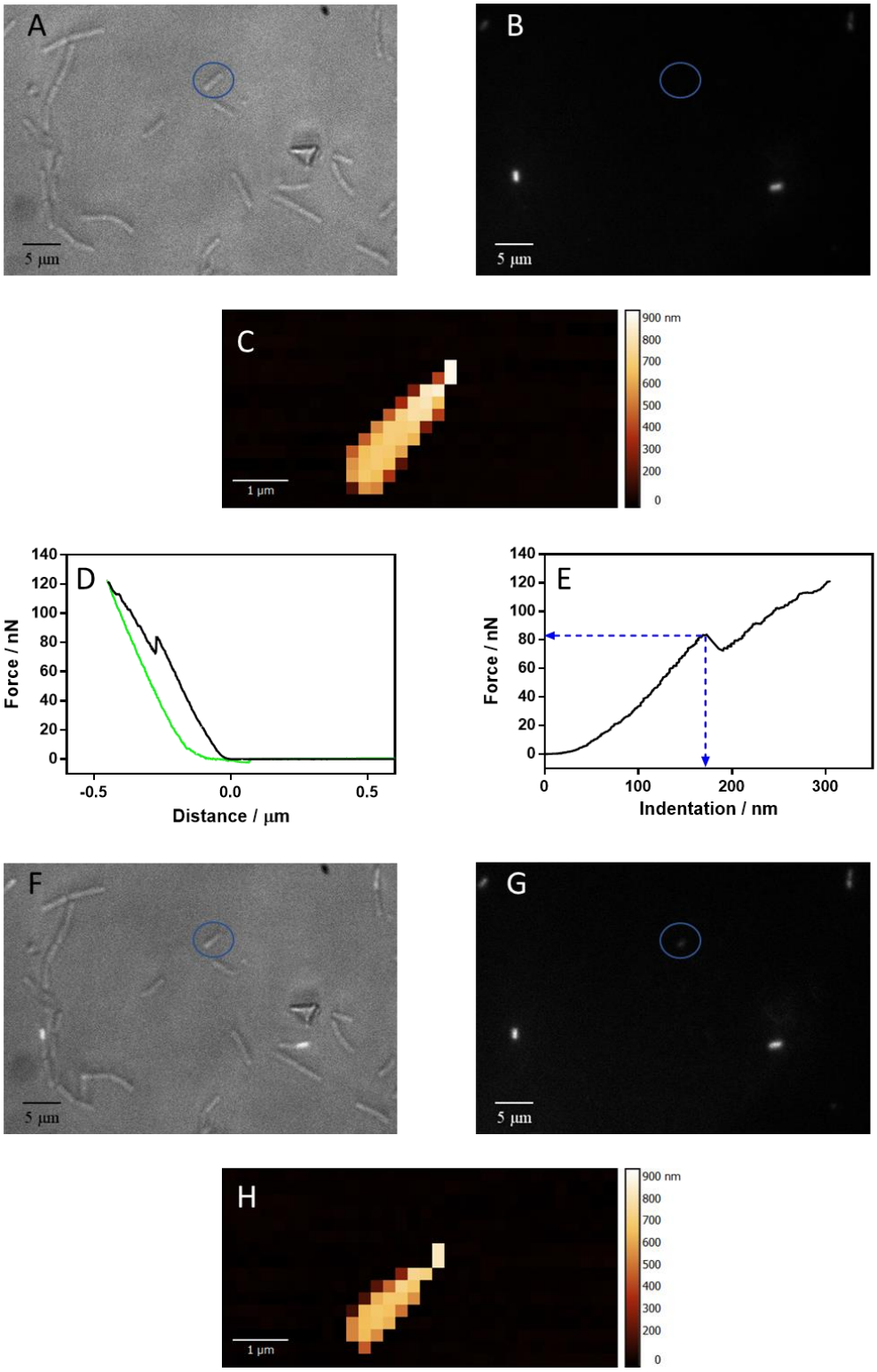

Figure 6.1: Preliminary cell wall integrity experiments on *B. subtilis*. (A) Brightfield and (B) PI fluorescence images of *B. subtilis* immobilized on 1:60 PLL-coated glass confirming that most bacteria do not show PI fluorescence before indentation with the AFM tip. (C) shows a low resolution AFM topography image of the bacterium marked in blue. (D) Force-distance curve (black is approach, green is retract). (D) Force-indentation curve showing a cell wall rupture event (blue arrows). (F) Overlaid fluorescence and brightfield and (G) fluorescence images after indentation of bacterium, showing PI staining. The AFM topography (H) image confirms that structural damage was inflicted on the indented bacterium.

Alternative immobilization methods based on physical confinement traps can overcome the challenge of bacteria poor immobilization under physiological conditions, and were successfully tested on *E. coli* and *B. subtilis.*[229], *S. aureus*[230] and *S. sciuri*[186] . However, this approach requires time consuming nanolithography complex and sophisticated procedures.

In any case, the possibility to perform these experiments for Gram-positive bacteria analogously to those carried out for *E. coli* could give a more complete and rigorous view of the role that the composition of the bacterial cell wall plays in their response to mechanically induced damage, providing a better understanding of the interactions between both types of bacteria and the topographical nanomaterials. There seems to be an established idea that Gram-negative bacteria are less resistant to nanostructures surfaces. This is attributed to the resistance that the greater layer of peptidoglycan gives to Gram-positive bacteria. It is suggested that the bactericidal effect depends on the physical properties and bacterial cell wall composition[38, 66, 82], where higher bactericidal effects are found for the Gram-negative bacteria, which are less rigid, so deforms more easily. However, factors like bacterial motility or shape, apart from nanopillar density and aspect ratio have been demonstrated to influence the bactericidal effect on both Gram-negative and Gram-positive bacteria[34, 38, 71, 85, 89]. On the other hand, the opposite trend is suggested for susceptibility to colloidal nanostructures. Some investigations showed that these colloidal nanostructures are more bactericidal on Gram-positive bacteria, because the additional membrane that Gram-negative possess gives them more protection and less sensitivity when penetrated by colloidal nanostructures.[38, 45, 49, 51] The complex wall of the Gram-negative bacteria (membrane-peptidoglycan-membrane) provides a more difficult framework to penetrate for colloidal nanostructures.

General conclusions

General conclusions

In this thesis, AFM and fluorescence microscopy have been combined simultaneously to study how bacterial cells respond to mechanically-induced damage. The main conclusions that can be extracted from the thesis are:

1) Correlative microscopy provides a powerful tool for studying biological systems in real time. Several technical challenges were found and overcome to successfully perform simultaneous nanoindentation and fluorescence imaging on living bacteria.

2) The forces required to puncture the bacterial cell wall of *E. coli* range from 20-25 nN depending on the immobilization strategy used. These values are larger than those reported in previous studies in other bacterial systems or using different techniques, and contribute to a better understanding on the forces involved in the interaction between bacteria and mechano-bactericidal nanomaterials.

3) There is a correlation between the magnitude of the force exerted on the bacterium and the loss of bacterial viability and integrity, as assessed by PI incorporation and AFM topography imaging. Thus, larger forces produce more structural damage.

4) PI fluorescence response upon cell wall rupture was not instantaneous. It was shown that the delay is mostly related to the fact that the AFM tip acts as a stopper that precludes PI incorporation.

5) Monitoring Min oscillations by fluorescence microscopy is useful to assess physiological state of bacteria and provides complementary information to PI. A halt of oscillations was observed when the bacterial membrane was ruptured.

6) Min oscillations also allowed studying more subtle fatigue effects upon application of low forces repeatedly without breaking the bacterial cell wall. These experiments, which would have not been possible with viability cell markers, can be interpreted in the context of the accumulated collisions of colloidal nanomaterials with bacteria.

Conclusiones generales

En esta tesis, AFM y fluorescencia se han combinado simultáneamente para estudiar cómo las células bacterianas responden al daño inducido mecánicamente. Las principales conclusiones que se pueden extraer de la tesis son:

1) La microscopía correlativa proporciona una herramienta poderosa para estudiar sistemas biológicos en tiempo real. Se encontraron y superaron varios desafíos técnicos para realizar con éxito la nanoindentación y seguimiento de la fluorescencia de forma simultánea en bacterias vivas.

2) Las fuerzas requeridas para perforar la pared bacteriana de *E. coli* varían entre 20-25 nN dependiendo de la estrategia de inmovilización utilizada. Estos valores son mayores que los reportados en estudios previos en otros sistemas bacterianos o mediante el uso de diferentes técnicas, y contribuyen a una mejor comprensión de las fuerzas involucradas en la interacción entre las bacterias y los nanomateriales mecano-bactericidas.

3) Existe una correlación entre la magnitud de la fuerza ejercida sobre la bacteria y la pérdida de la viabilidad e integridad bacteriana, según lo evaluado por la incorporación de PI y las imágenes de topografía AFM. Por lo tanto, fuerzas más grandes producen mayor daño estructural.

4) La respuesta de fluorescencia de PI tras la ruptura de la pared bacteriana no es instantánea. Se demostró que la demora está relacionada principalmente con el hecho de que la punta AFM actúa como un tapón que impide la incorporación de PI.

5) El seguimiento de las oscilaciones del sistema Min mediante microscopía de fluorescencia resulta útil para evaluar el estado fisiológico de las bacterias, proporcionando información complementaria a los experimentos con PI. La ruptura de la pared bacteriana tiene como consecuencia la detención de las oscilaciones de Min.

6) El seguimiento de las oscilaciones de Min permitió estudiar efectos de fatiga más sutiles, mediante la aplicación de pequeñas fuerzas de forma consecutiva sin llegar a romper la pared bacteriana. Estos experimentos no hubieran sido posibles con marcadores de viabilidad, y pueden interpretarse en el contexto de colisiones acumuladas de nanomateriales coloidales contra bacterias.

Appendix A

Calculation of the nano-mechanical properties of *E. coli* before cell wall rupture

Appendix A: Calculation of the nano-mechanical properties of *E. coli* before cell wall rupture

A.1 Introduction

This section provides a nanomechanical characterization of the intact bacterial cell wall in order to provide complementary information to the high force regime studied in the main part of the thesis. Several investigations been carried out to quantify the mechanical properties of bacteria, but there are two mainly parameters that better describe their structural material properties: Stiffness[46, 231-238] and Young's Modulus[166, 167, 171, 239-242].

Stiffness (*k*) is the extent to which an object resists deformation in response to an applied force.[243] For a deformable elastic body only in one direction, the stiffness is computed as:

$$k = \frac{F}{L} \qquad \text{Equation A.1}$$

Where,
F is the force applied on the body (N)
L is the displacement produced by the force (m)

Therefore, stiffness is an extrinsic property, which depends on the physical characteristics of the body (i.e material, size and shape).[244]

When the sample is indented by the AFM tip, the signal recorded by the photodiode corresponds to the linear deformation of the cantilever and the sample. A simple model assuming the AFM cantilever and the sample to be two ideal springs in series proposed by Arnoldi[232] is used to compute:

$$\frac{1}{k_{\mathrm{eff}}} = \frac{1}{k_{\mathrm{b}}} + \frac{1}{k_{\mathrm{c}}} \qquad \text{Equation A.2}$$

Where,
k_{b} is the stiffness of the bacterium (N/m)
k_{c} is the cantilever spring constant (N/m)
k_{eff} is the slope of the force-distance curve taken on the bacterium

The advantage this analysis is that it does not require the hypothesis of any model. The drawback of this method is that the geometry or the surface of the indenting probe is not taken into consideration. This means that it is difficult to compare data obtained

with different probes. In addition, the fact that a force–deformation curve is not linear over the whole range makes it difficult to set the range where the respective curve should be analyzed.[244] On the other hand, the elasticity (i.e. the ability of a material to recover its normal shape after being stretched or compressed) can be defined by its Young's Modulus (E, or tensile elasticity), which is characterized by the relationship between the applied stress on the material (force per unit area) and the resulting strain (fractional change in length) in the elastic behavior zone.[245, 246] For a perfectly elastic material, E is defined as:

$$E = \frac{\sigma}{\varepsilon} = \frac{stress}{strain}$$ Equation A.3

Young´s Modulus describes the ability of a material to resist elastic deformation to an applied stress, and contrary to stiffness, the Young´s Modulus is an intrinsic property of a material, which does not depend on the size or shape of the body.[244]

In order to calculate this parameter, it is necessary to introduce a mechanical model to predict the shape of the contact area between the AFM tip and bacteria, taking into account several assumptions based in the contact theory considered. The most widely used model for AFM nanoindentation data processing is the Hertz model.[247] However, the Hertz model can be applied only under specific conditions:

- Homogeneous sample (i.e. the material has uniform composition and uniform properties throughout).
- Isotropic sample (i.e. the properties of the material are the same in all directions).
- Linear elasticity response of the sample (i.e. stress is proportional to strain).
- Small deformations applied to the sample.
- Contact surface is flat.
- Infinite extended sample.
- Adhesionless and frictionless surfaces.

Despite bacteria, as biological materials, do not fulfill these required premises[248], some reasonable assumptions (discussed in the next section) can be applied to estimate the Young´s Modulus of bacteria.

In order to extract the mechanical properties discussed above, the force-distance curves were analyzed according the two different regions that can be found typically when indenting bacteria (Figure A.1). Before the tip makes contact with the bacterial surface (i.e. contact point, represented as (0,0)) the tip is far away from the bacterium and no deflection occurs; therefore, the slope is zero. This region is used to set the base line and zero cantilever deflection. Once the tip-bacterium contacts at (0,0), the tip begins to indent the bacterium. This indentation causes the slope of the curve to change

continuously until it reaches a compliance region, where the slope becomes constant just before the bacterial membrane is penetrated by the AFM tip (first peak). This region is governed by the Hooke´s law, where the bacterial spring constant can be obtained through the slope of the curve.

On the other hand, the non-linear regimen is analyzed with the Hertz model. As said before, the nonlinearity is due to the cell elasticity change during indentation.[231] This Hertzian model takes into account the continuously changes of the contact surface, which is one of the main reasons of this nonlinearity behavior. Nevertheless, only the first part of the curve is fitted, taking in consideration the Hertz model restrictions.

For both analyses, it has been assumed that the deflection of the cantilever comes only from the mechanical indentation of bacteria[232], while other possible interactions like electrostatic forces between tip-bacteria are not significant enough and can be neglected.[131]

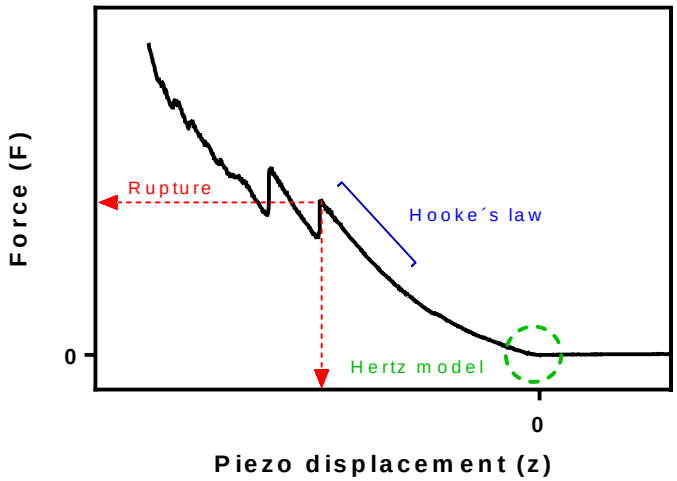

Figure A.1: Bacterial cell mechanical characterization. Force-distance curve of an indented *E. coli* cell, representing the different regions that can be found according to the cell mechanical behavior.

A.2 Results and discussion

A.2.1 Linear indentation analysis

Equation A.2 represents a spring system in series, in which the force applied at any piezo position (z) can be calculated as:

$$F(z) = k_{\mathrm{c}} \cdot d = k_{\mathrm{b}} \cdot \delta \qquad \text{Equation A.4}$$

The magnitude of the piezo movement is equal to the sum of the compression of the two springs, or:

$$z = d + \delta \qquad \text{Equation A.5}$$

Since the value of the linear slope, *s*, is the ratio of *d* to *z*, combining Equations A.4 and A.5 gives:

$$k_{\mathrm{b}} = k_{\mathrm{c}} \cdot \frac{s}{1-s} \qquad \text{Equation A.6}$$

In order to quantify the value of the linear slopes, it is necessary to analyze the raw data values in terms of deflection (*d*) vs piezo distance (*z*), where the slope was computed just before the first breaking point for each curve, for a piezo displacement down to 120 nm (see below). Figure A.2 shows the histogram distribution of the bacterial spring constant calculated with Equation A.6 for PLL and Cell-Tak™, where it can be observed that both histograms are rather similar. The obtained values are k_b = 0.090 ± 0.022 N/m (mean ± standard deviation) and 0.109 ± 0.032 N/m for PLL (n = 24) and Cell-Tak™ (n = 21), respectively. Similarly, a stiffness value for the preliminary experiment of *B. subitilis* (Figure 6.1) of 0.74 N/m was obtained, being approximately 7 times stiffer than *E. coli.*

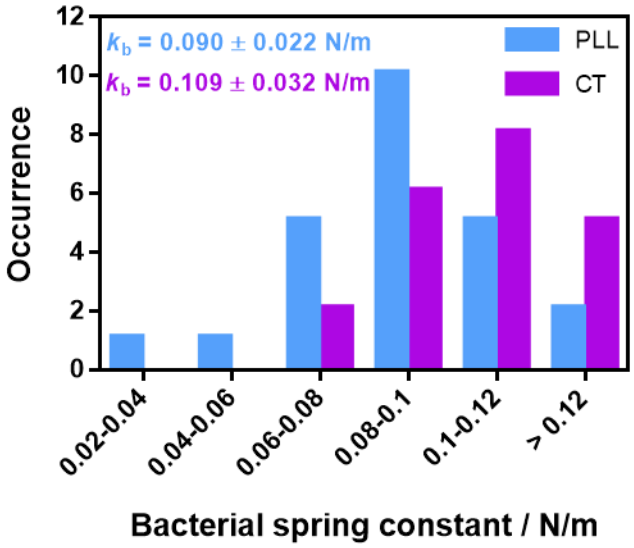

Figure A.2: Bacterial stiffness estimation. Bacterial spring constant distribution for *E. coli* cells immobilized in PLL (blue) and Cell-Tak™ (purple).

A.2.2 Non-linear indentation analysis

As previously mentioned, a Hertzian based model was used to estimate the Young´s Modulus of E. coli cells. The Hertz-Sneddon modification[249] for a spherical indenter was employed, in order to overcome the limitation regarding the maximum possible indentation with the small radius of the used tip:

$$F = \frac{E}{(1-\upsilon^2)} \cdot \left(\frac{R^2+a^2}{2} \cdot Log\left(\frac{R+a}{R-a}\right) - aR\right) \qquad \text{Equation A.7}$$

$$\delta = \frac{a}{2} \cdot Log\left(\frac{R+a}{R-a}\right) \qquad \text{Equation A.8}$$

Where,

R is the tip radius
a is the contact radius
υ is the Poisson ratio (assumed 0.5 for soft biological samples[244, 250, 251])

To solve Equations A.7 and A.8, AtomicJ software was used to analyze force-indentation curves and fit them with the Hertz-Sneddon model (See below).

To obtain a reliable estimation, only the first 50 nm of the force-indentation curve were fitted. In this small region, the bacterial cell can be approximately considered as an elastic half space.[252-258] An elastic half space is an isotropic and homogeneous material that is assumed to extend infinitely in all directions and in depth, with the top surface as a boundary.[259, 260] As it has been previously reported, if the indenter's radius is at least ten times smaller from each horizontal dimension of the sample, then the sample can be considered as an elastic half space.[260, 261] In this context, since the bacteria cell area is larger compared to the tip radius, one can assume as an approximation that the sample is flat. Finally, it is strongly recommended that the indentation depth should not exceed the 5-10 % of the bacteria thickness, not only to be considered as an infinitely extended sample but also to avoid measuring the substrate contribution (Buckle´s rule).[248, 262]

Figure A.3 shows the histogram distribution of the bacteria Young´s Modulus calculated through Equation A.7 and A.8 for PLL and Cell-Tak™. It can be observed that both histograms are similar, as for the bacterial spring constant. The obtained values are E = 1.4 ± 0.9 N/m (mean ± standard deviation) and 1.9 ± 0.9 N/m for PLL (n = 24) and Cell-Tak™ (n = 21), respectively. Similarly, a Young´s Modulus value for the preliminary experiment of *B. subtilis* (Figure 6.1) of 21.7 N/m was obtained, indicating higher resistance to be deformed elastically than *E. coli* cells.

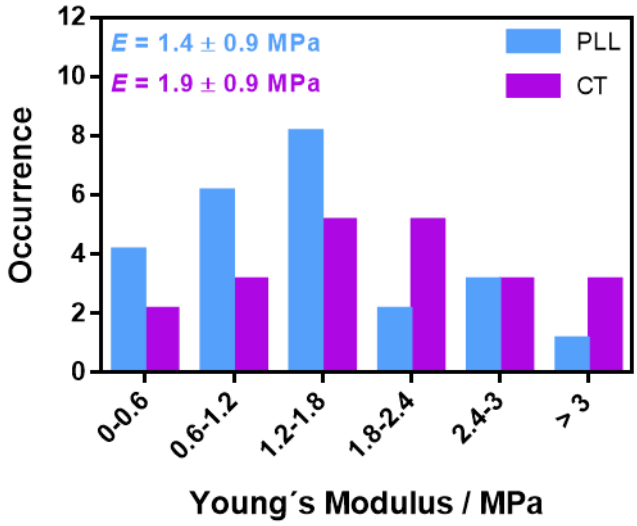

Figure A.3: Bacterial Young´s Modulus estimation. Young´s Modulus distribution for *E. coli* cells immobilized in PLL (blue) and Cell-Tak™ (purple).

A.3 Software analysis

This appendix provides the sequential data processing protocol performed with AFM specific software to obtain the results shown in this thesis. Force-distance curves were analyzed with JPK Data Processing[173] and AtomicJ software.[174] The first one is supplied with the JPK Nanowizard® system, but a license is needed to perform the analysis. AtomicJ is an open source JAVA™ application, which can be found in http://sourceforge.net/projects/jrobust in a compressed file, and can be employed by any user and able to open typical AFM-spectroscopy format files.

A.3.1. Linear indentation analysis

JPK Data Processing is able to compute the raw data from indentation analysis in terms of vertical deflection (d) vs piezo displacement (z), needed to obtain bacterial spring constant values[231]. Thus, the user can browse and load the raw data curves that will be displayed on the panel (Figure A.4). The user can set the contact point (zero force) and adjust the baseline by selection the range in the non-contact region of the curve.

Then, a straight line can be drawn delimiting the range of the curve to be adjusted. For this thesis, the slope before the rupture point down to 120 nm of the piezo displacement was measured. The software provides the value of the slope in the corresponding units (nm/μm), which must be converted in such a way that it is dimensionless (nm/nm).

Once the slope is obtained (s = 0.2936), Equation A.6 can be applied to obtain the bacterial spring constant (k_b), using the k_c calculated by thermal noise method[188] before every experiment (k_c = 0.2714 N/m for this case):

$$k_b = k_c \cdot \frac{s}{1-s} = 0.2714 \cdot \frac{0.2936}{1-0.2936} = 0.113 \ {}^{N}/_{m}$$

It should be noted that using a stiffer cantilever will increase the indentation of the cantilever (i.e. lower value of the slope), potentially making AFM measurements more destructive, but this would not change the spring constant of the bacterium. When imaging a hard surface (green line - reference) with an essentially infinite spring constant, such as a glass slide, s = 1 (nm/nm); $\Delta d/\Delta z$= 1, so: $\Delta d = \Delta z$. This means that all the piezo displacement is translated into only deflecting the cantilever and no indentation occurs on the sample. This is useful to appreciate visually how much a sample is being deformed based on the cantilever stiffness.

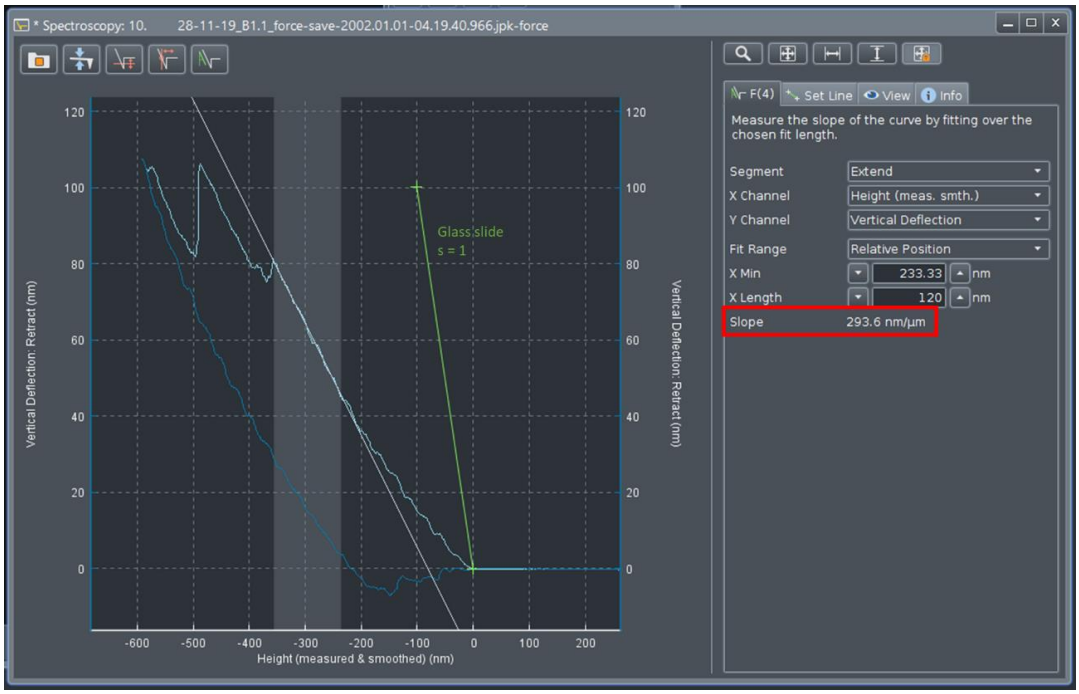

Figure A.4: JPK data processing. Screenshot of the JPK Data Processing software representing vertical deflection (*d*) – piezo displacement (*z*) curve of an *E. coli* cell, where the slope (white line) is obtained from the linear region of the approach curve (light blue line). Green line represents the same data recorded on the glass slide, where the whole piezo displacement fully corresponds to the deflection of the cantilever, with no indentation. Dark blue line corresponds to the retract part of the curve.

A.3.2. Non-linear indentation analysis

AtomicJ software was used to extract the Young´s Modulus from non-linear force (*F*) – indentation (δ) curves based on the Hertz-Sneddon model for spherical indenters[249]. The program computes the raw data and automatically converts it to *F-d* curves, subtracting the cantilever deflection in each point. In the processing panel (Figure A.5A), the user has to introduce the parameters necessary for fitting: Tip geometry (i.e. spherical), tip radius (i.e. 8 nm), Poisson ratio (i.e. 0.5 for biological samples), the baseline order (1-straight), the cantilever stiffness and sensitivity (in this case, they are automatically read from the JPK file) and the contact point algorithm. Here, user can both choose it visually (manual) or use iterative methods available on the software (automatic). In this thesis, manual estimation was chosen for those curves where there was an evident deviation of the contact point.

Once all parameters were introduced, the program presents the result of the fitting. Figure A.5B shows the analyzed force – distance curve, the estimated contact point (i.e. the point where the fit starts - red spot) and the transition point (i.e. the point which limits the fitting range - blue spot). The user now can move this point, in order to fit the desired range. As said in Appendix A, this point was 50 nm as a criterion. In the

"Indentation" tab (Figure A.5C), user can check how accurate the fit is to the selected model (green points are the experimental data, red line is the model fitting). Finally, a table with all the result is displayed as shown in Figure A.5D, showing the desired value of *E*, with the r^2 value related to the fitting.

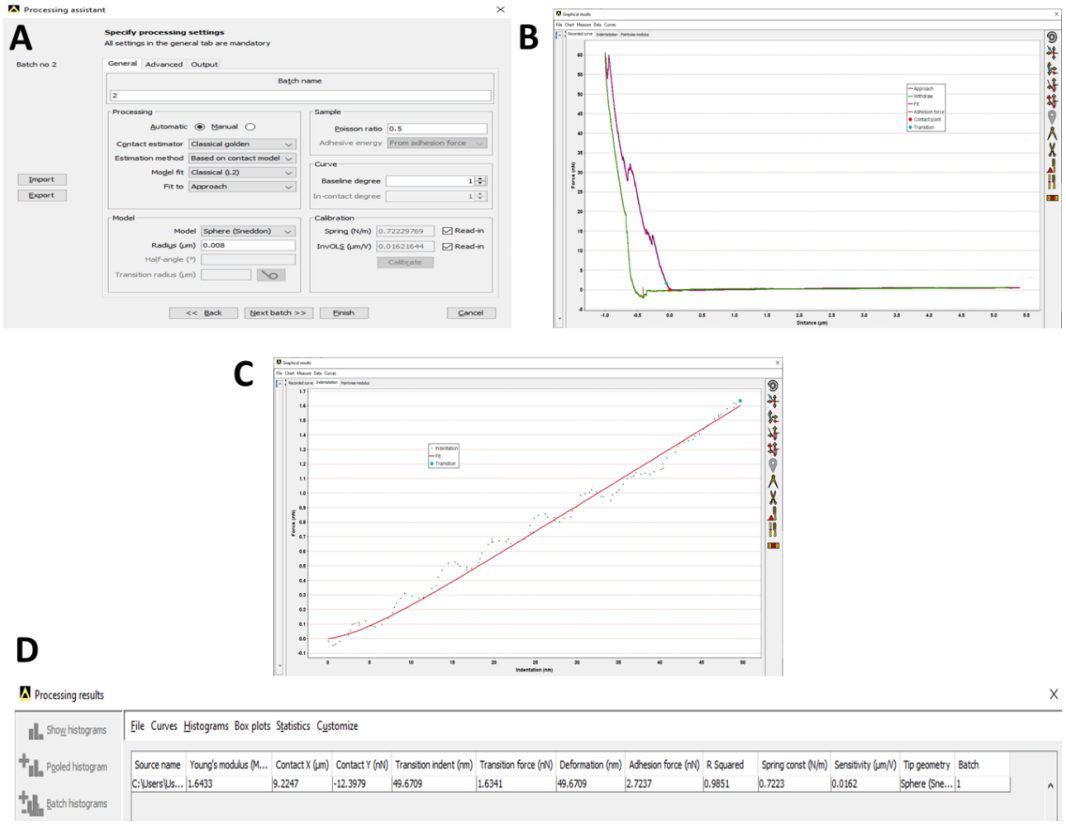

Figure A.5: AtomicJ data processing. Screenshots of the AtomicJ software analysis. (A) Processing assistant of the force-distance curves, where the key parameters of the fitting have to be introduced. (B) Force-distance curve (purple-approach and green-retract line) according to the estimated contact point (red spot) and the chosen transition point (blue spot) chosen. (C) Force-Indentation curve used for the fitted range (green points are experimental data and red line the fitting curve). (D) Summary of the results obtained for the fitting with the Hertz-Sneddon model.

A.4. Conclusion

Values of Young´s Modulus and bacterial spring constant presented above are in agreement with previous values for *E. coli* reported in bibliography[164, 232, 235, 263], and quite similar between PLL and Cell-Tak™. As said in Chapter 4, this was expected, due to a low impact of the adhesive on the cells during the immobilization process. Small differences observed are in agreement to the presence of the protein layer at the bottom of *E. coli* cells immobilized in Cell-Tak™, and in accordance with the values of the breaking force and indentation depth obtained in Chapter 4, where the bacteria immobilized in the Cell-Tak™ have a slightly higher breaking point, with a lower breaking indentation giving them some extra protection.

On the other hand, it is necessary to mention that due to the nature of the sharp tips used to perform the rupture of the bacterial membrane, the values of elasticity obtained for the first 50 nm would correspond to the local bacterial envelope and not for the whole bacterium. Indenting soft biological samples with sharps tips enables the measurement of mechanical properties, but only locally. This is very useful to characterize an inhomogeneous material within multiple materials or composition, but when trying to quantify a material as a whole, colloidal tips should be used to integrate properties over large indentation areas. Complex computational models are required to study a soft material in its whole, considering the substrate effect during indentation and precisely calculating the contact area between the tip and the sample, especially for sharps tips, where the sample will wrap the tip as the indentation is deeper.

References

References

1. Whitman, W. B.; Coleman, D. C.; Wiebe, W. J., Prokaryotes: The unseen majority. *Proceedings of the National Academy of Sciences* **1998,** *95* (12), 6578-6583.
2. Bacterial World. http://www.oum.ox.ac.uk/bacterialworld/.
3. Cooper, G. M., *The Cell: A Molecular Approach*. 2nd ed.; Sinauer Associates: 2000.
4. Zilber-Rosenberg, I.; Rosenberg, E., Role of microorganisms in the evolution of animals and plants: the hologenome theory of evolution. *FEMS Microbiology Reviews* **2008,** *32* (5), 723-735.
5. Pírez, M.; Mota, M., Morfología y estructura bacteriana. In *TEMAS DE BACTERIOLOGÍA Y VIROLOGÍA MÉDICA*, 2nd ed.; Oficina del libro FEFMUR: 2006.
6. What Is a Cell? https://www.nature.com/scitable/topicpage/what-is-a-cell-14023083/.
7. Auer, G. K.; Weibel, D. B., Bacterial Cell Mechanics. *Biochemistry* **2017,** *56* (29), 3710-3724.
8. Salton, M. R. J.; Kim, K.-S., Chapter 2: Structure. In *Medical Microbiology*, 4th ed.; Baron, S., Ed. University of Texas Medical Branch at Galveston: 1996.
9. Silhavy, T. J.; Kahne, D.; Walker, S., The bacterial cell envelope. *Cold Spring Harb Perspect Biol* **2010,** *2* (5), a000414-a000414.
10. Slavin, Y. N.; Asnis, J.; Häfeli, U. O.; Bach, H., Metal nanoparticles: understanding the mechanisms behind antibacterial activity. *Journal of Nanobiotechnology* **2017,** *15* (1), 65.
11. Kaiser, G. 2.2: The Cytoplasmic Membrane. https://bio.libretexts.org/Bookshelves/Microbiology/Book:_Microbiology_(Kaiser)/Unit_1:_Introduction_to_Microbiology_and_Prokaryotic_Cell_Anatomy/2:_The_Prokaryotic_Cell_-_Bacteria/2.2:_The_Cytoplasmic_Membrane.
12. Madigan, M. T.; Martinko, J. M.; Brock, T. D., *Brock biology of microorganisms*. Pearson Prentice Hall: Upper Saddle River, NJ, 1997.
13. Harvey, R. A.; Fisher, B. D.; Champe, P. C., *Microbiology*. 2nd ed.; 2007.
14. Gram, H. C., Über die isolierte Färbung der Schizomyceten in Schnitt- und Trockenpräparaten. *Fortschritte der Medizin (in German)* **1884,** *2*, 185–189.
15. Rogers, K.; Kadner, R. J. Bacteria. https://www.britannica.com/science/bacteria.
16. Luckey, T. D., Introduction to intestinal microecology. *The American Journal of Clinical Nutrition* **1972,** *25* (12), 1292-1294.
17. Sender, R.; Fuchs, S.; Milo, R., Revised Estimates for the Number of Human and Bacteria Cells in the Body. *PLOS Biology* **2016,** *14* (8), e1002533.
18. Mas-Moruno, C.; Su, B.; Dalby, M. J., Multifunctional Coatings and Nanotopographies: Toward Cell Instructive and Antibacterial Implants. *Advanced Healthcare Materials* **2019,** *8* (1), 1801103.
19. Goodman, S. B.; Yao, Z.; Keeney, M.; Yang, F., The future of biologic coatings for orthopaedic implants. *Biomaterials* **2013,** *34* (13), 3174-3183.
20. Busscher, H. J.; van der Mei, H. C.; Subbiahdoss, G.; Jutte, P. C.; van den Dungen, J. J. A. M.; Zaat, S. A. J.; Schultz, M. J.; Grainger, D. W., Biomaterial-Associated Infection: Locating the Finish Line in the Race for the Surface. *Science Translational Medicine* **2012,** *4* (153), 153rv10.
21. Norowski Jr, P. A.; Bumgardner, J. D., Biomaterial and antibiotic strategies for peri-implantitis: A review. *Journal of Biomedical Materials Research Part B: Applied Biomaterials* **2009,** *88B* (2), 530-543.
22. Banerjee, I.; Pangule, R. C.; Kane, R. S., Antifouling Coatings: Recent Developments in the Design of Surfaces That Prevent Fouling by Proteins, Bacteria, and Marine Organisms. *Advanced Materials* **2011,** *23* (6), 690-718.

23. Glinel, K.; Thebault, P.; Humblot, V.; Pradier, C. M.; Jouenne, T., Antibacterial surfaces developed from bio-inspired approaches. *Acta Biomaterialia* **2012,** *8* (5), 1670-1684.
24. Zhang, L.; Ning, C.; Zhou, T.; Liu, X.; Yeung, K. W. K.; Zhang, T.; Xu, Z.; Wang, X.; Wu, S.; Chu, P. K., Polymeric Nanoarchitectures on Ti-Based Implants for Antibacterial Applications. *ACS Applied Materials & Interfaces* **2014,** *6* (20), 17323-17345.
25. Hetrick, E. M.; Schoenfisch, M. H., Reducing implant-related infections: active release strategies. *Chemical Society Reviews* **2006,** *35* (9), 780-789.
26. Hickok, N. J.; Shapiro, I. M., Immobilized antibiotics to prevent orthopaedic implant infections. *Advanced Drug Delivery Reviews* **2012,** *64* (12), 1165-1176.
27. Boucher, H. W.; Talbot, G. H.; Bradley, J. S.; Edwards, J. E.; Gilbert, D.; Rice, L. B.; Scheld, M.; Spellberg, B.; Bartlett, J., Bad Bugs, No Drugs: No ESKAPE! An Update from the Infectious Diseases Society of America. *Clinical Infectious Diseases* **2009,** *48* (1), 1-12.
28. Levy, S. B.; Marshall, B., Antibacterial resistance worldwide: causes, challenges and responses. *Nature Medicine* **2004,** *10* (12), S122-S129.
29. Veerachamy, S.; Yarlagadda, T.; Manivasagam, G.; Yarlagadda, P. K. D. V., Bacterial adherence and biofilm formation on medical implants: A review. *Proceedings of the Institution of Mechanical Engineers, Part H: Journal of Engineering in Medicine* **2014,** *228* (10), 1083-1099.
30. Gristina, A. G., Biomaterial-centered infection: microbial adhesion versus tissue integration. *Science* **1987,** *237* (4822), 1588-1595.
31. Donlan, R. M., Biofilms: microbial life on surfaces. *Emerg Infect Dis* **2002,** *8* (9), 881-890.
32. Costerton, J. W., Introduction to biofilm. *International Journal of Antimicrobial Agents* **1999,** *11* (3), 217-221.
33. Costerton, J. W.; Stewart, P. S.; Greenberg, E. P., Bacterial Biofilms: A Common Cause of Persistent Infections. *Science* **1999,** *284* (5418), 1318-1322.
34. Elbourne, A.; Crawford, R. J.; Ivanova, E. P., Nano-structured antimicrobial surfaces: From nature to synthetic analogues. *Journal of Colloid and Interface Science* **2017,** *508*, 603-616.
35. Hasan, J.; Crawford, R. J.; Ivanova, E. P., Antibacterial surfaces: the quest for a new generation of biomaterials. *Trends in Biotechnology* **2013,** *31* (5), 295-304.
36. Neoh, K. G.; Kang, E. T., Combating Bacterial Colonization on Metals via Polymer Coatings: Relevance to Marine and Medical Applications. *ACS Applied Materials & Interfaces* **2011,** *3* (8), 2808-2819.
37. Harris, L. G.; Tosatti, S.; Wieland, M.; Textor, M.; Richards, R. G., Staphylococcus aureus adhesion to titanium oxide surfaces coated with non-functionalized and peptide-functionalized poly(l-lysine)-grafted-poly(ethylene glycol) copolymers. *Biomaterials* **2004,** *25* (18), 4135-4148.
38. Lin, N.; Berton, P.; Moraes, C.; Rogers, R. D.; Tufenkji, N., Nanodarts, nanoblades, and nanospikes: Mechano-bactericidal nanostructures and where to find them. *Advances in Colloid and Interface Science* **2018,** *252*, 55-68.
39. Tuson, H. H.; Weibel, D. B., Bacteria–surface interactions. *Soft Matter* **2013,** *9* (17), 4368-4380.
40. Lejeune, P., Contamination of abiotic surfaces: what a colonizing bacterium sees and how to blur it. *Trends in Microbiology* **2003,** *11* (4), 179-184.
41. Bazaka, K.; Crawford, R. J.; Ivanova, E. P., Do bacteria differentiate between degrees of nanoscale surface roughness? *Biotechnology Journal* **2011,** *6* (9), 1103-1114.
42. Anselme, K.; Davidson, P.; Popa, A. M.; Giazzon, M.; Liley, M.; Ploux, L., The interaction of cells and bacteria with surfaces structured at the nanometre scale. *Acta Biomaterialia* **2010,** *6* (10), 3824-3846.
43. Wang, Z.; Zhu, W.; Qiu, Y.; Yi, X.; von dem Bussche, A.; Kane, A.; Gao, H.; Koski, K.; Hurt, R., Biological and environmental interactions of emerging two-dimensional nanomaterials. *Chemical Society Reviews* **2016,** *45* (6), 1750-1780.

44. Kang, S.; Pinault, M.; Pfefferle, L. D.; Elimelech, M., Single-Walled Carbon Nanotubes Exhibit Strong Antimicrobial Activity. *Langmuir* **2007,** *23* (17), 8670-8673.
45. Liu, S.; Wei, L.; Hao, L.; Fang, N.; Chang, M. W.; Xu, R.; Yang, Y.; Chen, Y., Sharper and Faster "Nano Darts" Kill More Bacteria: A Study of Antibacterial Activity of Individually Dispersed Pristine Single-Walled Carbon Nanotube. *ACS Nano* **2009,** *3* (12), 3891-3902.
46. Liu, S.; Ng, A. K.; Xu, R.; Wei, J.; Tan, C. M.; Yang, Y.; Chen, Y., Antibacterial action of dispersed single-walled carbon nanotubes on Escherichia coli and Bacillus subtilis investigated by atomic force microscopy. *Nanoscale* **2010,** *2* (12), 2744-2750.
47. Liu, S.; Zeng, T. H.; Hofmann, M.; Burcombe, E.; Wei, J.; Jiang, R.; Kong, J.; Chen, Y., Antibacterial Activity of Graphite, Graphite Oxide, Graphene Oxide, and Reduced Graphene Oxide: Membrane and Oxidative Stress. *ACS Nano* **2011,** *5* (9), 6971-6980.
48. Hu, W.; Peng, C.; Luo, W.; Lv, M.; Li, X.; Li, D.; Huang, Q.; Fan, C., Graphene-Based Antibacterial Paper. *ACS Nano* **2010,** *4* (7), 4317-4323.
49. Akhavan, O.; Ghaderi, E., Toxicity of Graphene and Graphene Oxide Nanowalls Against Bacteria. *ACS Nano* **2010,** *4* (10), 5731-5736.
50. Palmieri, V.; Bugli, F.; Lauriola, M. C.; Cacaci, M.; Torelli, R.; Ciasca, G.; Conti, C.; Sanguinetti, M.; Papi, M.; De Spirito, M., Bacteria Meet Graphene: Modulation of Graphene Oxide Nanosheet Interaction with Human Pathogens for Effective Antimicrobial Therapy. *ACS Biomaterials Science & Engineering* **2017,** *3* (4), 619-627.
51. Linklater, D. P.; Baulin, V. A.; Juodkazis, S.; Ivanova, E. P., Mechano-bactericidal mechanism of graphene nanomaterials. *Interface Focus* **2018,** *8* (3), 20170060-20170060.
52. Mao, J.; Guo, R.; Yan, L.-T., Simulation and analysis of cellular internalization pathways and membrane perturbation for graphene nanosheets. *Biomaterials* **2014,** *35* (23), 6069-6077.
53. Chen, J.; Wang, X.; Han, H., A new function of graphene oxide emerges: inactivating phytopathogenic bacterium Xanthomonas oryzae pv. Oryzae. *Journal of Nanoparticle Research* **2013,** *15* (5), 1658.
54. Negoda, A.; Liu, Y.; Hou, W.-C.; Corredor, C.; Moghadam, B. Y.; Musolff, C.; Li, L.; Walker, W.; Westerhoff, P.; Mason, A. J.; Duxbury, P.; Posner, J. D.; Worden, R. M., Engineered nanomaterial interactions with bilayer lipid membranes: screening platforms to assess nanoparticle toxicity. *International Journal of Biomedical Nanoscience and Nanotechnology* **2013,** *3* (1-2), 52-83.
55. Moghadam, B. Y.; Hou, W.-C.; Corredor, C.; Westerhoff, P.; Posner, J. D., Role of nanoparticle surface functionality in the disruption of model cell membranes. *Langmuir : the ACS journal of surfaces and colloids* **2012,** *28* (47), 16318-16326.
56. Suresh, A. K.; Pelletier, D. A.; Doktycz, M. J., Relating nanomaterial properties and microbial toxicity. *Nanoscale* **2013,** *5* (2), 463-474.
57. Wang, L.; Hu, C.; Shao, L., The antimicrobial activity of nanoparticles: present situation and prospects for the future. *Int J Nanomedicine* **2017,** *12*, 1227-1249.
58. Tu, Y.; Lv, M.; Xiu, P.; Huynh, T.; Zhang, M.; Castelli, M.; Liu, Z.; Huang, Q.; Fan, C.; Fang, H.; Zhou, R., Destructive extraction of phospholipids from Escherichia coli membranes by graphene nanosheets. *Nature Nanotechnology* **2013,** *8* (8), 594-601.
59. Pham, V. T. H.; Truong, V. K.; Quinn, M. D. J.; Notley, S. M.; Guo, Y.; Baulin, V. A.; Al Kobaisi, M.; Crawford, R. J.; Ivanova, E. P., Graphene Induces Formation of Pores That Kill Spherical and Rod-Shaped Bacteria. *ACS Nano* **2015,** *9* (8), 8458-8467.
60. Perreault, F.; de Faria, A. F.; Nejati, S.; Elimelech, M., Antimicrobial Properties of Graphene Oxide Nanosheets: Why Size Matters. *ACS Nano* **2015,** *9* (7), 7226-7236.
61. Chong, Y.; Ge, C.; Fang, G.; Wu, R.; Zhang, H.; Chai, Z.; Chen, C.; Yin, J.-J., Light-Enhanced Antibacterial Activity of Graphene Oxide, Mainly via Accelerated Electron Transfer. *Environmental Science & Technology* **2017,** *51* (17), 10154-10161.
62. Elbourne, A.; Chapman, J.; Gelmi, A.; Cozzolino, D.; Crawford, R. J.; Truong, V. K., Bacterial-nanostructure interactions: The role of cell elasticity and adhesion forces. *Journal of Colloid and Interface Science* **2019,** *546*, 192-210.

63. Tripathy, A.; Sen, P.; Su, B.; Briscoe, W. H., Natural and bioinspired nanostructured bactericidal surfaces. *Advances in Colloid and Interface Science* **2017,** *248*, 85-104.
64. Ivanova, E. P.; Hasan, J.; Webb, H. K.; Truong, V. K.; Watson, G. S.; Watson, J. A.; Baulin, V. A.; Pogodin, S.; Wang, J. Y.; Tobin, M. J.; Löbbe, C.; Crawford, R. J., Natural Bactericidal Surfaces: Mechanical Rupture of Pseudomonas aeruginosa Cells by Cicada Wings. *Small* **2012,** *8* (16), 2489-2494.
65. Gangadoo, S.; Chandra, S.; Power, A.; Hellio, C.; Watson, G. S.; Watson, J. A.; Green, D. W.; Chapman, J., Biomimetics for early stage biofouling prevention: templates from insect cuticles. *Journal of Materials Chemistry B* **2016,** *4* (34), 5747-5754.
66. Hasan, J.; Webb, H. K.; Truong, V. K.; Pogodin, S.; Baulin, V. A.; Watson, G. S.; Watson, J. A.; Crawford, R. J.; Ivanova, E. P., Selective bactericidal activity of nanopatterned superhydrophobic cicada Psaltoda claripennis wing surfaces. *Applied Microbiology and Biotechnology* **2013,** *97* (20), 9257-9262.
67. Hasan, J.; Webb, H. K.; Truong, V. K.; Watson, G. S.; Watson, J. A.; Tobin, M. J.; Gervinskas, G.; Juodkazis, S.; Wang, J. Y.; Crawford, R. J.; Ivanova, E. P., Spatial Variations and Temporal Metastability of the Self-Cleaning and Superhydrophobic Properties of Damselfly Wings. *Langmuir* **2012,** *28* (50), 17404-17409.
68. Truong, V. K.; Geeganagamage, N. M.; Baulin, V. A.; Vongsvivut, J.; Tobin, M. J.; Luque, P.; Crawford, R. J.; Ivanova, E. P., The susceptibility of Staphylococcus aureus CIP 65.8 and Pseudomonas aeruginosa ATCC 9721 cells to the bactericidal action of nanostructured Calopteryx haemorrhoidalis damselfly wing surfaces. *Applied Microbiology and Biotechnology* **2017,** *101* (11), 4683-4690.
69. Bandara, C. D.; Singh, S.; Afara, I. O.; Wolff, A.; Tesfamichael, T.; Ostrikov, K.; Oloyede, A., Bactericidal Effects of Natural Nanotopography of Dragonfly Wing on Escherichia coli. *ACS Applied Materials & Interfaces* **2017,** *9* (8), 6746-6760.
70. Mainwaring, D. E.; Nguyen, S. H.; Webb, H.; Jakubov, T.; Tobin, M.; Lamb, R. N.; Wu, A. H. F.; Marchant, R.; Crawford, R. J.; Ivanova, E. P., The nature of inherent bactericidal activity: insights from the nanotopology of three species of dragonfly. *Nanoscale* **2016,** *8* (12), 6527-6534.
71. Kelleher, S. M.; Habimana, O.; Lawler, J.; O' Reilly, B.; Daniels, S.; Casey, E.; Cowley, A., Cicada Wing Surface Topography: An Investigation into the Bactericidal Properties of Nanostructural Features. *ACS Applied Materials & Interfaces* **2016,** *8* (24), 14966-14974.
72. Watson, G. S.; Green, D. W.; Schwarzkopf, L.; Li, X.; Cribb, B. W.; Myhra, S.; Watson, J. A., A gecko skin micro/nano structure – A low adhesion, superhydrophobic, anti-wetting, self-cleaning, biocompatible, antibacterial surface. *Acta Biomaterialia* **2015,** *21*, 109-122.
73. Green, D. W.; Lee, K. K.-H.; Watson, J. A.; Kim, H.-Y.; Yoon, K.-S.; Kim, E.-J.; Lee, J.-M.; Watson, G. S.; Jung, H.-S., High Quality Bioreplication of Intricate Nanostructures from a Fragile Gecko Skin Surface with Bactericidal Properties. *Scientific Reports* **2017,** *7* (1), 41023.
74. Li, X.; Cheung, G. S.; Watson, G. S.; Watson, J. A.; Lin, S.; Schwarzkopf, L.; Green, D. W., The nanotipped hairs of gecko skin and biotemplated replicas impair and/or kill pathogenic bacteria with high efficiency. *Nanoscale* **2016,** *8* (45), 18860-18869.
75. Liu, K.; Jiang, L., Bio-inspired design of multiscale structures for function integration. *Nano Today* **2011,** *6* (2), 155-175.
76. Minoura, K.; Yamada, M.; Mizoguchi, T.; Kaneko, T.; Nishiyama, K.; Ozminskyj, M.; Koshizuka, T.; Wada, I.; Suzutani, T., Antibacterial effects of the artificial surface of nanoimprinted moth-eye film. *PLOS ONE* **2017,** *12* (9), e0185366.
77. Viela, F.; Navarro-Baena, I.; Hernández, J. J.; Osorio, M. R.; Rodríguez, I., Moth-eye mimetic cytocompatible bactericidal nanotopography: a convergent design. *Bioinspiration & Biomimetics* **2018,** *13* (2), 026011.
78. Viela, F.; Navarro-Baena, I.; Jacobo-Martín, A.; Hernández, J. J.; Boyano-Escalera, M.; Osorio, M. R.; Rodríguez, I., Nano-engineering safer-by-design nanoparticle based moth-eye

mimetic bactericidal and cytocompatible polymer surfaces. *RSC Advances* **2018,** *8* (40), 22606-22616.
79. Yamada, M.; Minoura, K.; Mizoguchi, T.; Nakamatsu, K.; Taguchi, T.; Kameda, T.; Sekiguchi, M.; Suzutani, T.; Konno, S., Antibacterial effects of nanoimprinted moth-eye film in practical settings. *bioRxiv* **2018**, 325837.
80. Linklater, D. P.; Juodkazis, S.; Ivanova, E. P., Nanofabrication of mechano-bactericidal surfaces. *Nanoscale* **2017,** *9* (43), 16564-16585.
81. Ivanova, E. P.; Hasan, J.; Webb, H. K.; Gervinskas, G.; Juodkazis, S.; Truong, V. K.; Wu, A. H. F.; Lamb, R. N.; Baulin, V. A.; Watson, G. S.; Watson, J. A.; Mainwaring, D. E.; Crawford, R. J., Bactericidal activity of black silicon. *Nature Communications* **2013,** *4* (1), 2838.
82. Pogodin, S.; Hasan, J.; Baulin, V. A.; Webb, H. K.; Truong, V. K.; Phong Nguyen, T. H.; Boshkovikj, V.; Fluke, C. J.; Watson, G. S.; Watson, J. A.; Crawford, R. J.; Ivanova, E. P., Biophysical model of bacterial cell interactions with nanopatterned cicada wing surfaces. *Biophys J* **2013,** *104* (4), 835-840.
83. Fisher, L. E.; Yang, Y.; Yuen, M.-F.; Zhang, W.; Nobbs, A. H.; Su, B., Bactericidal activity of biomimetic diamond nanocone surfaces. *Biointerphases* **2016,** *11* (1), 011014.
84. Hu, H.; Siu, V. S.; Gifford, S. M.; Kim, S.; Lu, M.; Meyer, P.; Stolovitzky, G. A., Bio-inspired silicon nanospikes fabricated by metal-assisted chemical etching for antibacterial surfaces. *Applied Physics Letters* **2017,** *111* (25), 253701.
85. Linklater, D. P.; Nguyen, H. K. D.; Bhadra, C. M.; Juodkazis, S.; Ivanova, E. P., Influence of nanoscale topology on bactericidal efficiency of black silicon surfaces. *Nanotechnology* **2017,** *28* (24), 245301.
86. Susarrey-Arce, A.; Sorzabal-Bellido, I.; Oknianska, A.; McBride, F.; Beckett, A. J.; Gardeniers, J. G. E.; Raval, R.; Tiggelaar, R. M.; Diaz Fernandez, Y. A., Bacterial viability on chemically modified silicon nanowire arrays. *Journal of Materials Chemistry B* **2016,** *4* (18), 3104-3112.
87. May, P. W.; Clegg, M.; Silva, T. A.; Zanin, H.; Fatibello-Filho, O.; Celorrio, V.; Fermin, D. J.; Welch, C. C.; Hazell, G.; Fisher, L.; Nobbs, A.; Su, B., Diamond-coated 'black silicon' as a promising material for high-surface-area electrochemical electrodes and antibacterial surfaces. *Journal of Materials Chemistry B* **2016,** *4* (34), 5737-5746.
88. Hazell, G.; May, P. W.; Taylor, P.; Nobbs, A. H.; Welch, C. C.; Su, B., Studies of black silicon and black diamond as materials for antibacterial surfaces. *Biomaterials Science* **2018,** *6* (6), 1424-1432.
89. Diu, T.; Faruqui, N.; Sjöström, T.; Lamarre, B.; Jenkinson, H. F.; Su, B.; Ryadnov, M. G., Cicada-inspired cell-instructive nanopatterned arrays. *Scientific Reports* **2014,** *4* (1), 7122.
90. Bhadra, C. M.; Khanh Truong, V.; Pham, V. T. H.; Al Kobaisi, M.; Seniutinas, G.; Wang, J. Y.; Juodkazis, S.; Crawford, R. J.; Ivanova, E. P., Antibacterial titanium nano-patterned arrays inspired by dragonfly wings. *Scientific Reports* **2015,** *5* (1), 16817.
91. Cao, Y.; Su, B.; Chinnaraj, S.; Jana, S.; Bowen, L.; Charlton, S.; Duan, P.; Jakubovics, N. S.; Chen, J., Nanostructured titanium surfaces exhibit recalcitrance towards Staphylococcus epidermidis biofilm formation. *Scientific Reports* **2018,** *8* (1), 1071.
92. Jaggessar, A.; Mathew, A.; Wang, H.; Tesfamichael, T.; Yan, C.; Yarlagadda, P. K. D. V., Mechanical, bactericidal and osteogenic behaviours of hydrothermally synthesised TiO2 nanowire arrays. *Journal of the Mechanical Behavior of Biomedical Materials* **2018,** *80*, 311-319.
93. Sengstock, C.; Lopian, M.; Motemani, Y.; Borgmann, A.; Khare, C.; Buenconsejo, P. J. S.; Schildhauer, T. A.; Ludwig, A.; Köller, M., Structure-related antibacterial activity of a titanium nanostructured surface fabricated by glancing angle sputter deposition. *Nanotechnology* **2014,** *25* (19), 195101.
94. Hasan, J.; Jain, S.; Chatterjee, K., Nanoscale Topography on Black Titanium Imparts Multi-biofunctional Properties for Orthopedic Applications. *Scientific Reports* **2017,** *7* (1), 41118.

95. Sjöström, T.; Nobbs, A. H.; Su, B., Bactericidal nanospike surfaces via thermal oxidation of Ti alloy substrates. *Materials Letters* **2016,** *167*, 22-26.
96. Sakamoto, A.; Terui, Y.; Horie, C.; Fukui, T.; Masuzawa, T.; Sugawara, S.; Shigeta, K.; Shigeta, T.; Igarashi, K.; Kashiwagi, K., Antibacterial effects of protruding and recessed shark skin micropatterned surfaces of polyacrylate plate with a shallow groove. *FEMS Microbiology Letters* **2014,** *361* (1), 10-16.
97. Dickson, M. N.; Liang, E. I.; Rodriguez, L. A.; Vollereaux, N.; Yee, A. F., Nanopatterned polymer surfaces with bactericidal properties. *Biointerphases* **2015,** *10* (2), 021010-021010.
98. Chung, K. K.; Schumacher, J. F.; Sampson, E. M.; Burne, R. A.; Antonelli, P. J.; Brennan, A. B., Impact of engineered surface microtopography on biofilm formation of Staphylococcus aureus. *Biointerphases* **2007,** *2* (2), 89-94.
99. Linklater, D. P.; De Volder, M.; Baulin, V. A.; Werner, M.; Jessl, S.; Golozar, M.; Maggini, L.; Rubanov, S.; Hanssen, E.; Juodkazis, S.; Ivanova, E. P., High Aspect Ratio Nanostructures Kill Bacteria via Storage and Release of Mechanical Energy. *ACS Nano* **2018,** *12* (7), 6657-6667.
100. Wu, S.; Zuber, F.; Brugger, J.; Maniura-Weber, K.; Ren, Q., Antibacterial Au nanostructured surfaces. *Nanoscale* **2016,** *8* (5), 2620-2625.
101. Garnett, E.; Yang, P., Light Trapping in Silicon Nanowire Solar Cells. *Nano Letters* **2010,** *10* (3), 1082-1087.
102. Oh, J.; Yuan, H.-C.; Branz, H. M., An 18.2%-efficient black-silicon solar cell achieved through control of carrier recombination in nanostructures. *Nature Nanotechnology* **2012,** *7* (11), 743-748.
103. Yuan, H.-C.; Yost, V. E.; Page, M. R.; Stradins, P.; Meier, D. L.; Branz, H. M., Efficient black silicon solar cell with a density-graded nanoporous surface: Optical properties, performance limitations, and design rules. *Applied Physics Letters* **2009,** *95* (12), 123501.
104. Jeon, H. C.; Heo, C.-J.; Lee, S. Y.; Yang, S.-M., Hierarchically Ordered Arrays of Noncircular Silicon Nanowires Featured by Holographic Lithography Toward a High-Fidelity Sensing Platform. *Advanced Functional Materials* **2012,** *22* (20), 4268-4274.
105. Kim, W.; Ng, J. K.; Kunitake, M. E.; Conklin, B. R.; Yang, P., Interfacing Silicon Nanowires with Mammalian Cells. *Journal of the American Chemical Society* **2007,** *129* (23), 7228-7229.
106. Shalek, A. K.; Robinson, J. T.; Karp, E. S.; Lee, J. S.; Ahn, D.-R.; Yoon, M.-H.; Sutton, A.; Jorgolli, M.; Gertner, R. S.; Gujral, T. S.; MacBeath, G.; Yang, E. G.; Park, H., Vertical silicon nanowires as a universal platform for delivering biomolecules into living cells. *Proceedings of the National Academy of Sciences* **2010,** *107* (5), 1870.
107. Chen, L.; Liu, X.; Su, B.; Li, J.; Jiang, L.; Han, D.; Wang, S., Aptamer-Mediated Efficient Capture and Release of T Lymphocytes on Nanostructured Surfaces. *Advanced Materials* **2011,** *23* (38), 4376-4380.
108. Lee, S.-K.; Kim, G.-S.; Wu, Y.; Kim, D.-J.; Lu, Y.; Kwak, M.; Han, L.; Hyung, J.-H.; Seol, J.-K.; Sander, C.; Gonzalez, A.; Li, J.; Fan, R., Nanowire Substrate-Based Laser Scanning Cytometry for Quantitation of Circulating Tumor Cells. *Nano Letters* **2012,** *12* (6), 2697-2704.
109. Nguyen, D. H. K.; Pham, V. T. H.; Al Kobaisi, M.; Bhadra, C.; Orlowska, A.; Ghanaati, S.; Manzi, B. M.; Baulin, V. A.; Joudkazis, S.; Kingshott, P.; Crawford, R. J.; Ivanova, E. P., Adsorption of Human Plasma Albumin and Fibronectin onto Nanostructured Black Silicon Surfaces. *Langmuir* **2016,** *32* (41), 10744-10751.
110. Wang, X.; Bhadra, C. M.; Yen Dang, T. H.; Buividas, R.; Wang, J.; Crawford, R. J.; Ivanova, E. P.; Juodkazis, S., A bactericidal microfluidic device constructed using nano-textured black silicon. *RSC Advances* **2016,** *6* (31), 26300-26306.
111. Serrano, C.; García-Fernández, L.; Fernández-Blázquez, J. P.; Barbeck, M.; Ghanaati, S.; Unger, R.; Kirkpatrick, J.; Arzt, E.; Funk, L.; Turón, P.; del Campo, A., Nanostructured medical sutures with antibacterial properties. *Biomaterials* **2015,** *52*, 291-300.

112. Zheng, Y.; Li, J.; Liu, X.; Sun, J., Antimicrobial and osteogenic effect of Ag-implanted titanium with a nanostructured surface. *Int J Nanomedicine* **2012,** *7*, 875-884.
113. Tsimbouri, P. M.; Fisher, L.; Holloway, N.; Sjostrom, T.; Nobbs, A. H.; Meek, R. M. D.; Su, B.; Dalby, M. J., Osteogenic and bactericidal surfaces from hydrothermal titania nanowires on titanium substrates. *Scientific Reports* **2016,** *6* (1), 36857.
114. Hegab, H. M.; ElMekawy, A.; Zou, L.; Mulcahy, D.; Saint, C. P.; Ginic-Markovic, M., The controversial antibacterial activity of graphene-based materials. *Carbon* **2016,** *105*, 362-376.
115. Zou, X.; Zhang, L.; Wang, Z.; Luo, Y., Mechanisms of the Antimicrobial Activities of Graphene Materials. *Journal of the American Chemical Society* **2016,** *138* (7), 2064-2077.
116. Linklater, D. P.; Juodkazis, S.; Rubanov, S.; Ivanova, E. P., Comment on "Bactericidal Effects of Natural Nanotopography of Dragonfly Wing on Escherichia coli". *ACS Applied Materials & Interfaces* **2017,** *9* (35), 29387-29393.
117. Köller, M.; Ziegler, N.; Sengstock, C.; Schildhauer, T. A.; Ludwig, A., Bacterial cell division is involved in the damage of gram-negative bacteria on a nano-pillar titanium surface. *Biomedical Physics & Engineering Express* **2018,** *4* (5), 055002.
118. Romero-Vargas Castrillón, S.; Perreault, F.; de Faria, A. F.; Elimelech, M., Interaction of Graphene Oxide with Bacterial Cell Membranes: Insights from Force Spectroscopy. *Environmental Science & Technology Letters* **2015,** *2* (4), 112-117.
119. Suo, Z.; Avci, R.; Deliorman, M.; Yang, X.; Pascual, D. W., Bacteria Survive Multiple Puncturings of Their Cell Walls. *Langmuir* **2009,** *25* (8), 4588-4594.
120. Xue, F.; Liu, J.; Guo, L.; Zhang, L.; Li, Q., Theoretical study on the bactericidal nature of nanopatterned surfaces. *Journal of Theoretical Biology* **2015,** *385*, 1-7.
121. Rodrigues, D. F.; Elimelech, M., Toxic Effects of Single-Walled Carbon Nanotubes in the Development of E. coli Biofilm. *Environmental Science & Technology* **2010,** *44* (12), 4583-4589.
122. Brady-Estévez, A. S.; Kang, S.; Elimelech, M., A Single-Walled-Carbon-Nanotube Filter for Removal of Viral and Bacterial Pathogens. *Small* **2008,** *4* (4), 481-484.
123. Wang, Y.; Wang, J., Friction Determination by Atomic Force Microscopy in Field of Biochemical Science. *Micromachines* **2018,** *9* (7), 313.
124. Balke, N.; Jesse, S.; Carmichael, B.; Okatan, M. B.; Kravchenko, I. I.; Kalinin, S. V.; Tselev, A., Quantification of in-contact probe-sample electrostatic forces with dynamic atomic force microscopy. *Nanotechnology* **2017,** *28* (6), 065704.
125. Jiang, Y.; Turner, K. T., Measurement of the strength and range of adhesion using atomic force microscopy. *Extreme Mechanics Letters* **2016,** *9*, 119-126.
126. Wadas, A., Magnetic forces measured by atomic force microscopy. Theoretical approach. *Journal of Magnetism and Magnetic Materials* **1988,** *72* (3), 295-299.
127. Avila, A.; Bhushan, B., Electrical Measurement Techniques in Atomic Force Microscopy. *Critical Reviews in Solid State and Materials Sciences* **2010,** *35* (1), 38-51.
128. Thomas, G.; Burnham, N. A.; Camesano, T. A.; Wen, Q., Measuring the mechanical properties of living cells using atomic force microscopy. *J Vis Exp* **2013,** (76), 50497.
129. Kumar, S.; LeDuc, P. R., Dissecting the Molecular Basis of the Mechanics of Living Cells. *Experimental Mechanics* **2009,** *49* (1), 11-23.
130. Mertens, J.; Bondia, P.; Allende-Ballestero, C.; Carrascosa, J. L.; Flors, C.; Castón, J. R., Mechanics of Virus-like Particles Labeled with Green Fluorescent Protein. *Biophys J* **2018,** *115* (8), 1561-1568.
131. Vadillo-Rodriguez, V.; Beveridge, T. J.; Dutcher, J. R., Surface Viscoelasticity of Individual Gram-Negative Bacterial Cells Measured Using Atomic Force Microscopy. *Journal of Bacteriology* **2008,** *190* (12), 4225-4232.
132. Rief, M.; Gautel, M.; Oesterhelt, F.; Fernandez, J. M.; Gaub, H. E., Reversible Unfolding of Individual Titin Immunoglobulin Domains by AFM. *Science* **1997,** *276* (5315), 1109.

133. Hinterdorfer, P.; Baumgartner, W.; Gruber, H. J.; Schilcher, K.; Schindler, H., Detection and localization of individual antibody-antigen recognition events by atomic force microscopy. *Proc Natl Acad Sci U S A* **1996,** *93* (8), 3477-3481.
134. Binnig, G.; Quate, C. F.; Gerber, C., Atomic Force Microscope. *Physical Review Letters* **1986,** *56* (9), 930-933.
135. Binnig, G.; Rohrer, H.; Gerber, C.; Weibel, E., Surface Studies by Scanning Tunneling Microscopy. *Physical Review Letters* **1982,** *49* (1), 57-61.
136. Meyer, G.; Amer, N. M., Novel optical approach to atomic force microscopy. *Applied Physics Letters* **1988,** *53* (12), 1045-1047.
137. NanoWizard (R) AFM Handbook. Version 2.2a.
138. García, R.; Pérez, R., Dynamic atomic force microscopy methods. *Surface Science Reports* **2002,** *47* (6), 197-301.
139. de Pablo, P. J.; Colchero, J.; Gómez-Herrero, J.; Baró, A. M., Jumping mode scanning force microscopy. *Applied Physics Letters* **1998,** *73* (22), 3300-3302.
140. Eifert, A.; Kranz, C., Hyphenating Atomic Force Microscopy. *Analytical Chemistry* **2014,** *86* (11), 5190-5200.
141. Ando, T.; Bhamidimarri, S. P.; Brending, N.; Colin-York, H.; Collinson, L.; De Jonge, N.; de Pablo, P. J.; Debroye, E.; Eggeling, C.; Franck, C.; Fritzsche, M.; Gerritsen, H.; Giepmans, B. N. G.; Grunewald, K.; Hofkens, J.; Hoogenboom, J. P.; Janssen, K. P. F.; Kaufmann, R.; Klumperman, J.; Kurniawan, N.; Kusch, J.; Liv, N.; Parekh, V.; Peckys, D. B.; Rehfeldt, F.; Reutens, D. C.; Roeffaers, M. B. J.; Salditt, T.; Schaap, I. A. T.; Schwarz, U. S.; Verkade, P.; Vogel, M. W.; Wagner, R.; Winterhalter, M.; Yuan, H.; Zifarelli, G., The 2018 correlative microscopy techniques roadmap. *Journal of Physics D: Applied Physics* **2018,** *51* (44), 443001.
142. Zhou, L.; Cai, M.; Tong, T.; Wang, H., Progress in the Correlative Atomic Force Microscopy and Optical Microscopy. *Sensors* **2017,** *17* (4).
143. Hinterdorfer, P.; Schütz, G.; Kienberger, F.; Schindler, H., Detection and characterization of single biomolecules at surfaces. *Reviews in Molecular Biotechnology* **2001,** *82* (1), 25-35.
144. Dvorak, J. A., The application of atomic force microscopy to the study of living vertebrate cells in culture. *Methods* **2003,** *29* (1), 86-96.
145. Madl, J.; Rhode, S.; Stangl, H.; Stockinger, H.; Hinterdorfer, P.; Schütz, G. J.; Kada, G., A combined optical and atomic force microscope for live cell investigations. *Ultramicroscopy* **2006,** *106* (8), 645-651.
146. Hards, A.; Zhou, C.; Seitz, M.; Bräuchle, C.; Zumbusch, A., Simultaneous AFM Manipulation and Fluorescence Imaging of Single DNA Strands. *ChemPhysChem* **2005,** *6* (3), 534-540.
147. Wallace, M. I.; Molloy, J. E.; Trentham, D. R., Combined single-molecule force and fluorescence measurements for biology. *Journal of Biology* **2003,** *2* (3), 4.
148. Hecht, E.; Thompson, K.; Frick, M.; Wittekindt, O. H.; Dietl, P.; Mizaikoff, B.; Kranz, C., Combined Atomic Force Microscopy–Fluorescence Microscopy: Analyzing Exocytosis in Alveolar Type II Cells. *Analytical Chemistry* **2012,** *84* (13), 5716-5722.
149. Li, M.; Liu*, L.; Xi*, N.; Wang, Y.; Xiao, X.; Zhang, W., Quantitative Analysis of Drug-Induced Complement-Mediated Cytotoxic Effect on Single Tumor Cells Using Atomic Force Microscopy and Fluorescence Microscopy. *IEEE Transactions on NanoBioscience* **2015,** *14* (1), 84-94.
150. Fantner, G. E.; Barbero, R. J.; Gray, D. S.; Belcher, A. M., Kinetics of antimicrobial peptide activity measured on individual bacterial cells using high-speed atomic force microscopy. *Nature nanotechnology* **2010,** *5* (4), 280-285.
151. Kuyukina, M. S.; Ivshina, I. B.; Korshunova, I. O.; Rubtsova, E. V., Assessment of bacterial resistance to organic solvents using a combined confocal laser scanning and atomic force microscopy (CLSM/AFM). *Journal of Microbiological Methods* **2014,** *107*, 23-29.

152. Nishida, S.; Funabashi, Y.; Ikai, A., Combination of AFM with an objective-type total internal reflection fluorescence microscope (TIRFM) for nanomanipulation of single cells. *Ultramicroscopy* **2002,** *91* (1), 269-274.
153. Monserrate, A.; Casado, S.; Flors, C., Correlative Atomic Force Microscopy and Localization-Based Super-Resolution Microscopy: Revealing Labelling and Image Reconstruction Artefacts. *ChemPhysChem* **2014,** *15* (4), 647-650.
154. Jurado, R.; Castello, F.; Bondia, P.; Casado, S.; Flors, C.; Cuesta, R.; Domínguez-Vera, J. M.; Orte, A.; Gálvez, N. J. N., Apoferritin fibers: a new template for 1D fluorescent hybrid nanostructures. **2016,** *8* (18), 9648-9656.
155. Bondia, P.; Jurado, R.; Casado, S.; Domínguez-Vera, J. M.; Gálvez, N.; Flors, C., Hybrid Nanoscopy of Hybrid Nanomaterials. *Small* **2017,** *13* (17), 1603784.
156. Bondia, P.; Casado, S.; Flors, C., Correlative Super-Resolution Fluorescence Imaging and Atomic Force Microscopy for the Characterization of Biological Samples. In *Super-Resolution Microscopy: Methods and Protocols*, Erfle, H., Ed. Springer New York: New York, NY, 2017; pp 105-113.
157. Gonzalez-Carrero, S.; Bareño, L.; Debroye, E.; Martin, C.; Bondia, P.; Flors, C.; Galian, R. E.; Hofkens, J.; Pérez-Prieto, J., Linear assembly of lead bromide-based nanoparticles inside lead(ii) polymers prepared by mixing the precursors of both the nanoparticle and the polymer. *Chemical Communications* **2019,** *55* (20), 2968-2971.
158. Bondia, P.; Torra, J.; Tone, C. M.; Sawazaki, T.; del Valle, A.; Sot, B.; Nonell, S.; Kanai, M.; Sohma, Y.; Flors, C., Nanoscale View of Amyloid Photodynamic Damage. *Journal of the American Chemical Society* **2020,** *142* (2), 922-930.
159. Ortega-Esteban, A.; Bodensiek, K.; San Martín, C.; Suomalainen, M.; Greber, U. F.; de Pablo, P. J.; Schaap, I. A. T., Fluorescence Tracking of Genome Release during Mechanical Unpacking of Single Viruses. *ACS Nano* **2015,** *9* (11), 10571-10579.
160. Green, N. H.; Allen, S.; Davies, M. C.; Roberts, C. J.; Tendler, S. J. B.; Williams, P. M., Force sensing and mapping by atomic force microscopy. *TrAC Trends in Analytical Chemistry* **2002,** *21* (1), 65-74.
161. Dorobantu, L. S.; Goss, G. G.; Burrell, R. E., Atomic force microscopy: A nanoscopic view of microbial cell surfaces. *Micron* **2012,** *43* (12), 1312-1322.
162. Raskin, D. M.; de Boer, P. A., Rapid pole-to-pole oscillation of a protein required for directing division to the middle of Escherichia coli. *Proc Natl Acad Sci U S A* **1999,** *96* (9), 4971-4976.
163. Vadillo-Rodriguez, V.; Dutcher, J. R., Dynamic viscoelastic behavior of individual Gram-negative bacterial cells. *Soft Matter* **2009,** *5* (24), 5012-5019.
164. Vadillo-Rodríguez, V.; Dutcher, J. R., Viscoelasticity of the bacterial cell envelope. *Soft Matter* **2011,** *7* (9), 4101-4110.
165. Vadillo-Rodriguez, V.; Schooling, S. R.; Dutcher, J. R., In Situ Characterization of Differences in the Viscoelastic Response of Individual Gram-Negative and Gram-Positive Bacterial Cells. *Journal of Bacteriology* **2009,** *191* (17), 5518-5525.
166. Gavara, N., A beginner's guide to atomic force microscopy probing for cell mechanics. *Microscopy Research and Technique* **2017,** *80* (1), 75-84.
167. Neumann, T. J. J. I. A. R., Determining the elastic modulus of biological samples using atomic force microscopy. **2008**, 1-9.
168. Fabry, B.; Maksym, G. N.; Butler, J. P.; Glogauer, M.; Navajas, D.; Fredberg, J. J., Scaling the Microrheology of Living Cells. *Physical Review Letters* **2001,** *87* (14), 148102.
169. Deng, L.; Trepat, X.; Butler, J. P.; Millet, E.; Morgan, K. G.; Weitz, D. A.; Fredberg, J. J., Fast and slow dynamics of the cytoskeleton. *Nature Materials* **2006,** *5* (8), 636-640.
170. Fischer-Friedrich, E.; Toyoda, Y.; Cattin, C. J.; Müller, D. J.; Hyman, A. A.; Jülicher, F., Rheology of the Active Cell Cortex in Mitosis. *Biophys J* **2016,** *111* (3), 589-600.
171. Thomas, G.; Burnham, N. A.; Camesano, T. A.; Wen, Q. J. J., Measuring the mechanical properties of living cells using atomic force microscopy. **2013,** (76), e50497.

172. David, N.; Petr, K., Gwyddion: an open-source software for SPM data analysis. *Open Physics* **2012,** *10* (1), 181-188.
173. JPK Data Processing Software Manual. Version 4.2.
174. Hermanowicz, P.; Sarna, M.; Burda, K.; Gabryś, H., AtomicJ: An open source software for analysis of force curves. *Review of Scientific Instruments* **2014,** *85* (6), 063703.
175. Andor Solis software. http://www.andor.com/scientific-software/solis-software.
176. Rasband, W. S., ImageJ. Bethesda, MD: 1997.
177. Mary, H. KymographBuilder : Yet Another Kymograph Fiji plugin. https://imagej.net/KymographBuilder_:_Yet_Another_Kymograph_Fiji_plugin.
178. Nitzsche, B.; Bormuth, V.; Bräuer, C.; Howard, J.; Ionov, L.; Kerssemakers, J.; Korten, T.; Leduc, C.; Ruhnow, F.; Diez, S., Chapter 14 - Studying Kinesin Motors by Optical 3D-Nanometry in Gliding Motility Assays. In *Methods in Cell Biology*, Wilson, L.; Correia, J. J., Eds. Academic Press: 2010; Vol. 95, pp 247-271.
179. Jahn, K. A.; Barton, D. A.; Kobayashi, K.; Ratinac, K. R.; Overall, R. L.; Braet, F., Correlative microscopy: Providing new understanding in the biomedical and plant sciences. *Micron* **2012,** *43* (5), 565-582.
180. Eaton, P.; West, P., 3.3 Flying Tip. In *Atomic Force Microscopy*, 1st ed.; Press, O. U., Ed. 2010.
181. Lopez-Ayon, G. M.; Oliver, D. J.; Grutter, P. H.; Komarova, S. V., Deconvolution of Calcium Fluorescent Indicator Signal from AFM Cantilever Reflection. *Microscopy and Microanalysis* **2012,** *18* (4), 808-815.
182. Fernandes, T. F. D.; Saavedra, O.; Margeat, E.; Milhiet, P.-E.; Costa, L., Synchronous, Crosstalk-free Correlative AFM and Confocal Microscopies/Spectroscopies. *Scientific Reports* **2020,** *10* (1), 7098.
183. Schulz, O.; Zhao, Z.; Ward, A.; Koenig, M.; Koberling, F.; Liu, Y.; Enderlein, J.; Yan, H.; Ros, R., Tip induced fluorescence quenching for nanometer optical and topographical resolution. *Optical Nanoscopy* **2013,** *2* (1), 1.
184. Anger, P.; Bharadwaj, P.; Novotny, L., Enhancement and Quenching of Single-Molecule Fluorescence. *Physical Review Letters* **2006,** *96* (11), 113002.
185. Dufrêne, Y. F., Atomic force microscopy and chemical force microscopy of microbial cells. *Nature Protocols* **2008,** *3* (7), 1132-1138.
186. Louise Meyer, R.; Zhou, X.; Tang, L.; Arpanaei, A.; Kingshott, P.; Besenbacher, F., Immobilisation of living bacteria for AFM imaging under physiological conditions. *Ultramicroscopy* **2010,** *110* (11), 1349-1357.
187. Colville, K.; Tompkins, N.; Rutenberg, A. D.; Jericho, M. H., Effects of Poly(l-lysine) Substrates on Attached Escherichia coli Bacteria. *Langmuir* **2010,** *26* (4), 2639-2644.
188. Hutter, J. L.; Bechhoefer, J., Calibration of atomic-force microscope tips. *Review of Scientific Instruments* **1993,** *64* (7), 1868-1873.
189. Elbourne, A.; Cheeseman, S.; Atkin, P.; Truong, N. P.; Syed, N.; Zavabeti, A.; Mohiuddin, M.; Esrafilzadeh, D.; Cozzolino, D.; McConville, C. F.; Dickey, M. D.; Crawford, R. J.; Kalantar-Zadeh, K.; Chapman, J.; Daeneke, T.; Truong, V. K., Antibacterial Liquid Metals: Biofilm Treatment via Magnetic Activation. *ACS Nano* **2020,** *14* (1), 802-817.
190. Peterson, B. W.; Sharma, P. K.; van der Mei, H. C.; Busscher, H. J., Bacterial Cell Surface Damage Due to Centrifugal Compaction. *Applied and Environmental Microbiology* **2012,** *78* (1), 120-125.
191. Spurlin, T. A.; Gewirth, A. A., Poly-L-Lysine-Induced Morphology Changes in Mixed Anionic/Zwitterionic and Neat Zwitterionic-Supported Phospholipid Bilayers. *Biophys J* **2006,** *91* (8), 2919-2927.
192. Formosa-Dague, C.; Duval, R. E.; Dague, E., Cell biology of microbes and pharmacology of antimicrobial drugs explored by Atomic Force Microscopy. *Seminars in Cell & Developmental Biology* **2018,** *73*, 165-176.

193. Dufrêne, Y. F., Atomic Force Microscopy in Microbiology: New Structural and Functional Insights into the Microbial Cell Surface. *mBio* **2014,** *5* (4), e01363-14.
194. Kirchhoff, C.; Cypionka, H., Propidium ion enters viable cells with high membrane potential during live-dead staining. *Journal of Microbiological Methods* **2017,** *142*, 79-82.
195. Rosenberg, M.; Azevedo, N. F.; Ivask, A., Propidium iodide staining underestimates viability of adherent bacterial cells. *Scientific Reports* **2019,** *9* (1), 6483.
196. Shi, L.; Günther, S.; Hübschmann, T.; Wick, L. Y.; Harms, H.; Müller, S., Limits of propidium iodide as a cell viability indicator for environmental bacteria. *Cytometry Part A* **2007,** *71A* (8), 592-598.
197. Stiefel, P.; Schmidt-Emrich, S.; Maniura-Weber, K.; Ren, Q., Critical aspects of using bacterial cell viability assays with the fluorophores SYTO9 and propidium iodide. *BMC Microbiology* **2015,** *15* (1), 36.
198. Yang, Y.; Xiang, Y.; Xu, M., From red to green: the propidium iodide-permeable membrane of Shewanella decolorationis S12 is repairable. *Scientific Reports* **2015,** *5* (1), 18583.
199. Downing, B. P. B.; Rutenberg, A. D.; Touhami, A.; Jericho, M., Subcellular Min Oscillations as a Single-Cell Reporter of the Action of Polycations, Protamine, and Gentamicin on Escherichia coli. *PLOS ONE* **2009,** *4* (9), e7285.
200. Meacci, G.; Ries, J.; Fischer-Friedrich, E.; Kahya, N.; Schwille, P.; Kruse, K., Mobility of Min-proteins inEscherichia colimeasured by fluorescence correlation spectroscopy. *Physical Biology* **2006,** *3* (4), 255-263.
201. Hu, Z.; Lutkenhaus, J., Topological Regulation of Cell Division in E. coli: Spatiotemporal Oscillation of MinD Requires Stimulation of Its ATPase by MinE and Phospholipid. *Molecular Cell* **2001,** *7* (6), 1337-1343.
202. Rowlett, V. W.; Margolin, W., The Min system and other nucleoid-independent regulators of Z ring positioning. *Front Microbiol* **2015,** *6*, 478-478.
203. de Boer, P. A.; Crossley, R. E.; Hand, A. R.; Rothfield, L. I., The MinD protein is a membrane ATPase required for the correct placement of the Escherichia coli division site. *EMBO J* **1991,** *10* (13), 4371-4380.
204. Bisicchia, P.; Arumugam, S.; Schwille, P.; Sherratt, D., MinC, MinD, and MinE Drive Counter-oscillation of Early-Cell-Division Proteins Prior to Escherichia coli Septum Formation. *mBio* **2013,** *4* (6), e00856-13.
205. Touhami, A.; Jericho, M.; Rutenberg, A. D., Temperature Dependence of MinD Oscillation in Escherichia coli: Running Hot and Fast. *Journal of Bacteriology* **2006,** *188* (21), 7661-7667.
206. Barák, I., Open questions about the function and evolution of bacterial Min systems. *Front Microbiol* **2013,** *4*, 378-378.
207. Rowlett, V. W.; Margolin, W., The bacterial Min system. *Current Biology* **2013,** *23* (13), R553-R556.
208. Scheffers, D.-J., The effect of MinC on FtsZ polymerization is pH dependent and can be counteracted by ZapA. *FEBS Letters* **2008,** *582* (17), 2601-2608.
209. Juarez, J. R.; Margolin, W., Changes in the Min Oscillation Pattern before and after Cell Birth. *Journal of Bacteriology* **2010,** *192* (16), 4134.
210. Hale, C. A.; Meinhardt, H.; de Boer, P. A., Dynamic localization cycle of the cell division regulator MinE in Escherichia coli. *EMBO J* **2001,** *20* (7), 1563-1572.
211. Pazos, M.; Casanova, M.; Palacios, P.; Margolin, W.; Natale, P.; Vicente, M. J. P. O., FtsZ placement in nucleoid-free bacteria. **2014,** *9* (3).
212. Padan, E.; Schuldiner, S., [27] Intracellular pH regulation in bacterial cells. In *Methods in Enzymology*, Academic Press: 1986; Vol. 125, pp 337-352.
213. Yoshioka, K.; Takahashi, H.; Homma, T.; Saito, M.; Oh, K.-B.; Nemoto, Y.; Matsuoka, H., A novel fluorescent derivative of glucose applicable to the assessment of glucose uptake

activity of Escherichia coli. *Biochimica et Biophysica Acta (BBA) - General Subjects* **1996,** *1289* (1), 5-9.
214. Natarajan, A.; Srienc, F., Dynamics of Glucose Uptake by Single Escherichia coli Cells. *Metabolic Engineering* **1999,** *1* (4), 320-333.
215. Novo, D.; Perlmutter, N. G.; Hunt, R. H.; Shapiro, H. M., Accurate flow cytometric membrane potential measurement in bacteria using diethyloxacarbocyanine and a ratiometric technique. *Cytometry* **1999,** *35* (1), 55-63.
216. Hassan, M. M.; Butler, M. S.; Ranzoni, A.; Cooper, M. A., Detection and quantification of the heterogeneity of S. aureus bacterial populations to identify antibiotic-induced persistence. *bioRxiv* **2018**, 320093.
217. Micic, M.; Hu, D.; Suh, Y. D.; Newton, G.; Romine, M.; Lu, H. P., Correlated atomic force microscopy and fluorescence lifetime imaging of live bacterial cells. *Colloids and Surfaces B: Biointerfaces* **2004,** *34* (4), 205-212.
218. Lin, H.-J.; Herman, P.; Lakowicz, J. R., Fluorescence lifetime-resolved pH imaging of living cells. *Cytometry Part A* **2003,** *52A* (2), 77-89.
219. Sud, D.; Mehta, G.; Mehta, K.; Linderman, J.; Takayama, S.; Mycek, M.-A. In *Fluorescence Lifetime Imaging Microscopy (FLIM) Measures Oxygen Gradients in Microfluidic Bioreactors*, Biomedical Optics, Fort Lauderdale, Florida, 2006/03/19; Optical Society of America: Fort Lauderdale, Florida, 2006; p TuI52.
220. Torno, K.; Wright, B. K.; Jones, M. R.; Digman, M. A.; Gratton, E.; Phillips, M., Real-time Analysis of Metabolic Activity Within Lactobacillus acidophilus by Phasor Fluorescence Lifetime Imaging Microscopy of NADH. *Current Microbiology* **2013,** *66* (4), 365-367.
221. Froschauer, E. M.; Kolisek, M.; Dieterich, F.; Schweigel, M.; Schweyen, R. J., Fluorescence measurements of free [Mg2+] by use of mag-fura 2 in Salmonella enterica. *FEMS Microbiology Letters* **2004,** *237* (1), 49-55.
222. Luan, Y.; Liu, S.; Pihl, M.; van der Mei, H. C.; Liu, J.; Hizal, F.; Choi, C.-H.; Chen, H.; Ren, Y.; Busscher, H. J., Bacterial interactions with nanostructured surfaces. *Current Opinion in Colloid & Interface Science* **2018,** *38*, 170-189.
223. Trichet, L.; Le Digabel, J.; Hawkins, R. J.; Vedula, S. R. K.; Gupta, M.; Ribrault, C.; Hersen, P.; Voituriez, R.; Ladoux, B., Evidence of a large-scale mechanosensing mechanism for cellular adaptation to substrate stiffness. *Proceedings of the National Academy of Sciences* **2012,** *109* (18), 6933.
224. Di Cio, S.; Gautrot, J. E., Cell sensing of physical properties at the nanoscale: Mechanisms and control of cell adhesion and phenotype. *Acta Biomaterialia* **2016,** *30*, 26-48.
225. Ghassemi, S.; Meacci, G.; Liu, S.; Gondarenko, A. A.; Mathur, A.; Roca-Cusachs, P.; Sheetz, M. P.; Hone, J., Cells test substrate rigidity by local contractions on submicrometer pillars. *Proceedings of the National Academy of Sciences* **2012,** *109* (14), 5328-5333.
226. Blount, Z. D., The unexhausted potential of E. coli. *eLife* **2015,** *4*, e05826.
227. Typas, A.; Banzhaf, M.; Gross, C. A.; Vollmer, W., From the regulation of peptidoglycan synthesis to bacterial growth and morphology. *Nature Reviews Microbiology* **2012,** *10* (2), 123-136.
228. Roszak, D. B.; Colwell, R. R., Survival strategies of bacteria in the natural environment. *Microbiol Rev* **1987,** *51* (3), 365-379.
229. Peric, O.; Hannebelle, M.; Adams, J. D.; Fantner, G. E., Microfluidic bacterial traps for simultaneous fluorescence and atomic force microscopy. *Nano Research* **2017,** *10* (11), 3896-3908.
230. Kailas, L.; Ratcliffe, E. C.; Hayhurst, E. J.; Walker, M. G.; Foster, S. J.; Hobbs, J. K., Immobilizing live bacteria for AFM imaging of cellular processes. *Ultramicroscopy* **2009,** *109* (7), 775-780.
231. Velegol, S. B.; Logan, B. E., Contributions of Bacterial Surface Polymers, Electrostatics, and Cell Elasticity to the Shape of AFM Force Curves. *Langmuir* **2002,** *18* (13), 5256-5262.

232. Arnoldi, M.; Fritz, M.; Bäuerlein, E.; Radmacher, M.; Sackmann, E.; Boulbitch, A., Bacterial turgor pressure can be measured by atomic force microscopy. *Physical Review E* **2000,** *62* (1), 1034-1044.
233. Sullivan, C. J.; Venkataraman, S.; Retterer, S. T.; Allison, D. P.; Doktycz, M. J., Comparison of the indentation and elasticity of E. coli and its spheroplasts by AFM. *Ultramicroscopy* **2007,** *107* (10), 934-942.
234. Yao, X.; Walter, J.; Burke, S.; Stewart, S.; Jericho, M. H.; Pink, D.; Hunter, R.; Beveridge, T. J., Atomic force microscopy and theoretical considerations of surface properties and turgor pressures of bacteria. *Colloids and Surfaces B: Biointerfaces* **2002,** *23* (2), 213-230.
235. Chen, Y.-Y.; Wu, C.-C.; Hsu, J.-L.; Peng, H.-L.; Chang, H.-Y.; Yew, T.-R., Surface Rigidity Change of Escherichia coli after Filamentous Bacteriophage Infection. *Langmuir* **2009,** *25* (8), 4607-4614.
236. Arnoldi, M.; Kacher, C. M.; Bäuerlein, E.; Radmacher, M.; Fritz, M., Elastic properties of the cell wall of Magnetospirillum gryphiswaldense investigated by atomic force microscopy. *Applied Physics A* **1998,** *66* (1), S613-S617.
237. Gaboriaud, F.; Bailet, S.; Dague, E.; Jorand, F., Surface Structure and Nanomechanical Properties of Shewanella putrefaciens Bacteria at Two pH values (4 and 10) Determined by Atomic Force Microscopy. *Journal of Bacteriology* **2005,** *187* (11), 3864.
238. Volle, C. B.; Ferguson, M. A.; Aidala, K. E.; Spain, E. M.; Núñez, M. E., Spring constants and adhesive properties of native bacterial biofilm cells measured by atomic force microscopy. *Colloids and Surfaces B: Biointerfaces* **2008,** *67* (1), 32-40.
239. McKee, C. T.; Last, J. A.; Russell, P.; Murphy, C. J., Indentation versus tensile measurements of Young's modulus for soft biological tissues. *Tissue Eng Part B Rev* **2011,** *17* (3), 155-164.
240. Ma, D.; Ong, C. W.; Wong, S. F.; He, J., New Method for Determining Young's Modulus by Non-ideally Sharp Indentation. *Journal of Materials Research* **2005,** *20* (6), 1498-1506.
241. Roa, J. J.; Oncins, G.; Diaz, J.; Sanz, F.; Segarra, M., Calculation of Young's Modulus Value by Means of AFM. *Recent Patents on Nanotechnology* **2011,** *5* (1), 27-36.
242. Tranchida, D.; Piccarolo, S., On the Use of the Nanoindentation Unloading Curve to Measure the Young's Modulus of Polymers on a Nanometer Scale. *Macromolecular Rapid Communications* **2005,** *26* (22), 1800-1804.
243. Baumgart, F., Stiffness — an unknown world of mechanical science? *Injury* **2000,** *31*, 14-84.
244. Carl, P.; Schillers, H., Elasticity measurement of living cells with an atomic force microscope: data acquisition and processing. *Pflügers Archiv - European Journal of Physiology* **2008,** *457* (2), 551.
245. Truesdell, C.; Euler, L., *The Rational Mechanics of Flexible Or Elastic Bodies, 1638-1788: Introduction to Leonhardi Euleri Opera Omnia Vol X Et XI Seriei Secundae*. Orell Füssli: 1960.
246. Young, T., *A course of lectures on natural philosophy and the mechanical arts*. Taylor and Walton: 1845; Vol. 1.
247. Hertz, H. R., Ueber die Berührung fester elastischer Körper. *Journal für die reine und angewandte Mathematik* **1882,** *1882* (92), 156-171.
248. Krieg, M.; Fläschner, G.; Alsteens, D.; Gaub, B. M.; Roos, W. H.; Wuite, G. J. L.; Gaub, H. E.; Gerber, C.; Dufrêne, Y. F.; Müller, D. J., Atomic force microscopy-based mechanobiology. *Nature Reviews Physics* **2019,** *1* (1), 41-57.
249. Sneddon, I. N., The relation between load and penetration in the axisymmetric boussinesq problem for a punch of arbitrary profile. *International Journal of Engineering Science* **1965,** *3* (1), 47-57.
250. Domke, J.; Radmacher, M., Measuring the Elastic Properties of Thin Polymer Films with the Atomic Force Microscope. *Langmuir* **1998,** *14* (12), 3320-3325.

251. Guz, N.; Dokukin, M.; Kalaparthi, V.; Sokolov, I., If Cell Mechanics Can Be Described by Elastic Modulus: Study of Different Models and Probes Used in Indentation Experiments. *Biophys J* **2014,** *107* (3), 564-575.
252. Zhou, Z. L.; Ngan, A. H. W.; Tang, B.; Wang, A. X., Reliable measurement of elastic modulus of cells by nanoindentation in an atomic force microscope. *Journal of the Mechanical Behavior of Biomedical Materials* **2012,** *8*, 134-142.
253. Faria, E. C.; Ma, N.; Gazi, E.; Gardner, P.; Brown, M.; Clarke, N. W.; Snook, R. D., Measurement of elastic properties of prostate cancer cells using AFM. *Analyst* **2008,** *133* (11), 1498-1500.
254. Lekka, M.; Laidler, P.; Gil, D.; Lekki, J.; Stachura, Z.; Hrynkiewicz, A. Z., Elasticity of normal and cancerous human bladder cells studied by scanning force microscopy. *European Biophysics Journal* **1999,** *28* (4), 312-316.
255. Li, Q. S.; Lee, G. Y. H.; Ong, C. N.; Lim, C. T., AFM indentation study of breast cancer cells. *Biochemical and Biophysical Research Communications* **2008,** *374* (4), 609-613.
256. Lekka, M.; Gil, D.; Pogoda, K.; Dulińska-Litewka, J.; Jach, R.; Gostek, J.; Klymenko, O.; Prauzner-Bechcicki, S.; Stachura, Z.; Wiltowska-Zuber, J.; Okoń, K.; Laidler, P., Cancer cell detection in tissue sections using AFM. *Archives of Biochemistry and Biophysics* **2012,** *518* (2), 151-156.
257. Lekka, M., Discrimination Between Normal and Cancerous Cells Using AFM. *Bionanoscience* **2016,** *6*, 65-80.
258. Tian, M.; Li, Y.; Liu, W.; Jin, L.; Jiang, X.; Wang, X.; Ding, Z.; Peng, Y.; Zhou, J.; Fan, J.; Cao, Y.; Wang, W.; Shi, Y., The nanomechanical signature of liver cancer tissues and its molecular origin. *Nanoscale* **2015,** *7* (30), 12998-13010.
259. Kontomaris, S.-V.; Malamou, A., The harmonic motion of a rigid cylinder on an elastic half-space. *European Journal of Physics* **2019,** *41* (1), 015003.
260. Kontomaris, S. V.; Malamou, A., Hertz model or Oliver & Pharr analysis? Tutorial regarding AFM nanoindentation experiments on biological samples. *Materials Research Express* **2020,** *7* (3), 033001.
261. Kontomaris, S.-V.; Stylianou, A.; Malamou, A.; Stylianopoulos, T., A discussion regarding the approximation of cylindrical and spherical shaped samples as half spaces in AFM nanoindentation experiments. *Materials Research Express* **2018,** *5* (8), 085402.
262. Kontomaris, S. V.; Yova, D.; Stylianou, A.; Balogiannis, G., The effects of UV irradiation on collagen D-band revealed by atomic force microscopy. *Scanning* **2015,** *37* (2), 101-111.
263. Cerf, A.; Cau, J.-C.; Vieu, C.; Dague, E., Nanomechanical Properties of Dead or Alive Single-Patterned Bacteria. *Langmuir* **2009,** *25* (10), 5731-5736.